Shot peening speed measurements using lidar technology

Angelou, Nikolas; Zhang, Xiaodan; Sjöholm, Mikael; Lorentzen, Lars; Huang, Xiaoxu

Publication date:
2017

Document Version
Publisher's PDF, also known as Version of record

Shot peening speed measurements using lidar technology

E-0151

Nikolas Angelou, Xiaodan Zhang,
Mikael Sjöholm, Lars Lorentzen and
Xiaoxu Huang
DTU Wind Energy
December 2017
ISBN:978-87-93549-19-7

DTU Wind Energy
Department of Wind Energy

Contents

1. Introduction

The shot peening technique is used for the surface modification of metallic components that are part of wind turbines, such as gears, bolts and blade coatings to prevent erosion. An important parameter of this technique is the dynamic energy of emitted shots. In this context the objective of this project is to present a proof of concept measurement method for the evaluation of the speed of the shots.

A remote sensing laser anemometer was selected as a probing instrument of the peening shots' speed since it avoids any disturbances to the flow from the presence of an in-situ instrument. Furthermore, the risk of damaging the peening machine by installing an instrument inside the chamber during operation is eliminated by this approach.

Laser anemometers are being researched and developed in the department of Wind Energy, mainly in the framework of the WindScanner.dk infrastructure project [1], but also validated and used in monitoring the wind conditions around wind turbines (wake and inflow), over complex terrain as well as offshore.

2. Shot peening machine

The shot peening machine used in this experiment was manufactured by Shanghai Carthing Machinery CO., LTD and it is installed in the laboratory of the Section for Materials Science and Characterization of the Department of Wind Energy of DTU.

2.1 Shot peening mechanism

The shot peening machine is connected with an air compressor to supply the necessary pressured air to push the shots out of the gun. The mechanism is shown in Figure 1, together with the two different types of shots (ceramic and steel) and the peening machine. The maximum shot peening pressure is 80 PSI. The stage for fixing the sample can rotate with a speed between 2 and 20 rpm and can move up and down with a speed between 100 and 1000 mm/min.

2.2 Shot materials

The shot materials used in this proof of concept experiment are made from steel and ceramic material. The conditioned steel cut wire shots have two diameter sizes: 0.6 mm and 1.0 mm with the Vickers hardness 640~700 at the load of 0.5/1 kg, while the ceramic shots with the Vickers hardness around 700 have four

diameter sizes: 63~125 µm, 150~210 µm, 300~425 µm and 600~850 µm. The composition of the ceramic shots used is 60~70% ZrO_2, 28~33% SiO_2 and <10% Al_2O_3.

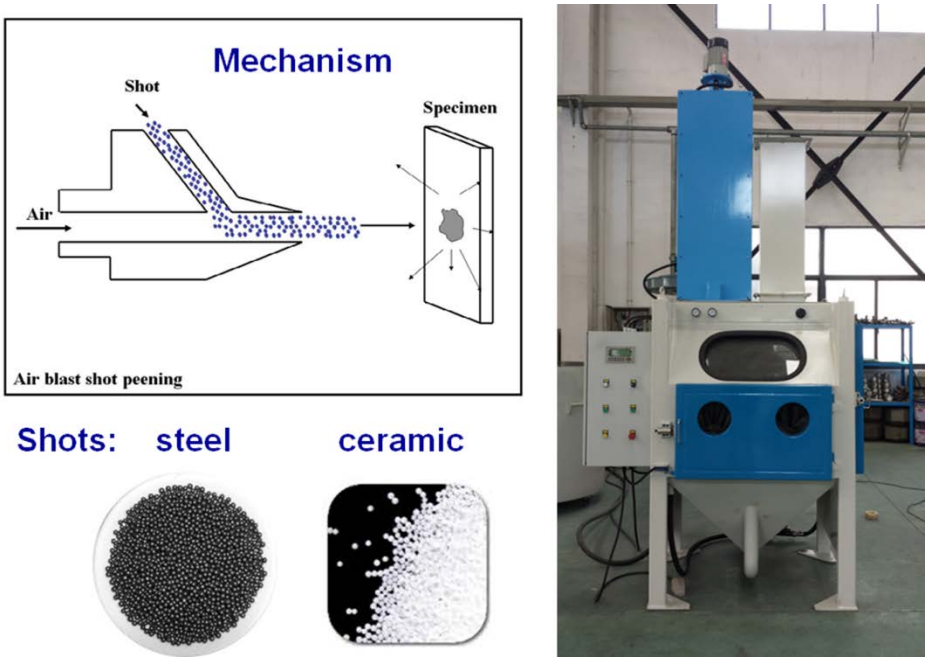

Figure 1 Sketch showing the shot peening mechanism, shots and shot peening machine.

3. Remote Measurement Technique

3.1 Principle

A laser anemometer is often addressed with the acronym lidar (light detection and ranging), because of the similar measuring principle. The laser light is transmitted in the atmosphere through a telescope, and its configuration can be adjusted to focus the laser light in a distance of interest. The transmitted light through its propagation in the atmosphere is scattered by particles that appear in the air (aerosols). Under windy conditions, air volumes that contain aerosols move relative to the telescope of the lidar. This movement induce a shift in the frequency of the light scattered (Doppler Effect). A tiny portion of the scattered light is scattered back to the telescope and through that into the detection module of the lidar.

3.2 Instrument

For the purposes of this experiment, a continuous-wave (cw), coherent, mono-axial, Doppler wind lidar was selected. It consists of three main components: a laser source, a detection system and a transceiver. The laser source and the detection system were selected to be the same as the ones used in the second generation of the short-range WindScanner (swrs) [2]. As a transceiver a small telescope, hereafter denoted as lidic, was used which was developed in the context of the project *Wind Turbine improvements by wind-lidar based preview and Control* [3]. The performance of such an arrangement has been tested in measuring the wind both

outdoors [4] and indoors (in wind tunnels) [5]. The tests revealed a high correlation between the wind measurements of a lidic and reference sensors, proving its high measuring performance.

3.2.1 Technical Specifications

The sampling rate of the detection system of the lidar was 250 MS/s. A 1024-point Fast-Fourier Transform (FFT) was applied to that signal to create 244141 spectra per second. These spectra were subsequently averaged to reduce the variance of the noise and resulted to 400 spectra per second. The resulting averaged spectra, denoted as laser Doppler spectra, were represented by 1024 bins with a frequency resolution of 244 kHz (0.19 m/s).

3.2.2 Calibration

For the needs of the experiment, the focus distance of the lidic was adjusted to be the minimum possible ~70 cm. Subsequently the diameter of the laser beam was measured using a beam profiler in a series of points, separated by a distance of 1 cm, around the expected focus distance.

The measurements revealed that the focus distance was indeed found at 73 cm away from the lidic and furthermore the expansion of the laser beam was in a good agreement with the theoretical expansion of an untruncated Gaussian laser beam (see Figure 2).

In such a case the probe length of a measurement is defined by a parameter called Rayleigh length, which describes the distance where the radius of the laser beam is increased by a factor of $\sqrt{2}$ relative to the minimum beam radius (beam waist), which was measured to be 0.06 mm.

That is slightly larger than the theoretical expected beam waist radius, which is 0.05 m. This difference is probably due to a small offset of the effective radius of the laser beam on the telescopic focussing lens, which is estimated to be 7.5 mm. The probe length is estimated to be equal to 8.29 mm, approximately two orders of magnitude larger than the beam diameter. Therefore, the measurements of the lidar are expected to be acquired over a line.

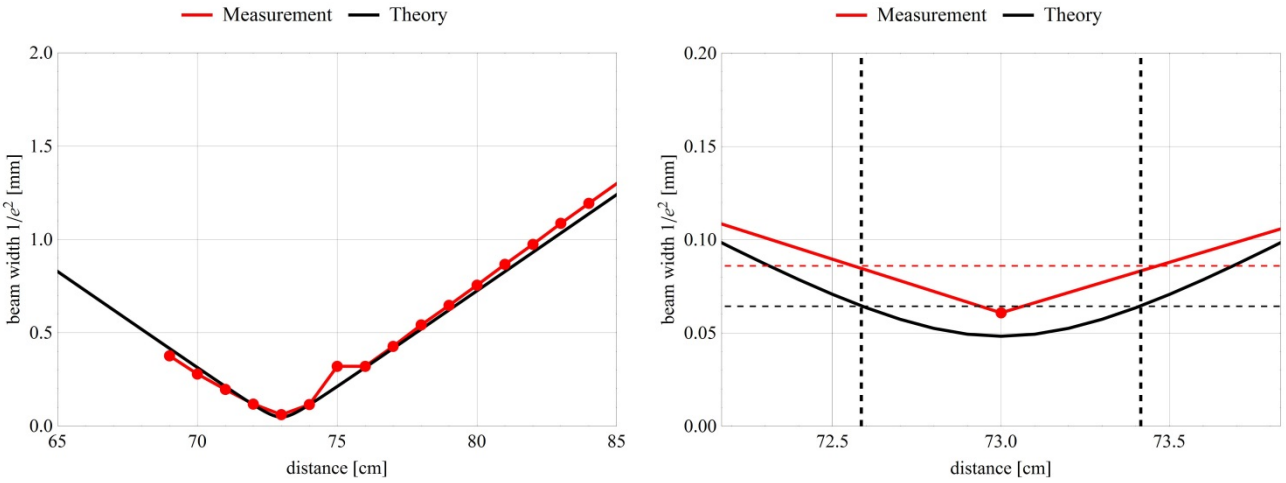

Figure 2 Measured (red) radius of a laser beam trace focused at 73 cm and theoretical model (black) of the expected beam diameter of a Gaussian laser beam.

The parameters describing the operation of the lidar used are presented in Table 1.

Parameter	Value
Wavelength [nm]	1565
Averaging rate [Hz]	400
Min speed [m/s]	0.19
Max speed [m/s]	97.8
Speed resolution [m/s]	0.19
Focus distance [m]	0.73
Probe length [mm]	8.29

Table 1 Operation parameters of the laser anemometer used in the experiment.

4. Experimental setup

For the needs of the experiment, the lidic telescope was mounted on a robotic arm (UR5), developed and manufactured by Universal Robots (see Figure 3). Using the robotic arm, the lidic was elevated high enough to be able to transmit the laser light into the peening machine through a window.

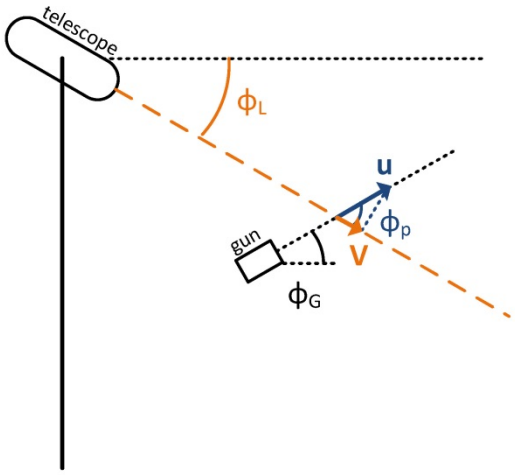

Figure 3 Picture of the lidic mounted on a Universal Robots robotic arm (left) and a drawing of the direction of the line-of-sight of the lidic relative to the shooting direction of the peening gun (right).

Two green pointing lasers were mounted on the rear part of the lidic and directed in a way that intersected at the position of the focus distance of the lidic (see Figure 4).

Figure 4 Top (Left) and side (Right) view of the lidar telescope. In the top photo the traces of the two pointing-laser beam, used for the alignment of the lidic with the peening gun, can be seen.

Using the two green pointing lasers trace and by adjusting the position of the robotic arm, the line-of-sight of the lidic was aligned with the shooting direction of the peening machine, while the focus distance was positioned 50 mm in front of the gun.

Based on the geometry of the setup (see Figure 3, right) the lidar was measuring the radial component of the projected speed vector of the peening shots emitted. The resulting speed measured can be associated with the speed of the shots by the following equation:

$$V = u\ \cos(\varphi_L + \varphi_G)$$

The lidic was measured to have a tilt angle (φ_L) equal to 34°, while the gun of the peening machine was aligned horizontally (φ_G=0). The angle between the line-of-sight of the lidar and the shooting direction of the peening machine, along with the probe length of the lidar measurements, created an effective measurement volume with a length equal to 6.87 mm and a width of 4.63 mm (see Figure 5).

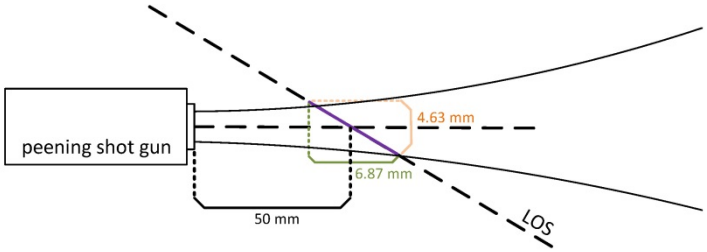

Figure 5 Drawing of the dimensions of the effective measurement volume of the lidar.

5. Measurements

The lidar measurements of the speed of the peening shots were acquired during two different experiments. The experimental setup used was similar, with varying configuration parameters for different shots. The robotic arm positioned the lidic so as to bring the focus point 50 mm in front of the gun barrel of the peening machine for all the measurements. Subsequently the gun barrel was moved manually relatively to focus point of the lidar in order to provide observations of how the speed of the shots slows down with distance. In each distance, the pressure of the air that pushes the shots was increased from either 30 or 40 to 80 PSI with a step of 10 PSI.The different configurations are presented in the following table.

Type	Size [mm]	Measuring distance [mm]	Pressure [PSI]
Ceramic	0.063~0.125	51 – 100 – 150	30 – 80
Ceramic	0.150~0.210	50	40 – 80
Ceramic	0.300~0.425	50	40 – 80
Ceramic	0.600~0.850	58 – 109 -160	30 – 80
Steel	0.600	50	40 – 80
Steel	1.000	50 – 100	40 – 80

Table 2 List of the different configuration of the experimental setup used during the measurement campaign.

6. Data Analysis

An example of a measured laser Doppler spectrum is presented in Figure 6, where the distribution of energy in different speed bins is depicted after averaging 400 FFTs. The x-axis presents the radial speed projected to the direction of the peening shot gun (u). It is interesting to observe that the spectrum consists of a high energy component in the speed area between 18-20 m/s, but due to the low energy components that appears between 25 – 40 m/s, the speed estimation (red line) is shifted to higher speeds.

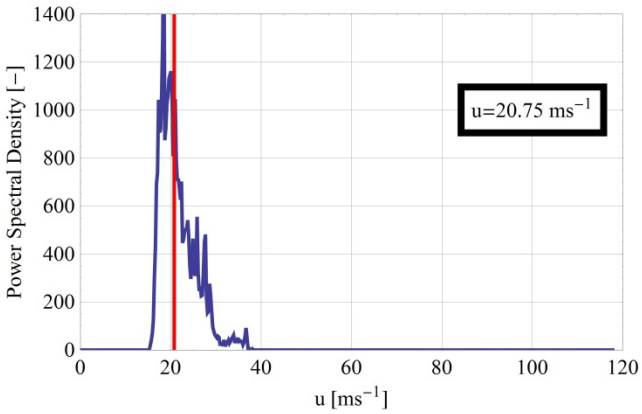

Figure 6 Example of a laser Doppler spectrum acquired by the lidar.

A 1-second time series of the laser Doppler spectra are presented in Figure 7, where the energy in different velocity bins is described by a contour plot along with the estimated speed of each spectrum.

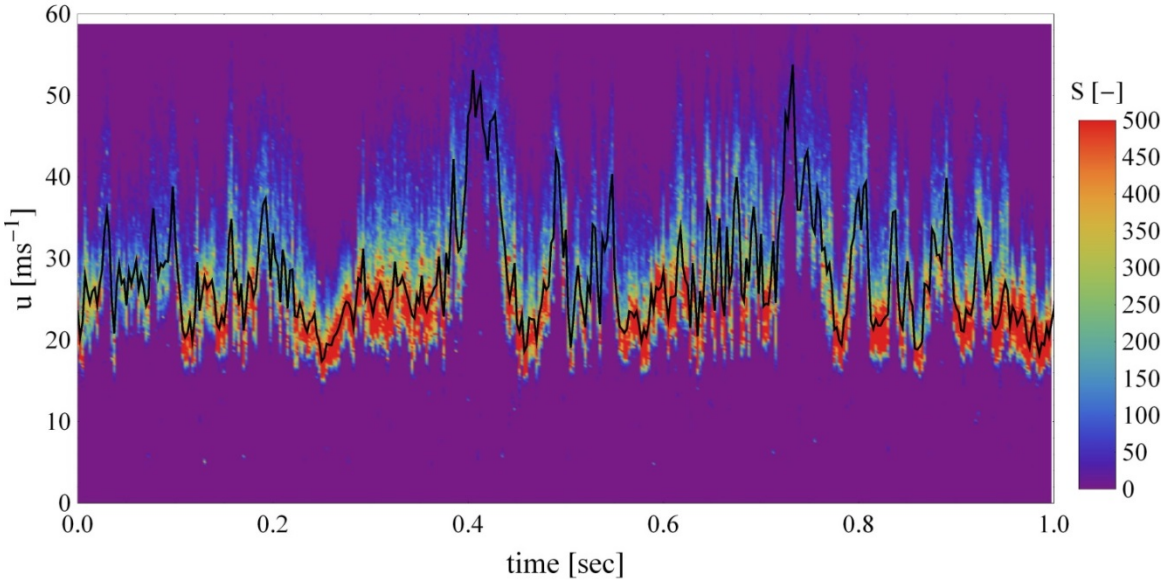

Figure 7 One second time series of laser Doppler spectra (contour plot) and corresponding estimation of the speed (black line).

In the Figure 8, a sample time series of the speed of 0.2 mm ceramic peening shots is presented. The first shots are emitted after the 4th second of data acquisition. Then few bursts of shots follow for the next 3-4 seconds. The bursts appear as a sudden increase of the speed and are associated with laser Doppler spectra with a higher maximum energy as it can be seen in Figure 9. After those events the flow of the shots becomes more stable for a period of a little bit less than 20 seconds. A 10-seconds and 1-second window of the time series in Figure 8 are presented in Figure 10. Towards the end of the emission of the shots, a few shots appear to have very high speeds that reach the maximum detectable speed (100 m/s) and decrease within 5 seconds.

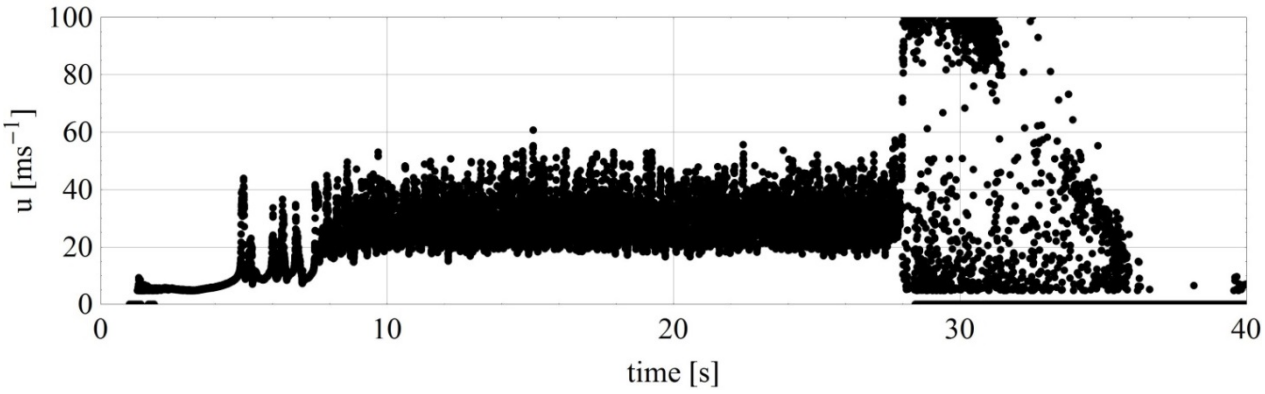

Figure 8 Example of a 30-second time series of the ceramic shots speed measured at 50 mm in front of the peening shots gun.

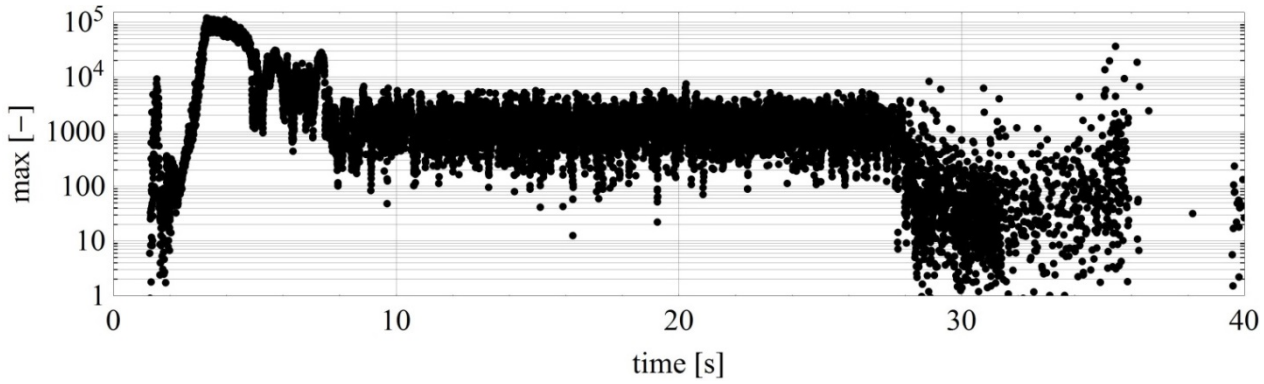

Figure 9 Example of the time series of the maximum values of laser Doppler spectra measuring the speed of ceramic shots.

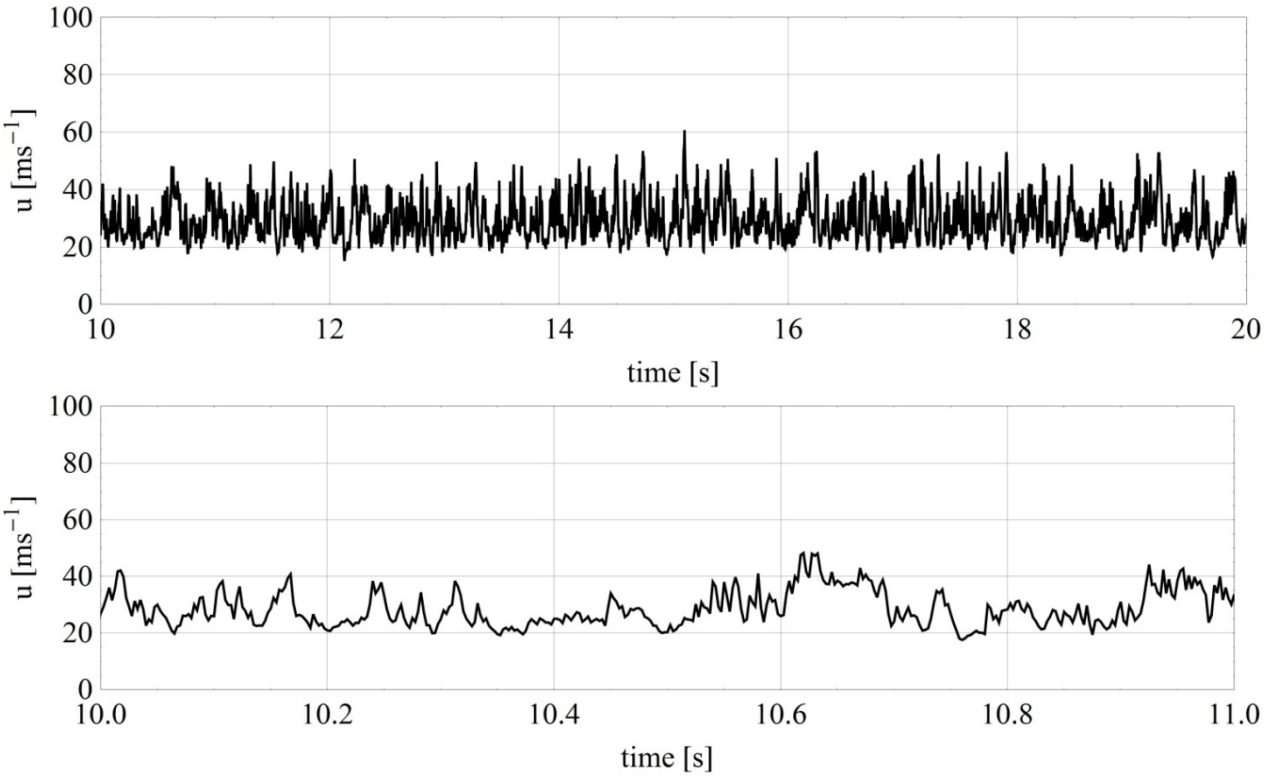

Figure 10 Example of a 10-second (top) and 1-second (bottom) time series of the ceramic shots speed from the measurement period presented in Figure 6.

The variations in the speed appear to be related to the maximum intensity in the laser Doppler spectra, as it can be seen in Figure 11, where the *u* velocity of the shots is presented versus the maximum value of the corresponding laser Doppler spectra.

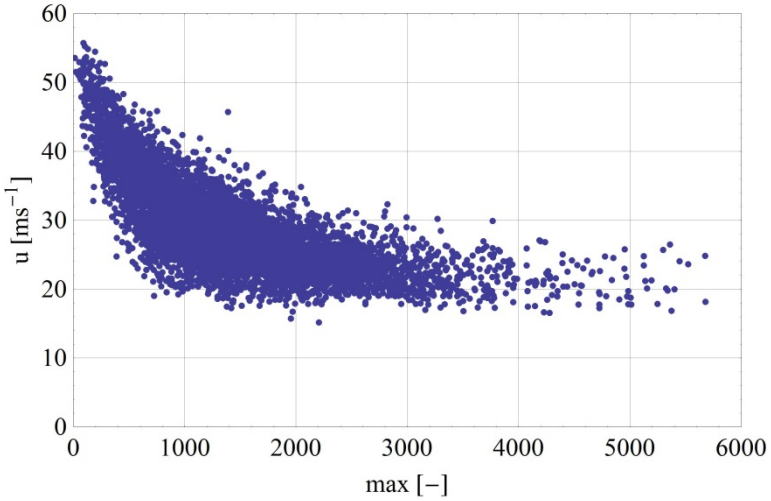

Figure 11 Velocity of the ceramic shots versus the maximum value of the corresponding laser Doppler spectra.

For the determination of the statistics of the velocity of the different shots a period between 15 – 20 seconds was selected from each run. In Figure 12, the average spectrum of such a period is presented, normalized to represent a probability distribution, along with the histogram of the corresponding velocity estimations. The appearing offset between the two is due to the high velocity signals that appear in the individual laser Doppler spectra that shift the estimation of the characteristic velocity to a higher level.

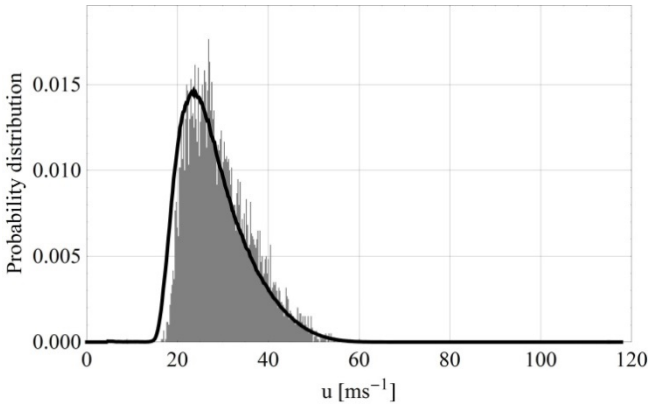

Figure 12 Probability density function and histogram of the measured speeds for one of the time series.

7. Results

7.1 Tables

The results of the speed measurements of the ceramic and steel shots are summarized in the following tables. In the tables are included the air pressure, the duration of the shots flow over which the statistical analysis took place and the corresponding results.

Diameter [mm]	Distance [mm]	Pressure [PSI]	Run [-]	Duration [sec]	mean u [m/s]	std u [m/s]	min u [m/s]	max u [m/s]
0.063~0.125	51	30	1	36	34,4	7,8	53,3	11,4
	51	30	2	17	35,5	7,8	53,6	13,5
	51	40	1	7	41,4	9,0	63,1	16,4
	51	40	2	7	41,9	8,5	60,6	17,2
	51	40	3	6,5	41,7	8,5	59,5	17,6
	51	50	1	15	45,3	9,7	70,9	17,9
	51	50	2	15	46,7	9,7	70,7	18,9
	51	50	3	11	46,9	9,9	70,7	18,7
	51	60	1	7	51,6	12,0	83,1	21,8
	51	60	2	10	50,6	11,0	78,8	19,1
	101	30	1	4	32,8	6,70	47,1	12,9
	101	30	2	6	32,2	7,10	50,7	12,4
	101	40	1	10	39,5	8,5	66,1	15,6
	101	40	2	10	40,1	8,8	66,7	15,6
	101	50	1	10	48,6	13	97,4	13
	101	50	2	11	48,1	12,7	97,2	12,7
	101	60	1	46	49,7	10,6	85,3	19,6
	101	60	2	17	50,2	11	91,1	19,7
	150	30	1	29	30,5	7,10	54	11
	150	30	2	16	30,8	7,10	54,8	10,7
	150	40	1	8	38,2	8,6	66,8	16,2
	150	40	2	8	38,1	8,7	62,7	15
	150	50	1	9	43	9,2	73,4	17,7
	150	50	2	8	32,2	9,1	69,8	19
	150	60	1	8	50,3	10,7	87,9	20,3
	150	60	2	10	51,1	13,1	98,1	13,1

Table 3 Statistics of the ceramic peening shots speed measured at 51, 101 and 150 mm in front of the gun barrel.

Diameter [mm]	Pressure [PSI]	Run [-]	Duration [sec]	mean u [m/s]	std u [m/s]	min u [m/s]	max u [m/s]
0.150~0.210	40	1	15	29,3	6,9	15,2	60,8
	40	2	15	29,3	7,1	8,8	59,9
	50	1	15	32,5	7,7	5,4	95,4
	50	2	15	32,4	7,4	5,5	95,0
	60	1	15	34,7	8,0	5,1	100,0
	60	2	15	34,7	7,8	5,2	102,1
	70	1	15	36,5	8,3	6,6	103,6
	70	2	15	36,5	7,9	15,6	102,9
	80	1	15	38,8	8,7	5,5	106,7
	80	2	15	38,2	7,9	10,5	101,4
0.300~0.425	40	1	15	31,5	7,4	10,9	64,5
	40	2	15	31,6	6,9	16,9	53,0
	50	1	15	35,4	7,3	7,6	61,5
	50	2	15	35,7	7,3	7,6	62,0
	60	1	15	38,4	7,4	6,8	68,6
	60	2	15	38,1	6,9	12,3	71,6
	70	1	10	38,7	7,1	13,7	86,1
	70	2	15	39,6	6,8	17,4	75,1
	80	1	10	41,2	7,6	6,2	88,6
	80	2	10	40,9	6,9	8,4	84,9

Table 4 Statistics of the ceramic peening shots speed measured at 50 mm in front of the gun barrel.

Diameter [mm]	Distance [mm]	Pressure [PSI]	Run [-]	Duration [sec]	mean u [m/s]	std u [m/s]	min u [m/s]	max u [m/s]
0.600~0.850	58	30	1	25	25,0	0,90	28,4	21,0
	58	30	2	12	25,8	1,20	31,7	4,4
	58	40	1	4	31,7	1,20	35,4	27,4
	58	50	1	6	35,6	1,60	41,4	31,1
	58	60	1	4	39,5	1,60	46,8	35,0
	109	30	1	6	26,6	2,80	46,0	21,9
	109	30	2	8	19,8	2,70	40,7	11,4
	109	40	1	8	30,5	1,20	34,1	26,9
	109	50	1	9	34,6	1,40	40,1	30,7
	109	60	1	5	38,5	1,10	42,0	35,3
	160	30	1	7	25,4	1,40	29,8	21,2
	160	30	2	7	25,3	1,50	30,8	21,6
	160	40	1	8	31,1	1,40	35,2	26,9
	160	50	1	7	35,4	1,60	40,3	30,8
	160	60	1	4	39,7	1,70	44,8	34,6

Table 5 Statistics of the ceramic peening shots speed measured at 58, 109 and 160 mm in front of the gun barrel.

Diameter [mm]	Distance [mm]	Pressure [PSI]	Run [-]	Duration [sec]	mean u [m/s]	std u [m/s]	min u [m/s]	max u [m/s]
0.6	50	40	1	20	6,4	2,8	4,8	34,6
	50	40	2	20	12,9	4,8	5,2	42,7
	50	50	1	20	21,8	2,8	11,2	36,6
	50	50	2	20	22,0	2,3	12,9	31,1
	50	60	1	15	24,5	1,5	18,9	34,9
	50	60	2	15	24,8	1,5	19,9	32,1
	50	70	1	15	27,3	1,5	22,2	36,6
	50	70	2	15	26,7	1,4	21,4	34,3
	50	80	1	15	29,0	1,5	22,7	35,6
	50	80	2	15	28,9	1,5	24	37,5
	100	80	1	15	27,9	1,3	20,8	34,6
	100	80	2	15	27,9	1,3	23,3	34,4
	100	70	1	15	25,5	1,2	21,1	34,7
	100	70	2	15	25,5	1,3	19,1	33,6
	100	60	1	15	23,2	1,2	19,3	31,4
	100	60	2	15	23,2	1,2	19,5	28,8
	100	50	1	15	20,6	1,8	13,0	30,9
	100	50	2	15	20,4	2,2	12,5	34,4
	100	40	1	15	16,7	2,5	9,4	28,4
	100	40	2	15	17,0	3,0	9,3	31,4
1.0	50	40	1	20	18,9	2,1	5,8	29,2
	50	40	2	20	18,8	2,0	11,6	29,1
	50	50	1	15	22,0	1,6	17,1	31,2
	50	50	2	15	22,0	1,6	14,9	30,9
	50	60	1	15	25,6	2,5	19,5	50,4
	50	60	2	15	25,2	1,7	19,4	35,8
	50	70	1	15	27,1	1,6	21,1	36,9
	50	70	2	15	27,1	1,7	11,7	35,9
	50	80	1	15	29,7	1,9	22,3	42,0
	50	80	2	15	29,5	1,9	7,3	42,0

Table 6 Statistics of the steel peening shots speed measured at 50 and 100 mm in front of the gun barrel.

7.2 Plots

In the following figures the results presented in the Tables 3 – 5 are plotted. In the figures a. the mean (blue dots), b. the standard deviation (light blue area) and c. the minimum and maximum (red dots) are plotted versus the different pressure levels. Additionally a linear fit of the mean speed of the shots is included. The results of the linear fit are presented in the Table 7.

Type	Size [mm]	Distance [mm]	Run [-]	Slope [ms^{-1}/PSI]	Offset [ms^{-1}]	Figure [#]
Ceramic	0.063 – 0.125	51	1	0.55	18.2	13
	0.063 – 0.125	51	2	0.50	21.1	13
	0.063 – 0.125	100	1	0.60	15.7	14
	0.063 – 0.125	100	2	0.62	14.7	14
	0.063 – 0.125	150	1	0.64	11.6	15
	0.063 – 0.125	150	2	0.55	13.3	15
	0.150 – 0.210	50	1	0.23	20.56	16
	0.150 – 0.210	50	2	0.22	21.08	16
	0.300 – 0.425	50	1	0.23	23.42	17
	0.300 – 0.425	50	2	0.22	23.68	17
	0.600 – 0.850	58	1	0.47	11.6	18
	0.600 – 0.850	109	1	0.45	12.1	19
	0.600 – 0.850	160	1	0.51	9.7	20
Steel	0.6	50	1	0.24	9,79	21
	0.6	50	2	0.23	10.91	21
	0.6	100	1	0.27	6.40	22
	0.6	100	2	0.27	6.66	22
	1.0	50	1	0.27	8,64	23
	1.0	50	2	0.27	8.62	23

Table 7 Slope and offset results of a linear interpolation of the velocity versus pressure values for different shots.

In the figures it can be observed that the mean velocity is increasing along with the increase of the pressure. The variation of the speed, as expressed by the standard deviation values, appears to be uncorrelated with the pressure, but rather with the size of the shots.

7.2.1 Ceramic 0.063~0.125 mm

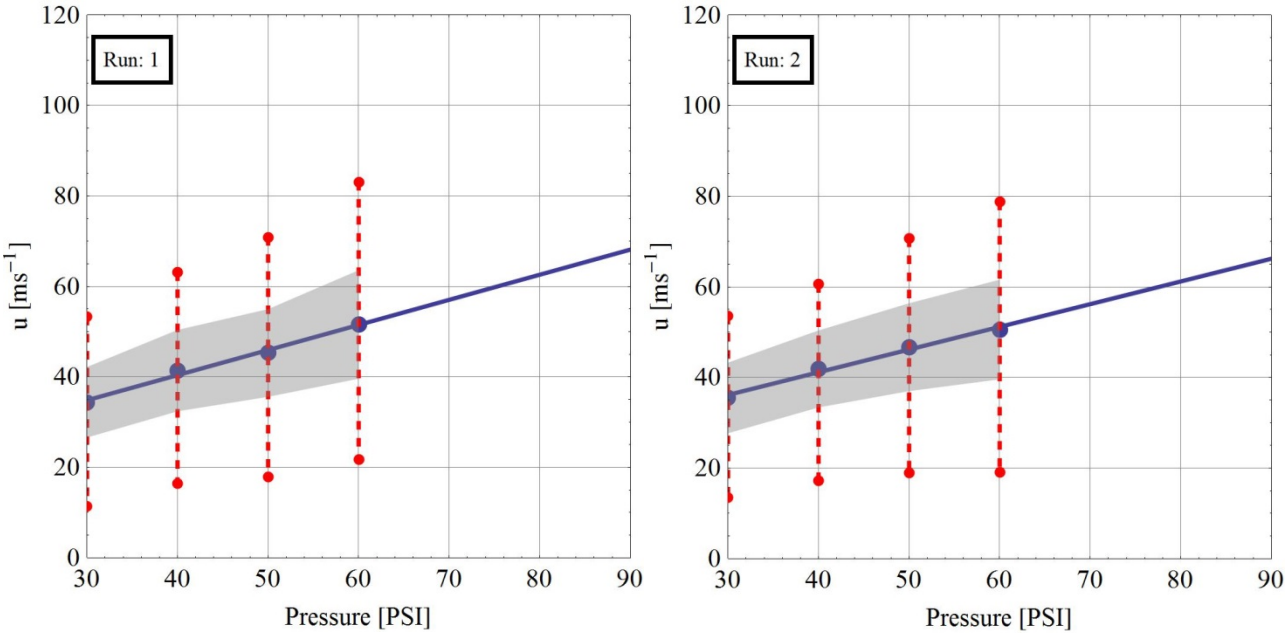

Figure 13 Results of the ceramic 0.063~0.125 mm peen shots speed at 51 mm for two different runs.

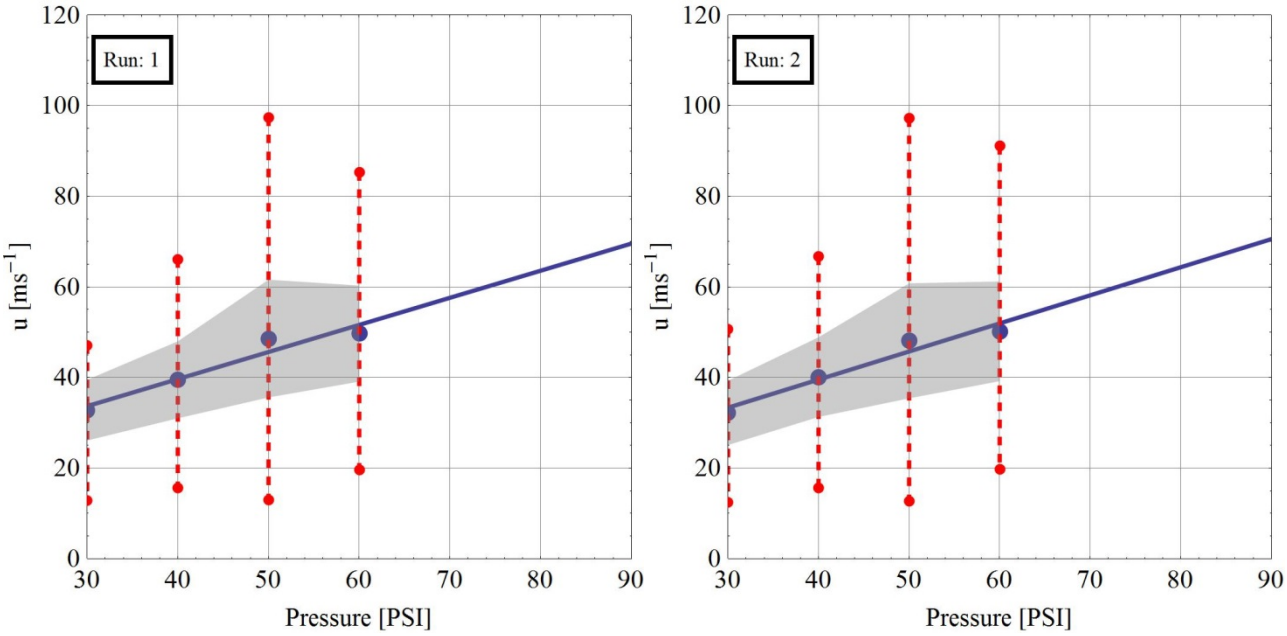

Figure 14 Results of the ceramic 0.063~0.125 mm peen shots speed at 100 mm for two different runs.

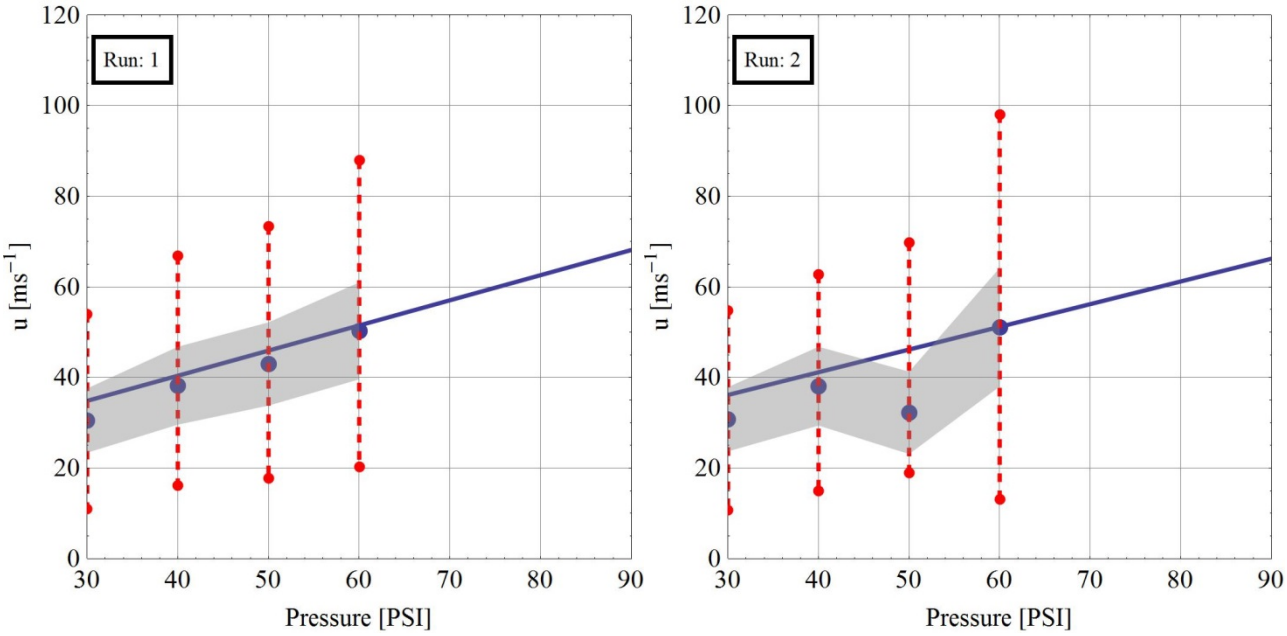

Figure 15 Results of the ceramic 0.063~0.125 mm peen shots speed at 151 mm for two different runs.

7.2.2 Ceramic 0.150~0.210 mm

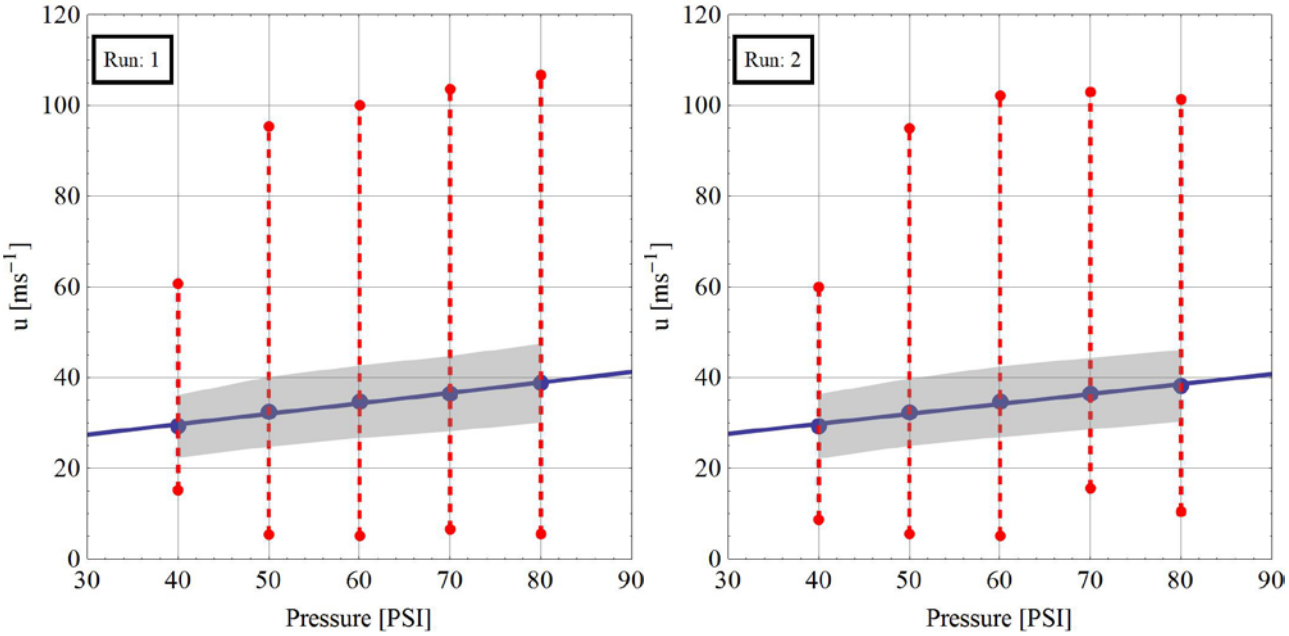

Figure 16 Results of the ceramic 0.150~0.210 mm peen shots speed at 50 mm for two different runs.

7.2.3 Ceramic 0.300~0.425 mm

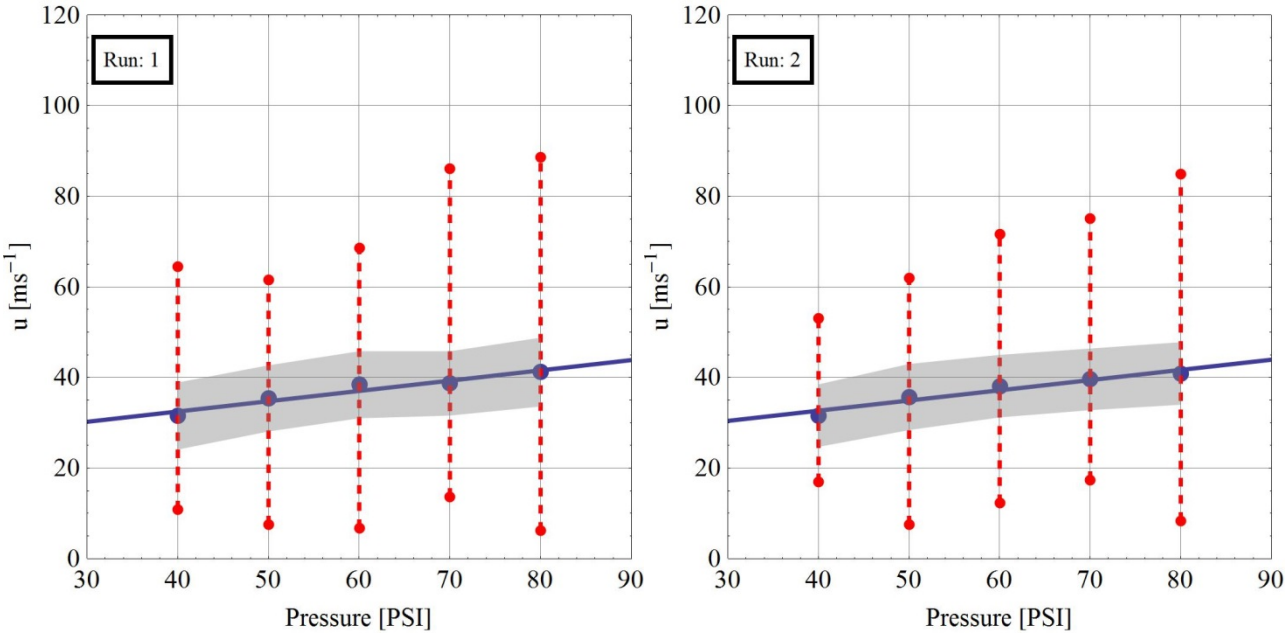

Figure 17 Results of the ceramic 0.300~0.425 mm peen shots speed at 50 mm for two different runs.

7.2.4 Ceramic 0.600~0.850 mm

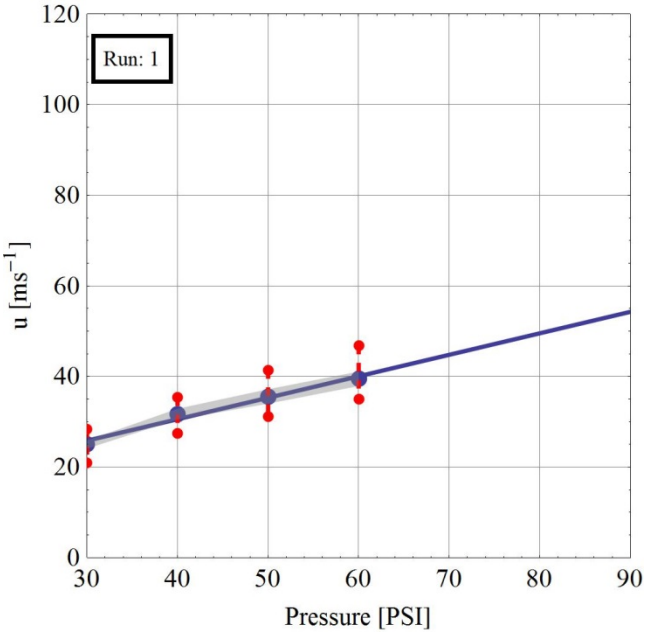

Figure 18 Results of the ceramic 0.600~0.850 mm peen shots speed at 58 mm.

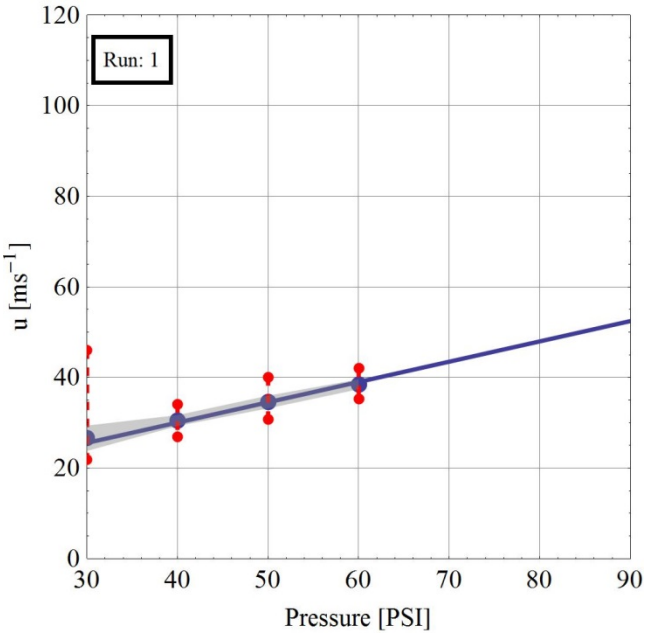

Figure 19 Results of the ceramic 0.600~0.850 mm peen shots speed at 109 mm.

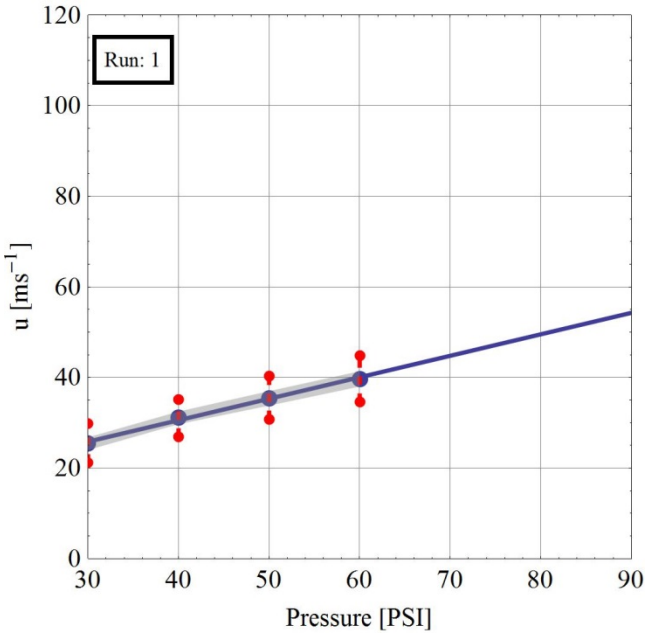

Figure 20 Results of the ceramic 0.600~0.850 mm peen shots speed at 160 mm.

7.2.5 Steel 0.6 mm

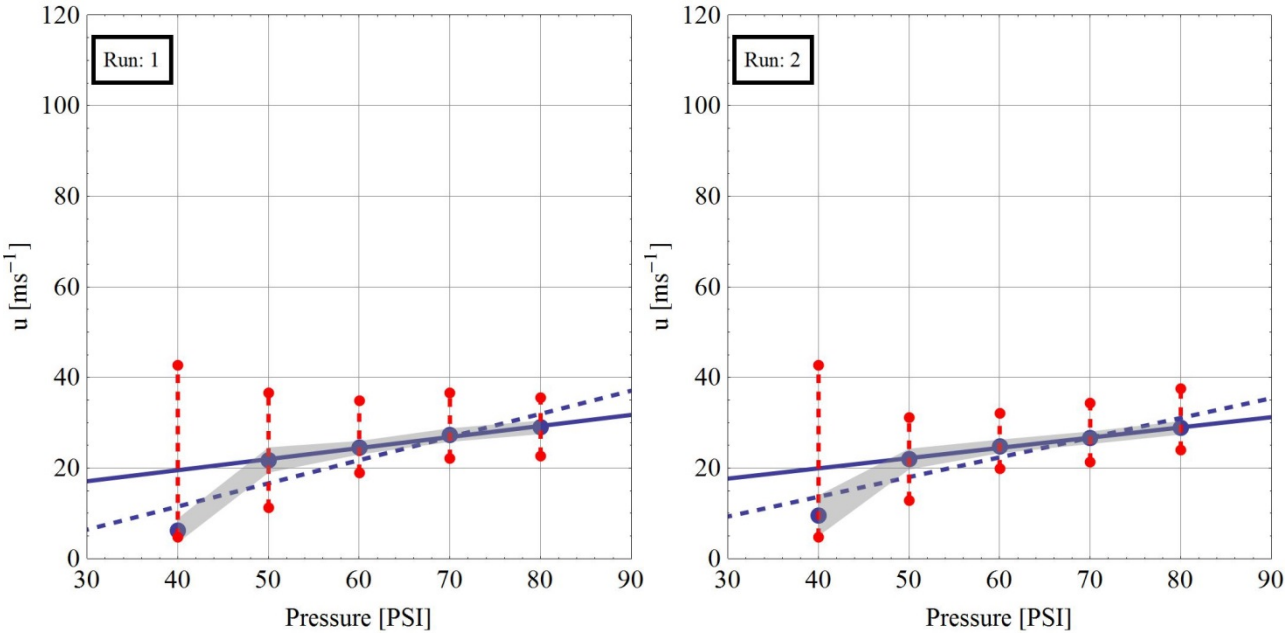

Figure 21 Results of the steel 0.6 mm peen shots for two different runs at 50 mm. The dashed blue line represents the linear fit when all the points are taken into account and the solid blue line when the speed at 40 PSI is treated as an outlier and it is excluded from the linear regression.

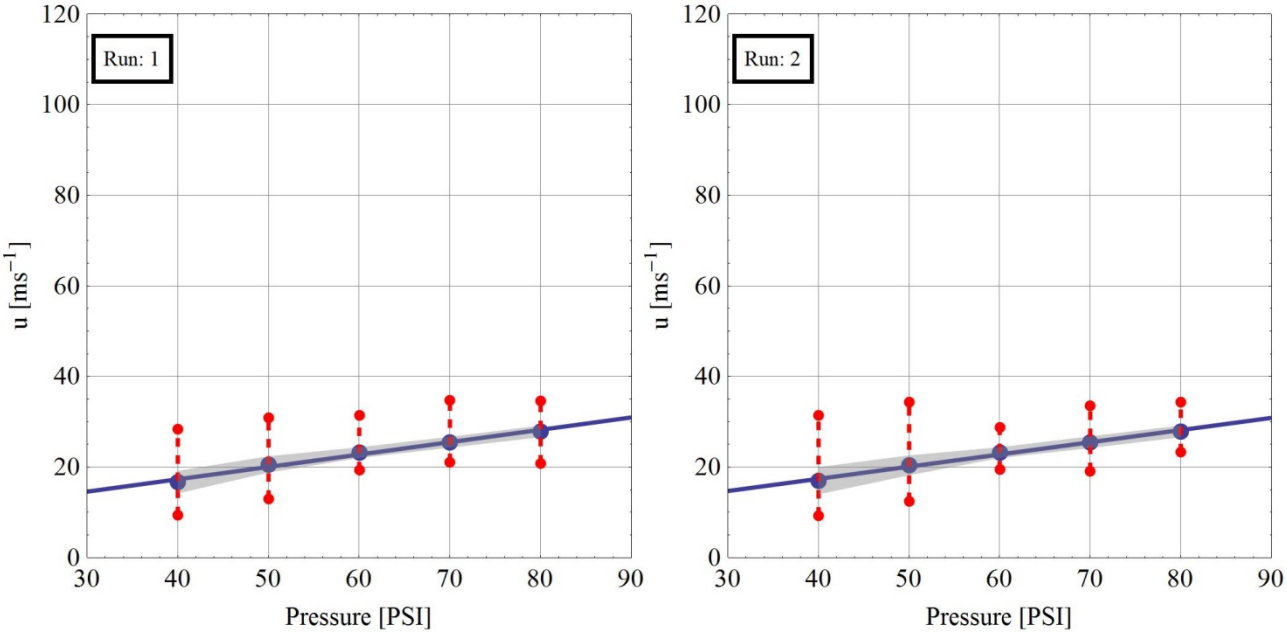

Figure 22 Results of the steel 0.6 mm peen shots for two different runs at 100 mm.

7.2.6 Steel 0.8 mm

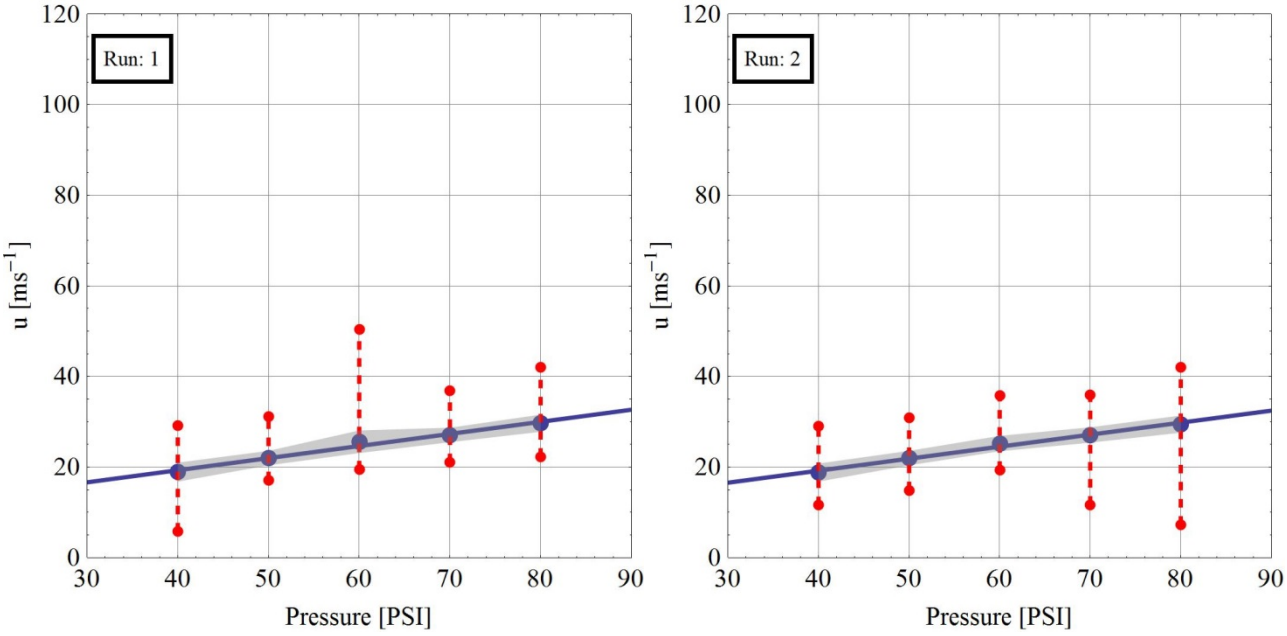

Figure 23 Results of the steel 1.0 mm peen shots for two different runs at 50 mm.

In the case of the 0.6 mm steel shots measurements were acquired in two different distances, the results are presented in Figure 24.

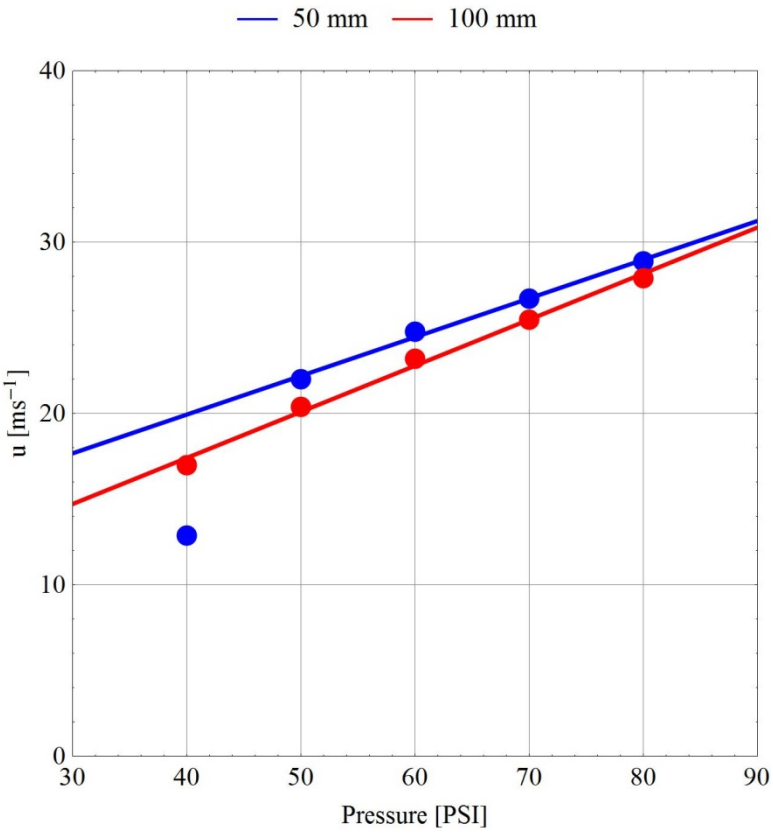

Figure 24 Mean velocities of 0.6 steel shots for different pressure levels in two different distances equal to 50 and 100 mm, respectively.

Summary

In the framework of the internal DTU cross-sectional project *Gear*, it was attempted the use of lidar remote sensing technology to evaluate the performance of a shot peening machine. Lidars are widely used in atmospheric studies and in specific in the DTU Wind Energy department for the probing of the atmospheric wind conditions.

In this study a lidar is used for the first time to monitor the speed of the emitted shots from a peening machine. The motivation behind this experiment was that the shot peening technique is applied for the surface modification of metallic components in the Wind Energy sector and a crucial parameter for its operation is the kinetic energy of the emitted shots.

Overall, the experiment can be described as a successful proof-of-concept where the advantages of laser based remote sensing have been used to provide feedback on the operation of a shot peening machine.

During the measurement campaigns acquisition of good quality data was achieved, through which it was possible to get an insight on how different pressure levels, used to emit the peening shots, are affecting the speed of peening shots of different size and chemical composition.

In the report are included the results of linear regression that can be used to predict the speed of particles in different distances away from the peening machine at different pressures. Moreover, a catalogue of plots for all the measured runs is included in the Appendix.

References

[1] Mikkelsen, T., Siggaard Knudsen, S., Sjöholm, M., Angelou, N., & Pedersen, A. T. (2012). WindScanner.eu - a new Remote Sensing Research Infrastructure for On- and Offshore Wind Energy. In Proceedings of the International Conference on Wind Energy: Materials, Engineering, and Policies (WEMEP-2012).

[2] Abari CF, Pedersen AT, Mann J. 2014. An all-fiber image-reject homodyne coherent Doppler wind lidar. Optics Express. 22(21):25880-25894.

[3] Pedersen AT, Sjöholm M, Angelou N, Mikkelsen T, Montes BF, Engholm Pedersen J, Slinger C, Harris M. 2013. Full-Scale Field Test of a Blade-Integrated Dual-Telescope Wind Lidar. Poster session presented at European Wind Energy Conference & Exhibition 2013, Vienna, Austria.

[4] Abari CF, Pedersen AT, Dellwik E, Mann J. 2015. Performance evaluation of an all-fiber image-reject homodyne coherent Doppler wind lidar. Atmospheric Measurement Techniques. 8(10):4145-4153

[5] Pedersen AT, Montes BF, Pedersen JE, Harris M, Mikkelsen T. 2012. Demonstration of short-range wind lidar in a high-performance wind tunnel. In Proceedings of EWEA 2012. European Wind Energy Association (EWEA).

Appendix – First Experiment

Ceramic bolts 0.063~0.125 mm

50 mm: 30 PSI

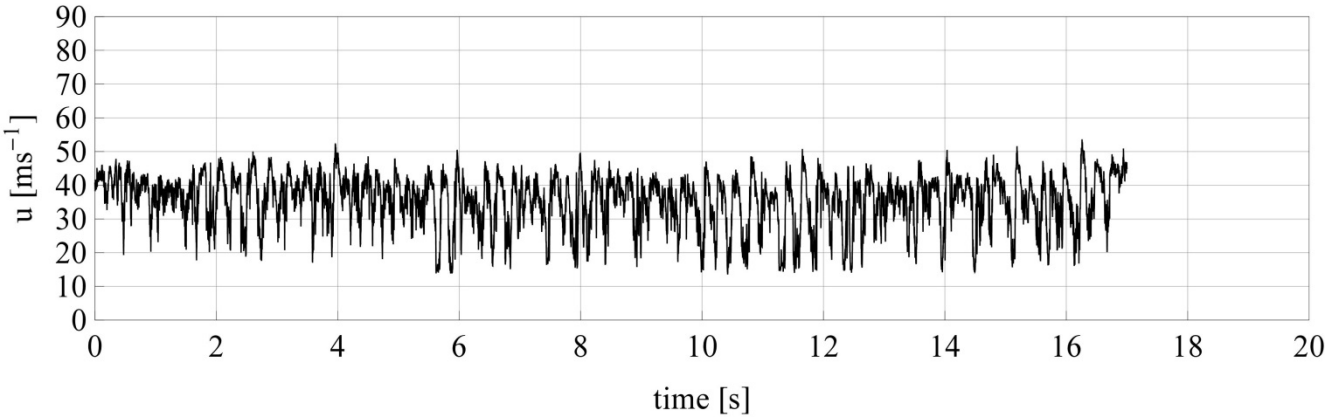

Figure 25 Time series of the speed of the peening shots (run 1).

50 mm: 40 PSI

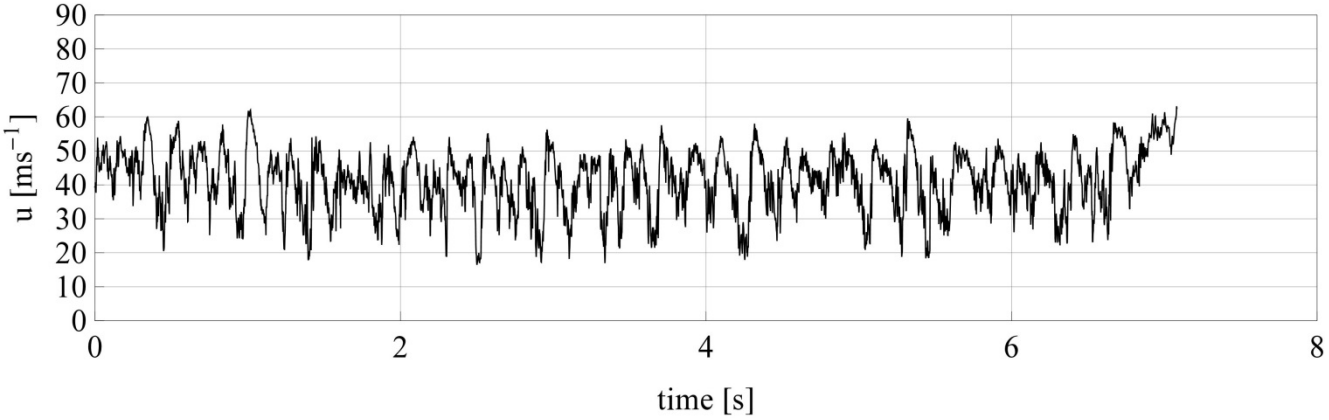

Figure 26 Time series of the speed of the peening shots (run 1).

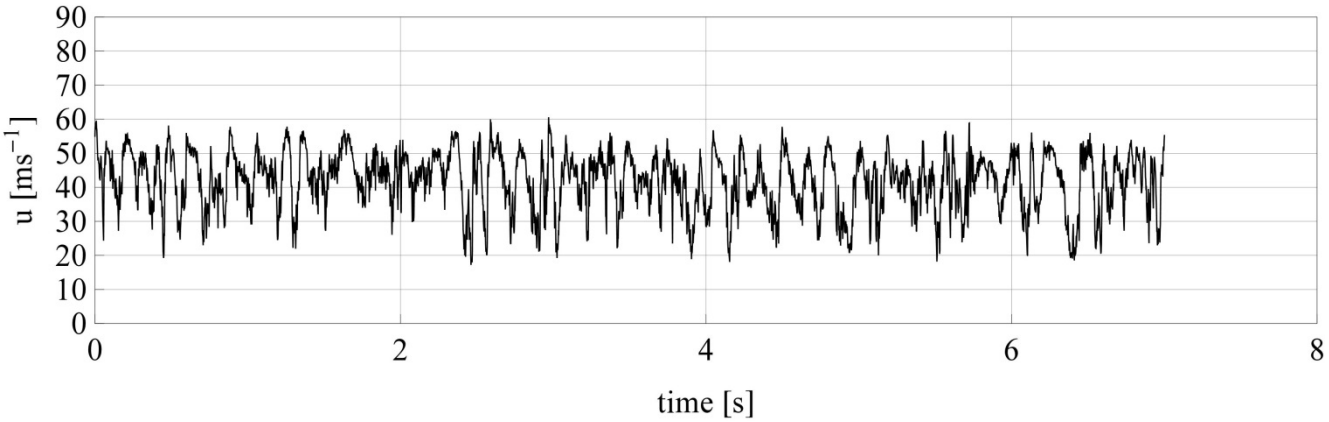

Figure 27 Time series of the speed of the peening shots (run 2).

50 mm: 50 PSI

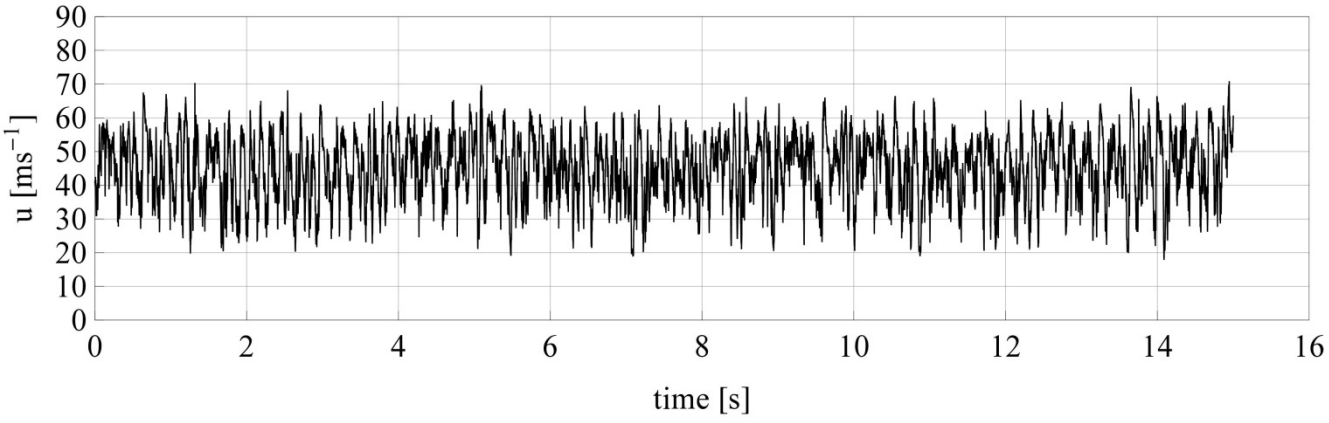

Figure 28 Time series of the speed of the peening shots (run 1).

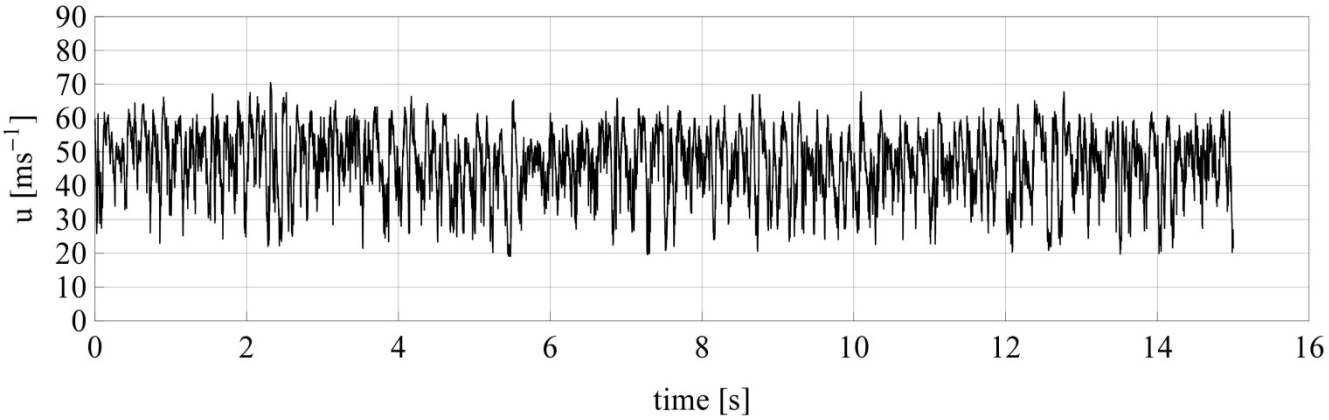

Figure 29 Time series of the speed of the peening shots (run 2).

50 mm: 60 PSI

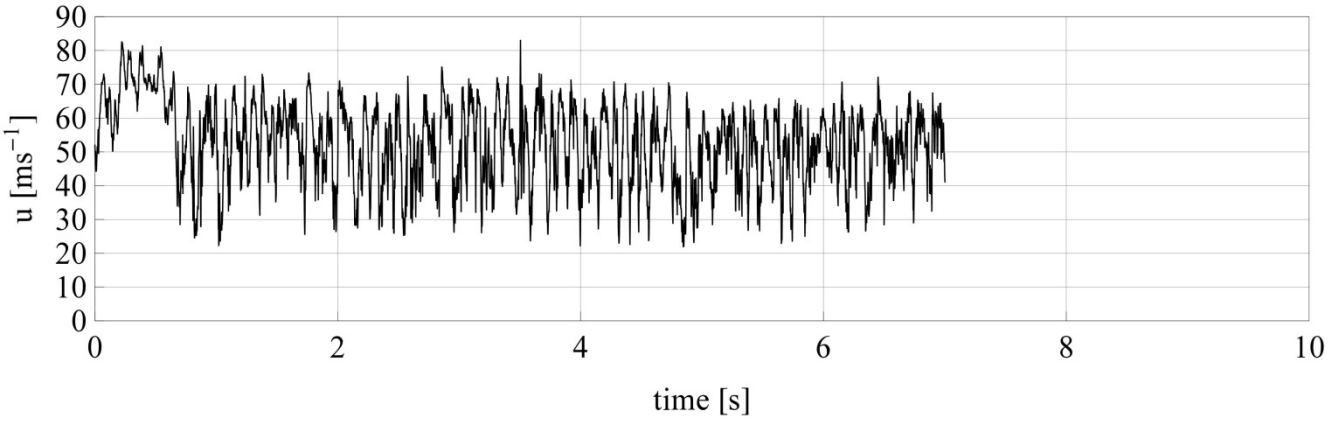

Figure 30 Time series of the speed of the peening shots (run 1).

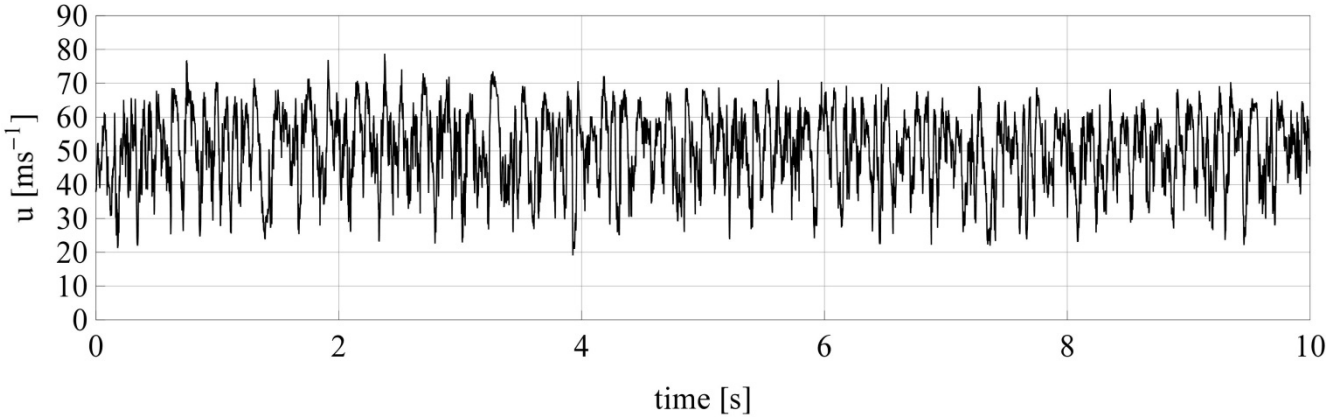

Figure 31 Time series of the speed of the peening shots (run 2).

100 mm: 30 PSI

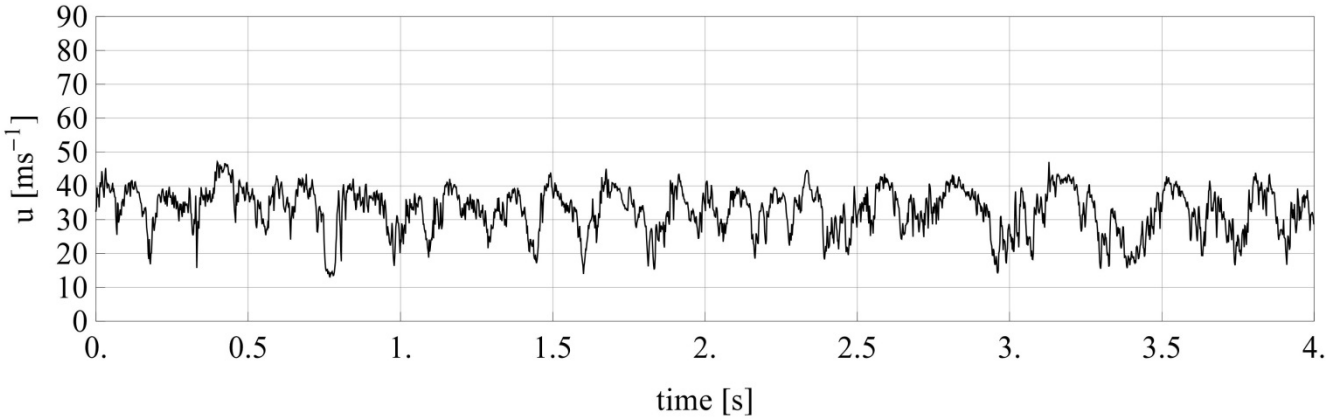

Figure 32 Time series of the speed of the peening shots (run 1).

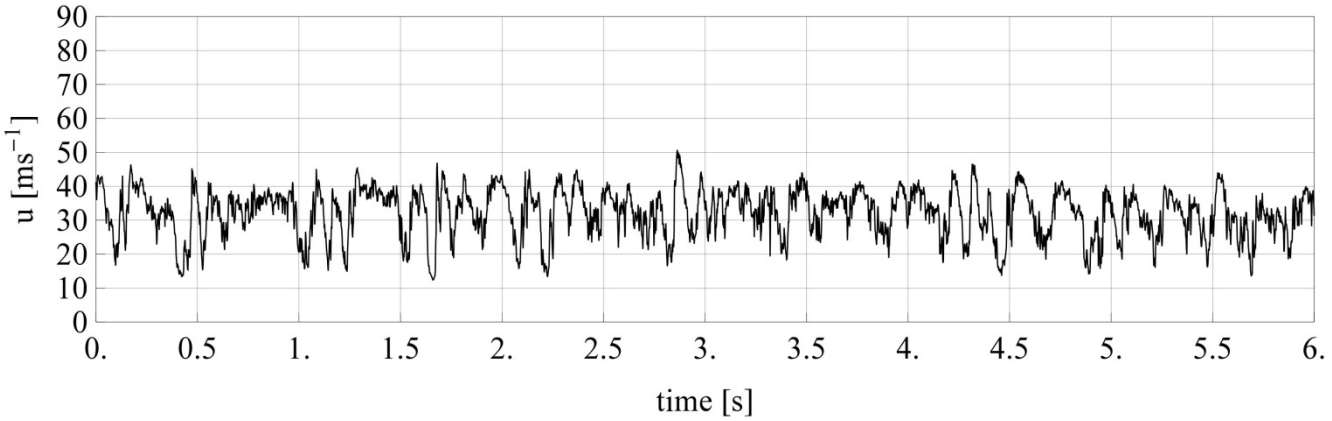

Figure 33 Time series of the speed of the peening shots (run 2).

100 mm: 40 PSI

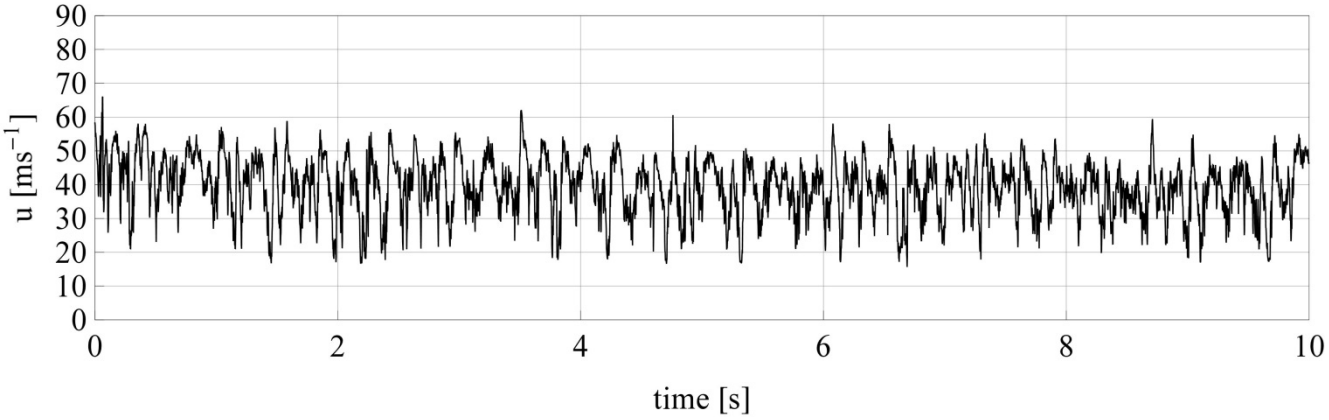

Figure 34 Time series of the speed of the peening shots (run 1).

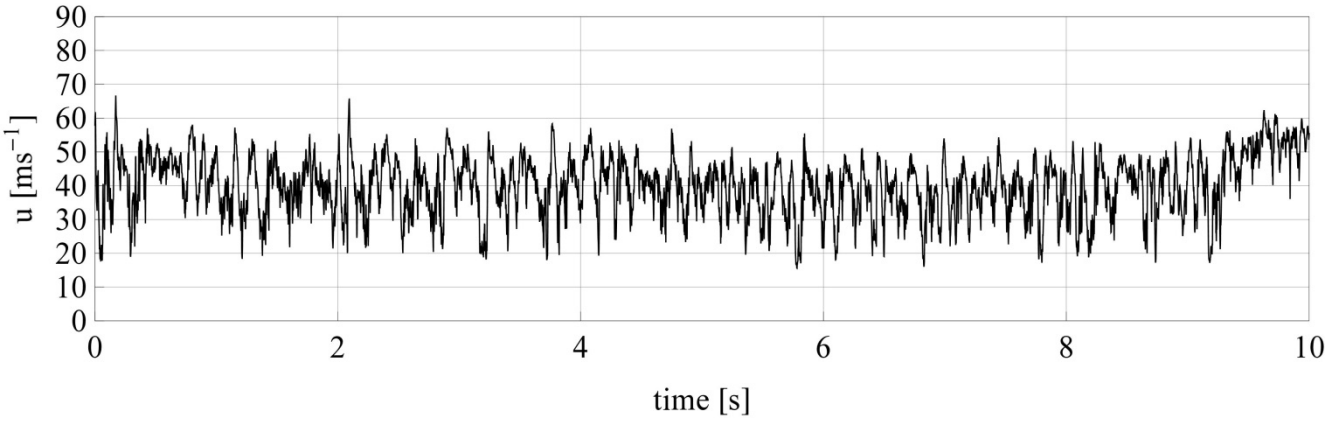

Figure 35 Time series of the speed of the peening shots (run 2).

100 mm: 50 PSI

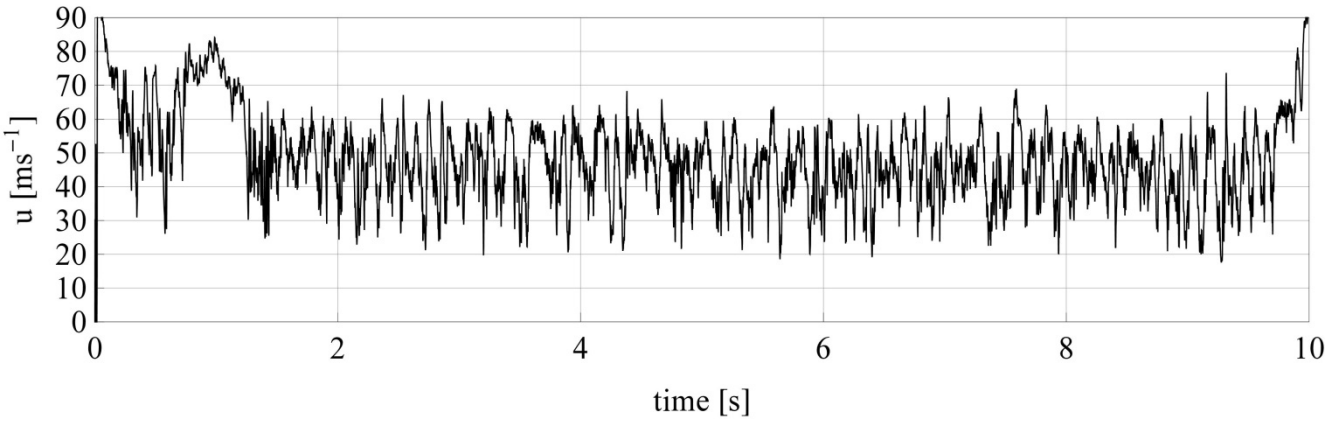

Figure 36 Time series of the speed of the peening shots (run 1).

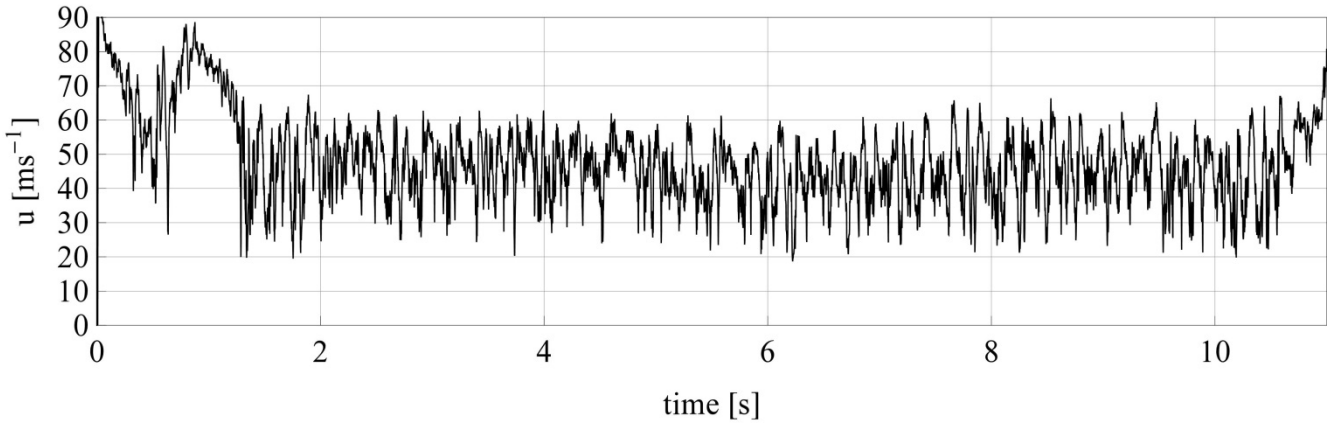

Figure 37 Time series of the speed of the peening shots (run 2).

100 mm: 60 PSI

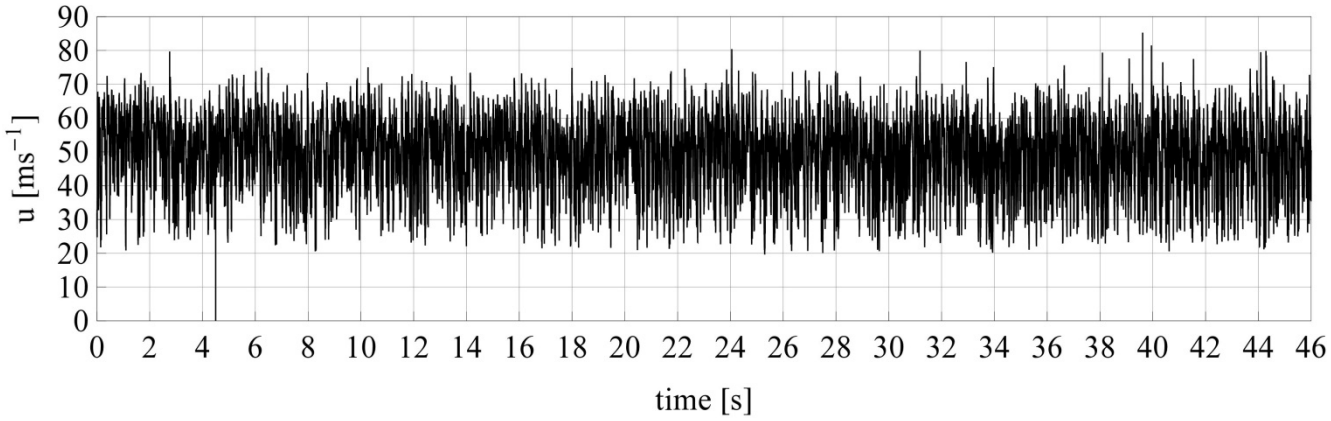

Figure 38 Time series of the speed of the peening shots (run 1).

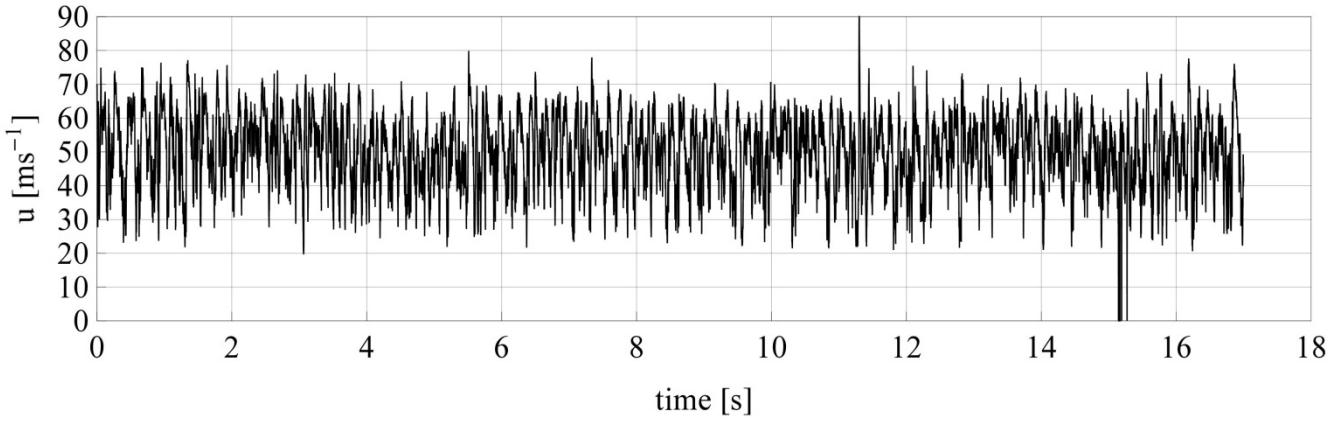

Figure 39 Time series of the speed of the peening shots (run 2).

150 mm: 30 PSI

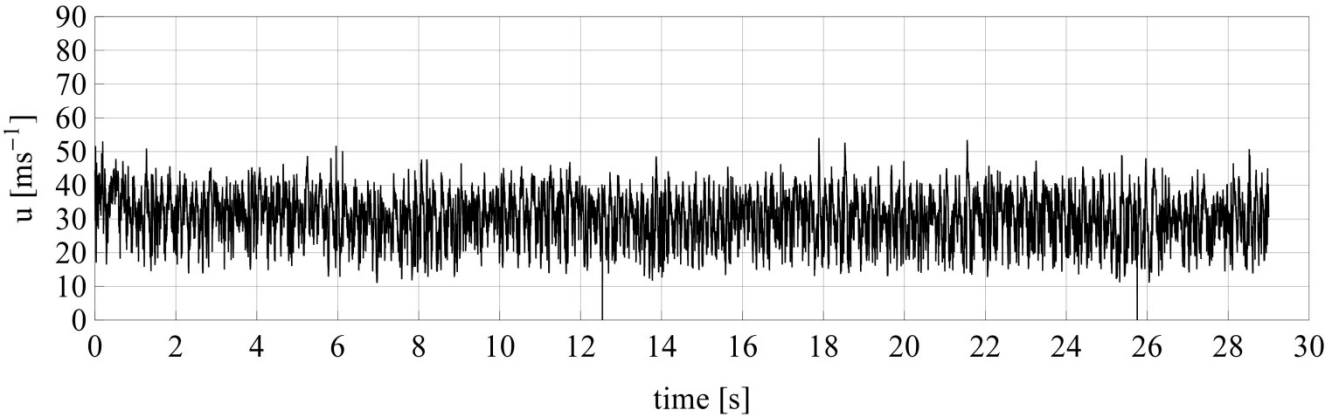

Figure 40 Time series of the speed of the peening shots (run 1).

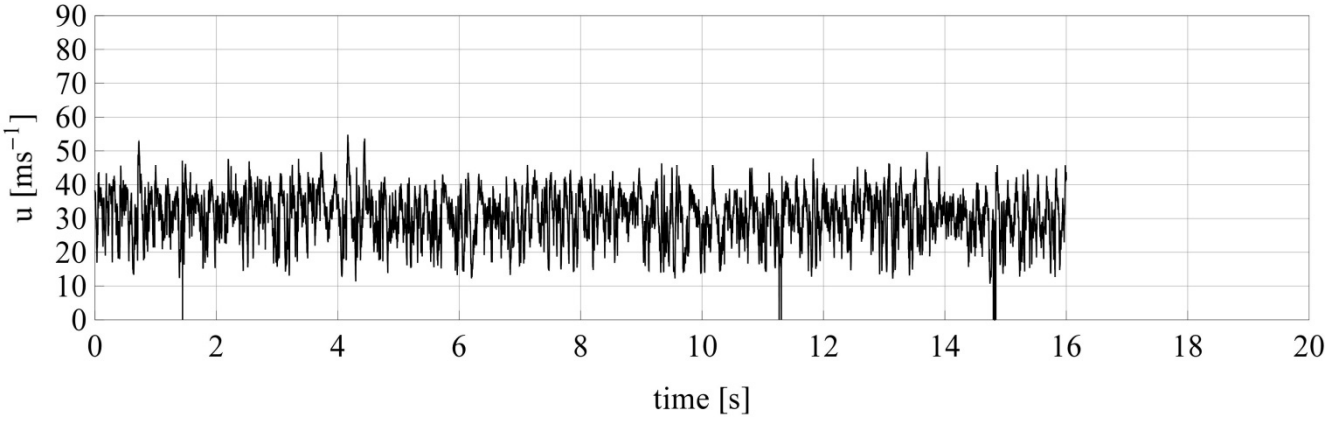

Figure 41 Time series of the speed of the peening shots (run 2).

150 mm: 40 PSI

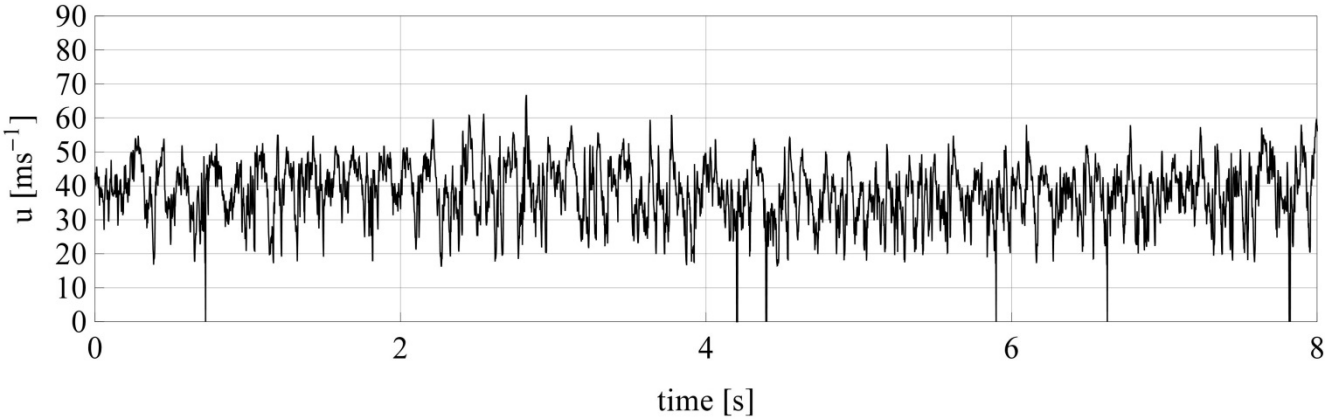

Figure 42 Time series of the speed of the peening shots (run 1).

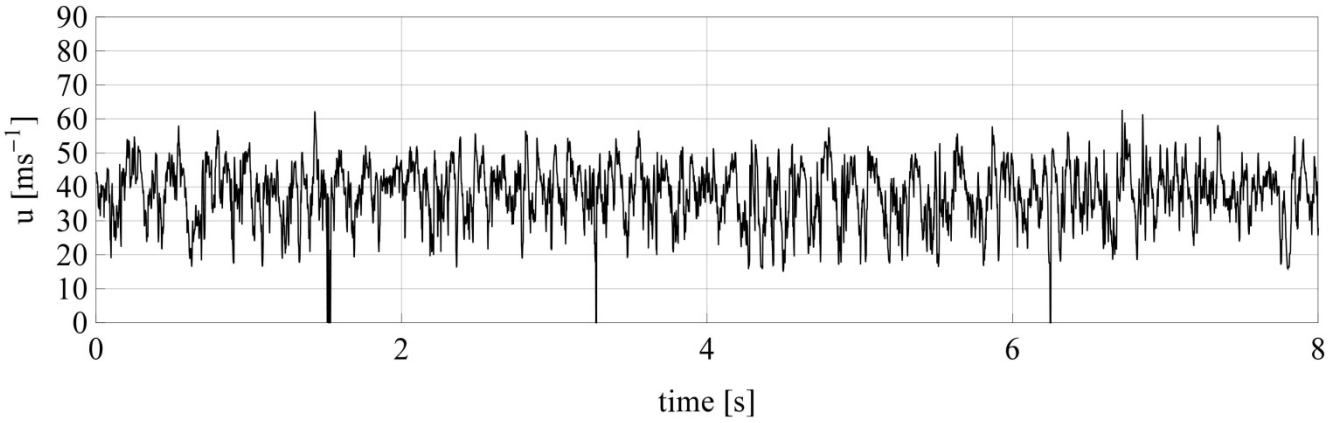

Figure 43 Time series of the speed of the peening shots (run 2).

150 mm: 50 PSI

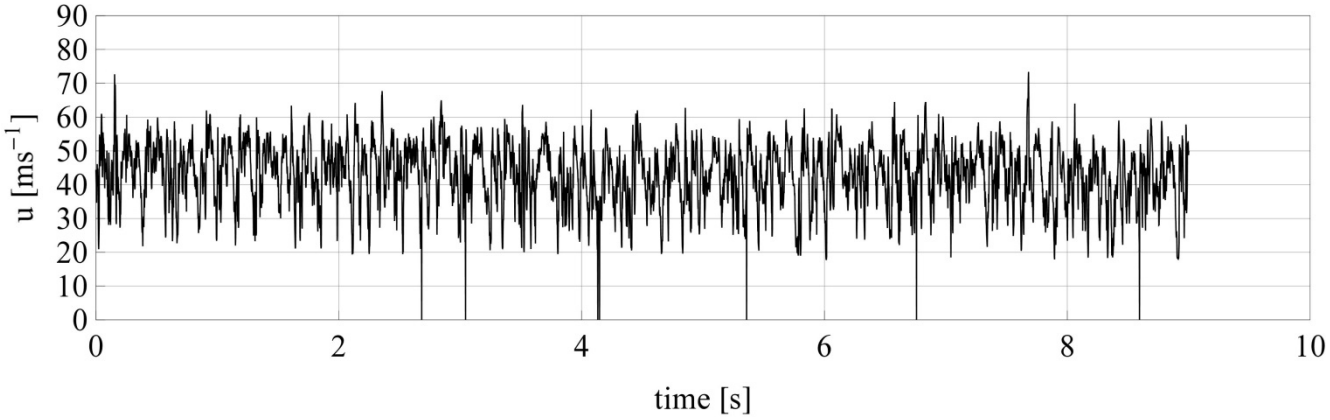

Figure 44 Time series of the speed of the peening shots (run 1).

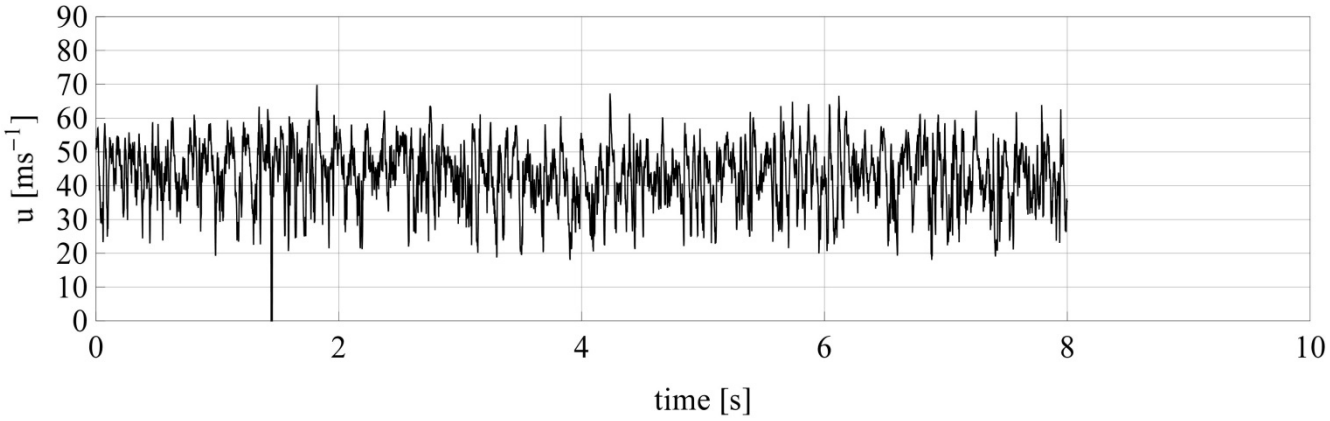

Figure 45 Time series of the speed of the peening shots (run 2).

150 mm: 60 PSI

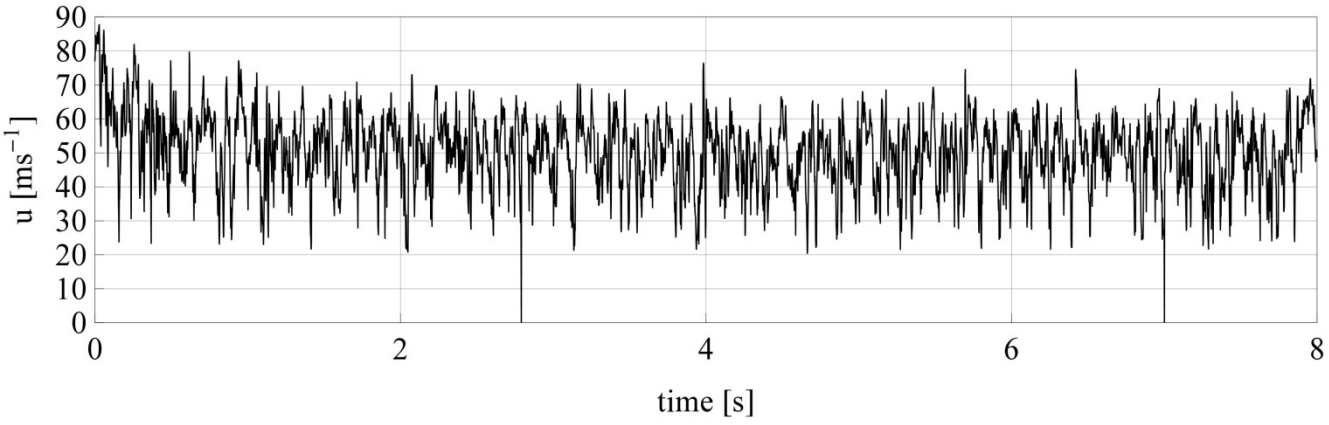

Figure 46 Time series of the speed of the peening shots (run 1).

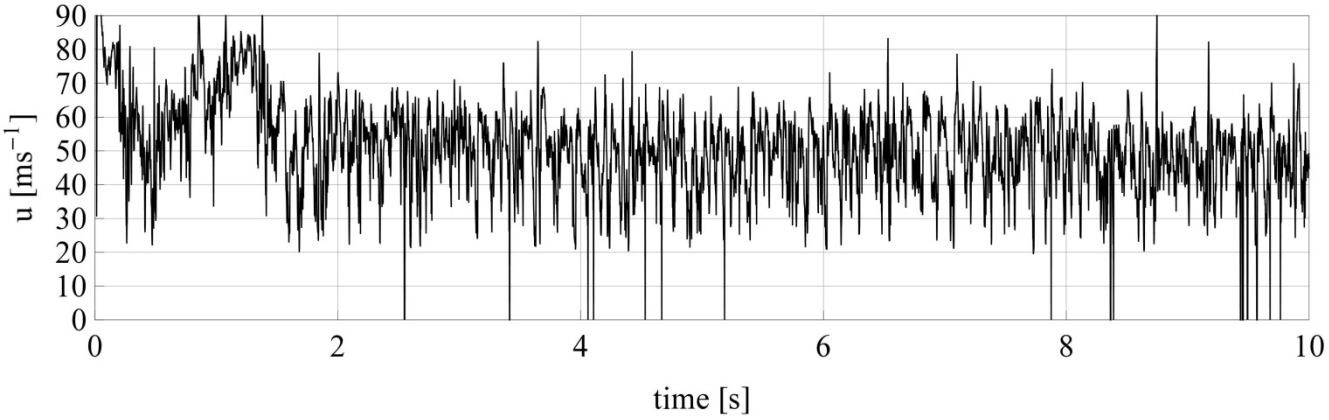

Figure 47 Time series of the speed of the peening shots (run 2).

Ceramic bolts 0.600~0.850 mm

50 mm: 30 PSI

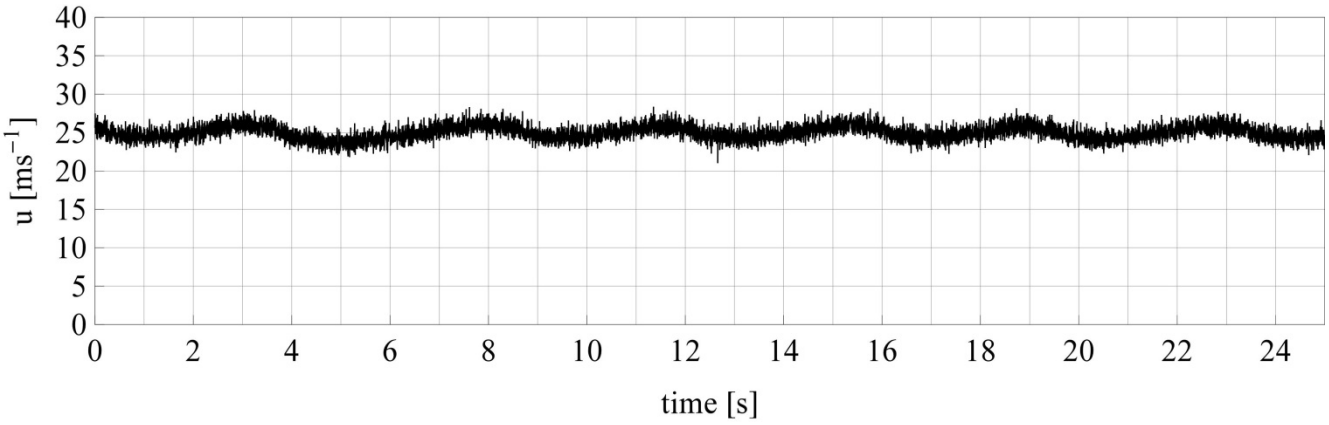

Figure 48 Time series of the speed of the peening shots (run 1).

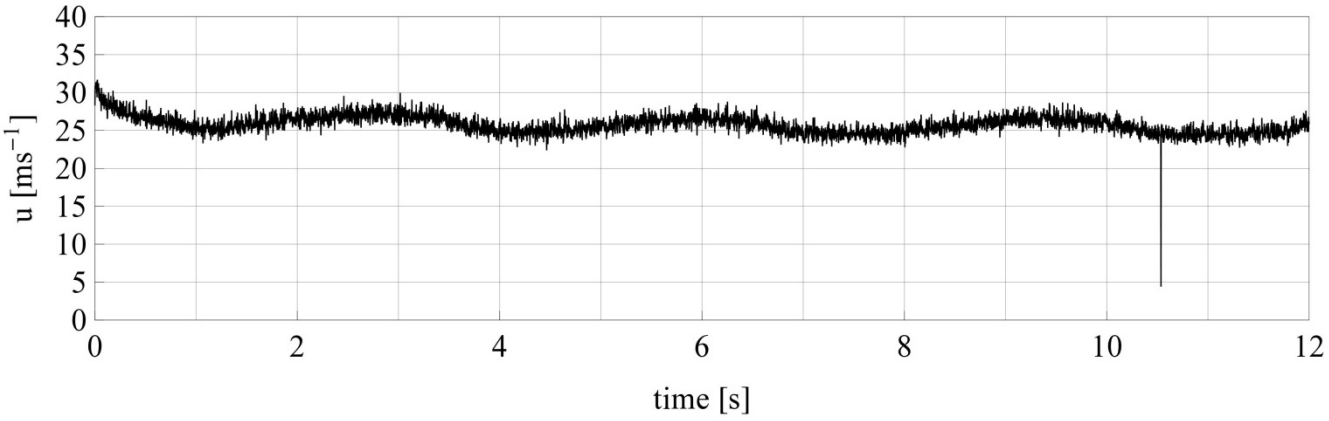

Figure 49 Time series of the speed of the peening shots (run 2).

100 mm: 30 PSI

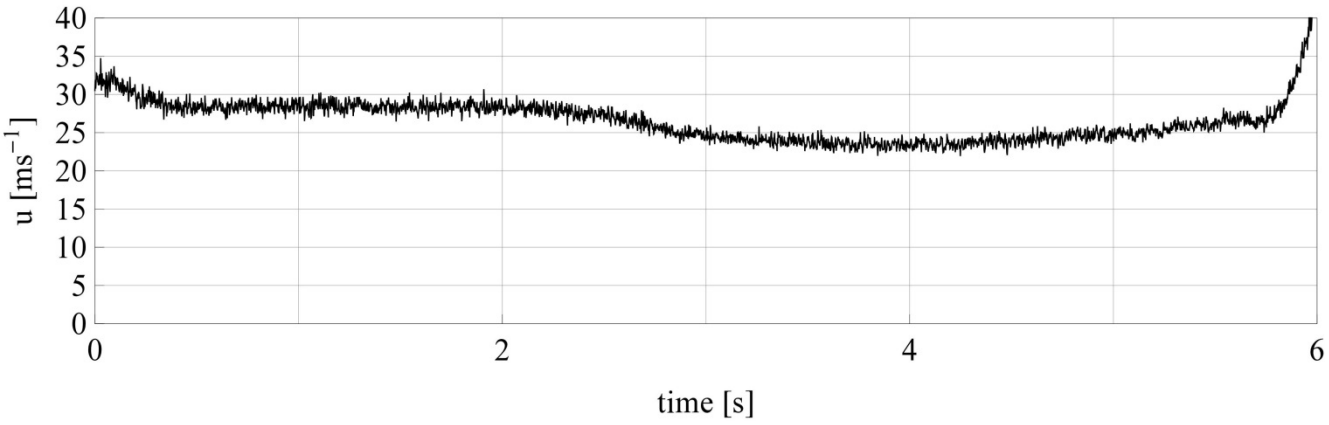

Figure 50 Time series of the speed of the peening shots (run 1).

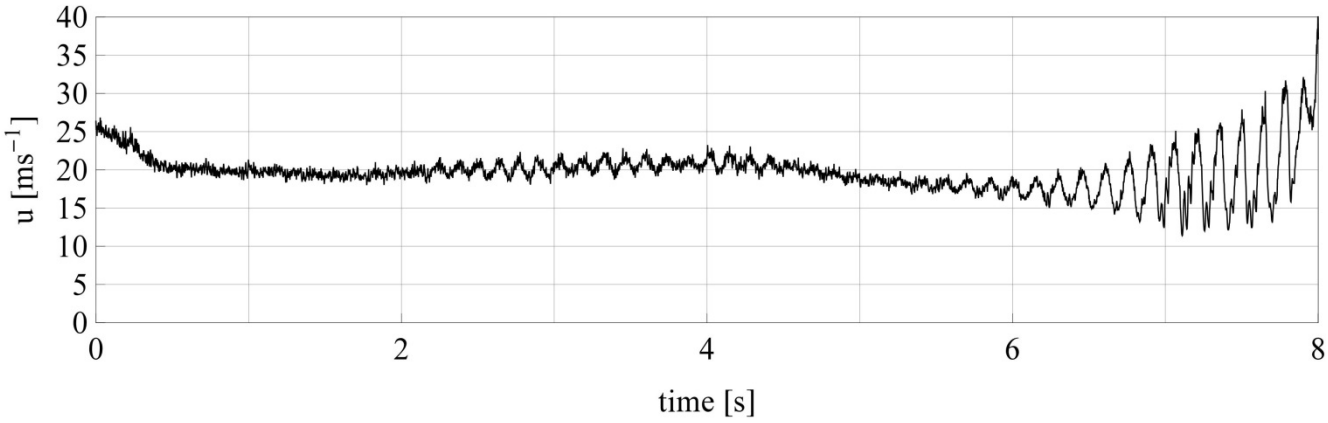

Figure 51 Time series of the speed of the peening shots (run 2).

150 mm: 30 PSI

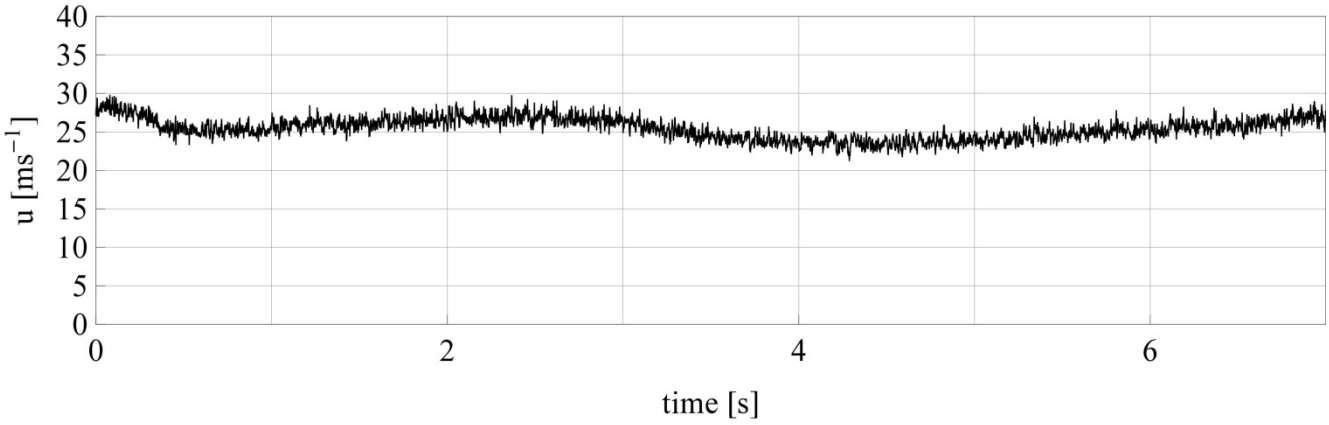

Figure 52 Time series of the speed of the peening shots (run 1).

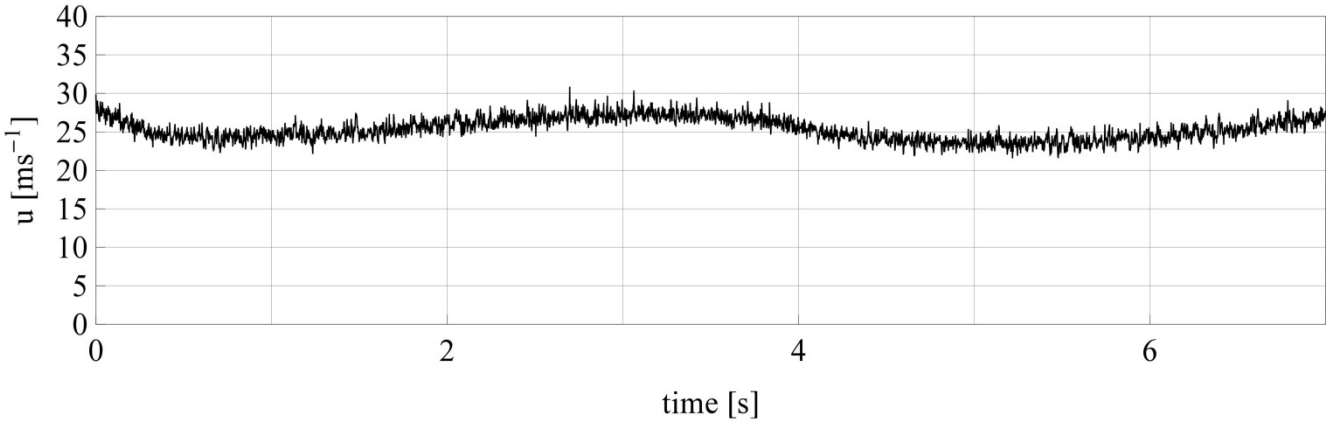

Figure 53 Time series of the speed of the peening shots (run 2).

Appendix – Second Experiment

Ceramic bolts 0.2 mm @ 50 mm: 40 PSI

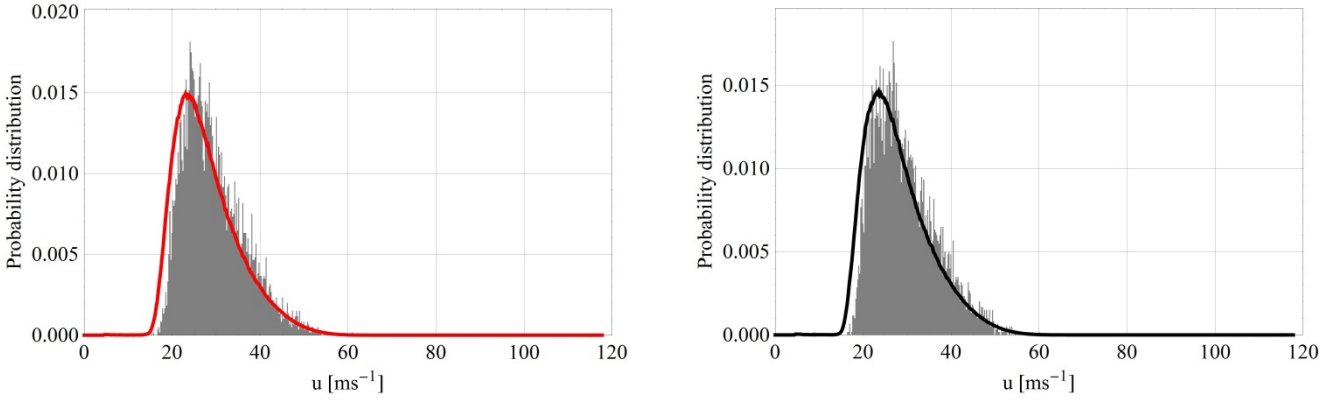

Figure 54 Probability density function and histogram of the measured speeds for two runs.

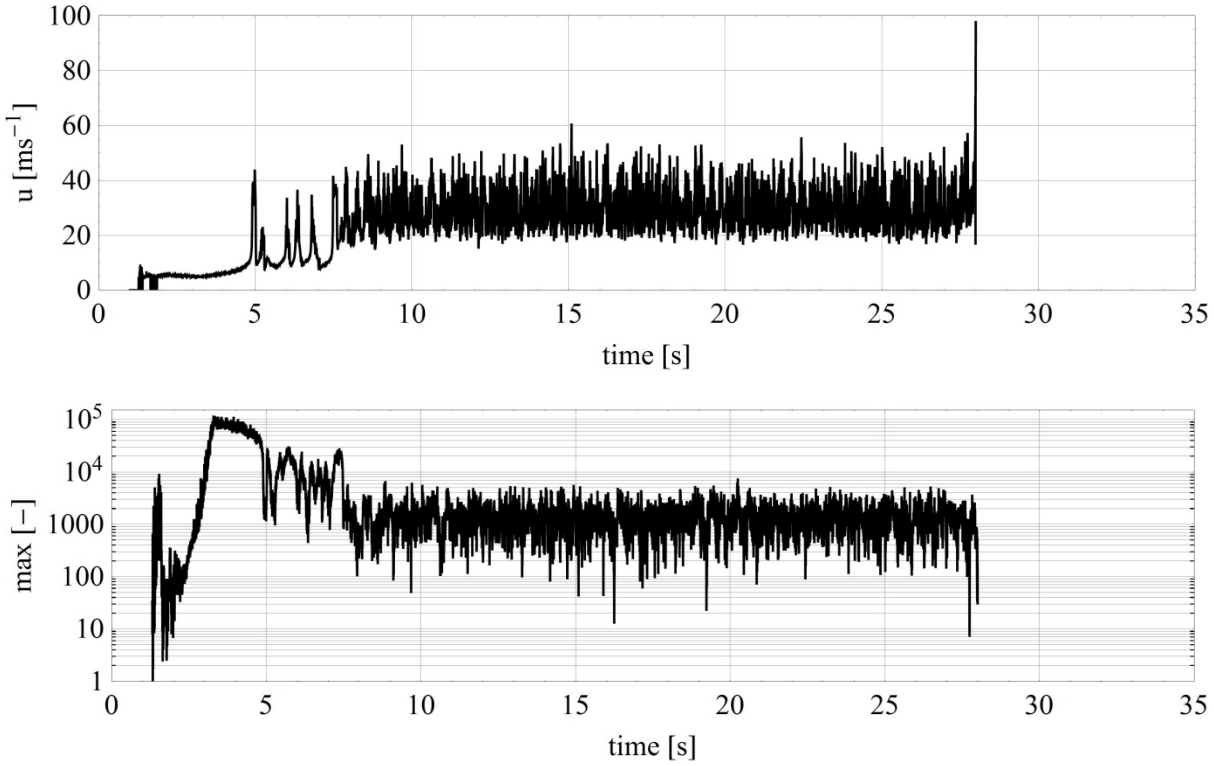

Figure 55 Time series of the velocity and the corresponding maximum value of the laser Doppler spectra of the first run.

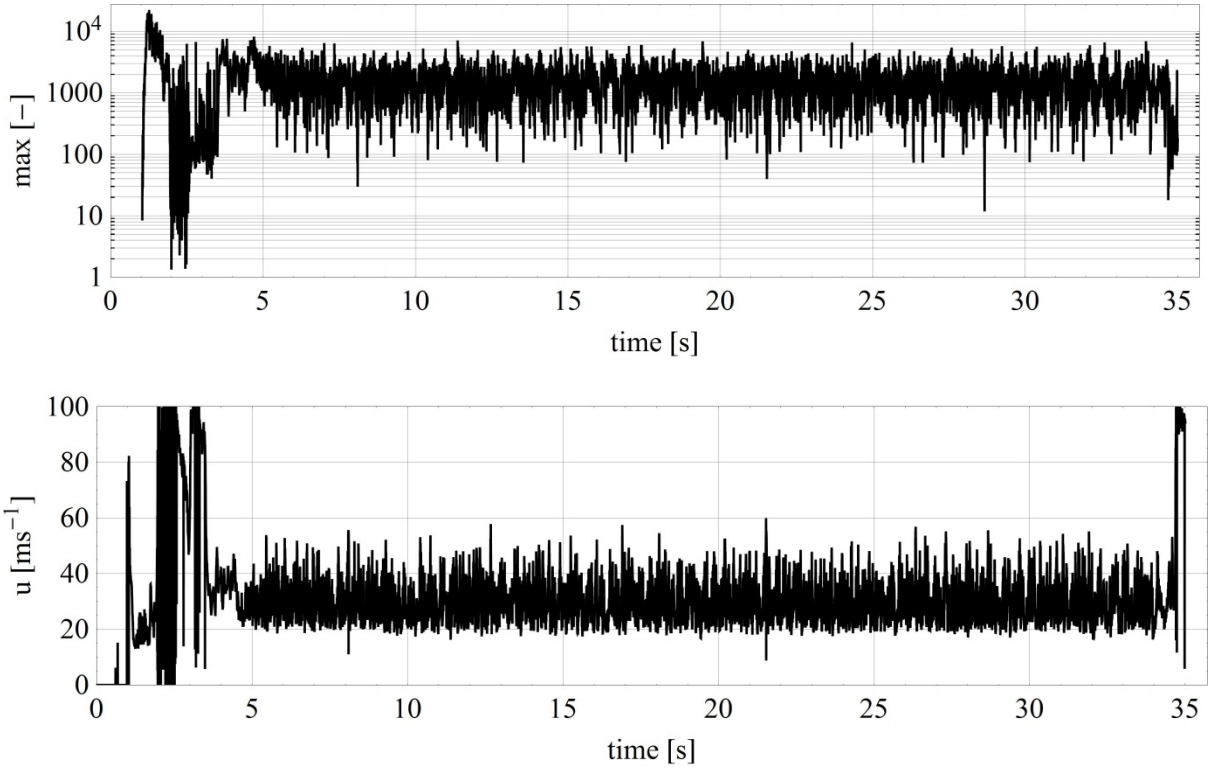

Figure 56 Time series of the velocity and the corresponding maximum value of the laser Doppler spectra of the second run.

Ceramic bolts 0.2 mm @ 50 mm: 50 PSI

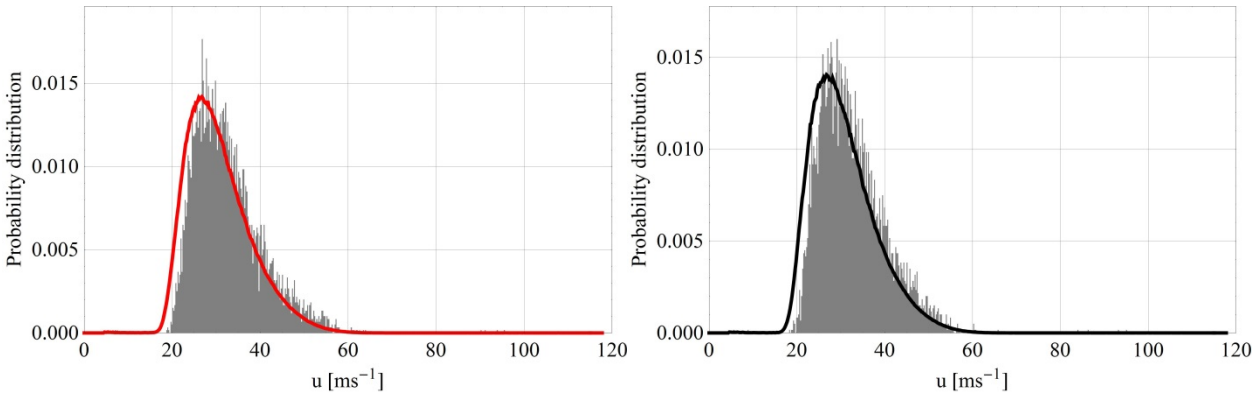

Figure 57 Probability density function and histogram of the measured speeds for two runs.

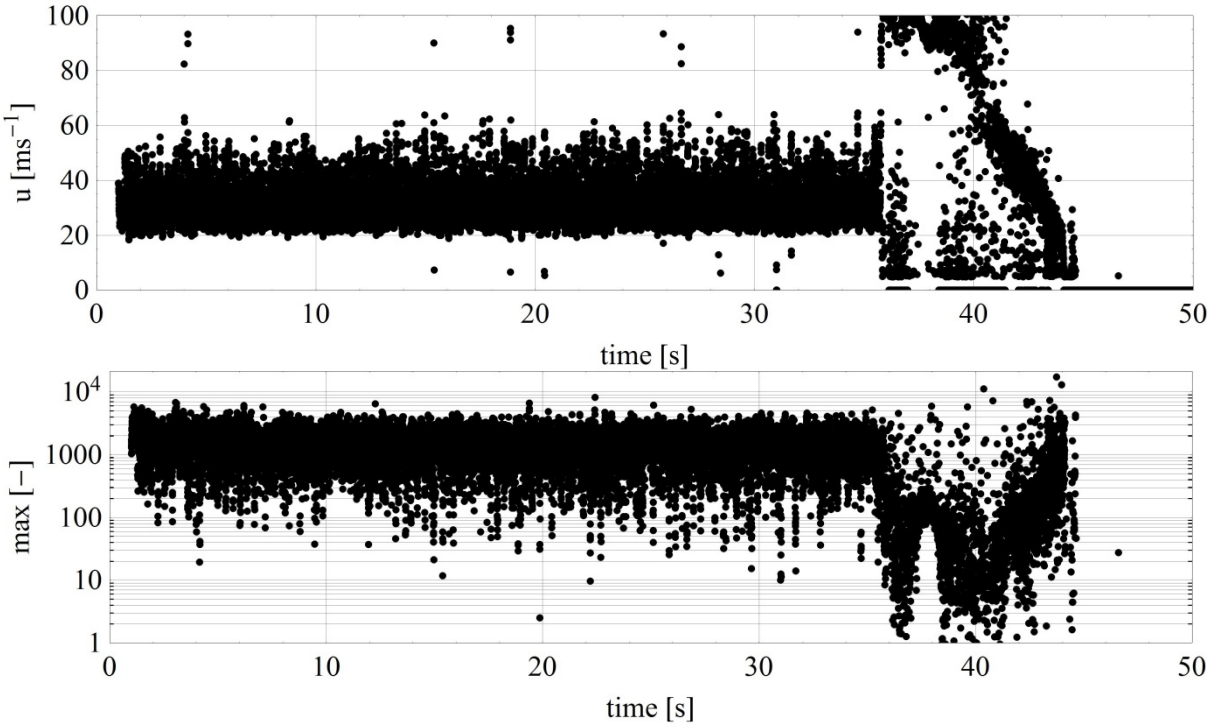

Figure 58 Time series of the velocity and the corresponding maximum value of the laser Doppler spectra of the first run.

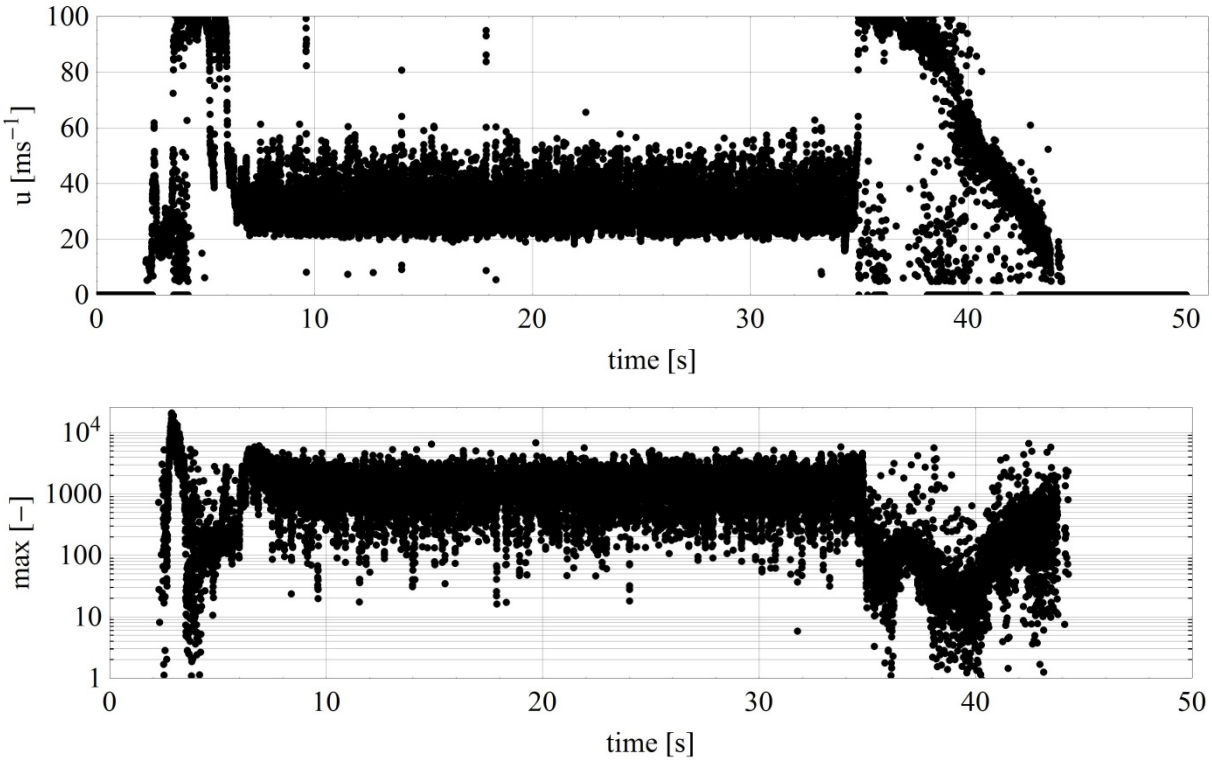

Figure 59 Time series of the velocity and the corresponding maximum value of the laser Doppler spectra of the second run.

Ceramic bolts 0.2 mm @ 50 mm: 60 PSI

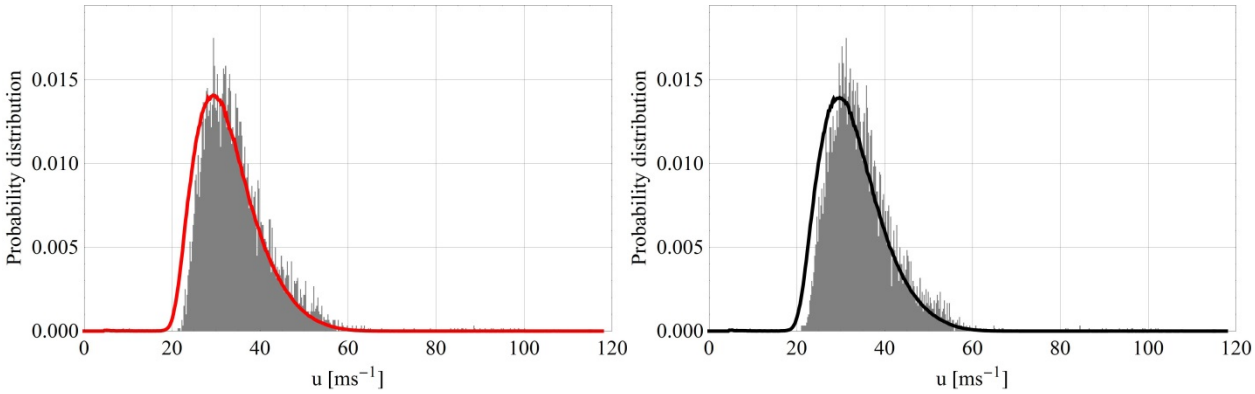

Figure 60 Probability density function and histogram of the measured speeds for two runs.

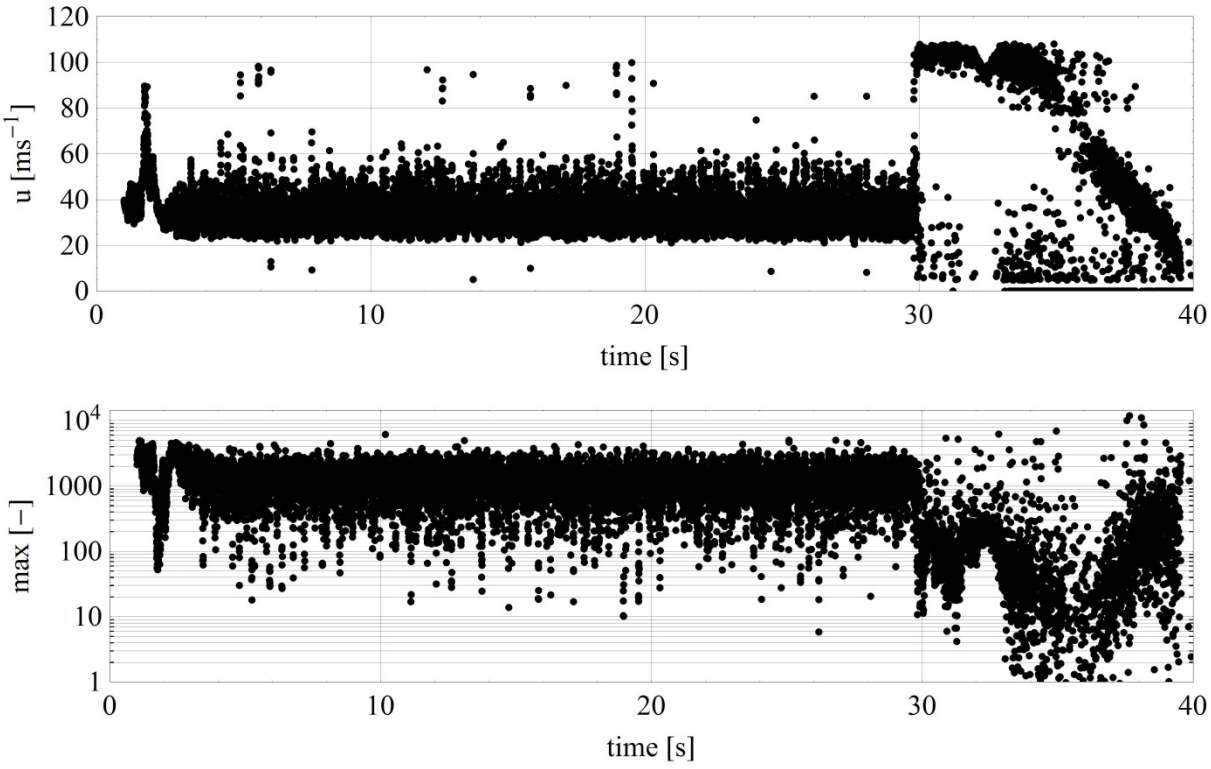

Figure 61 Time series of the velocity and the corresponding maximum value of the laser Doppler spectra of the first run.

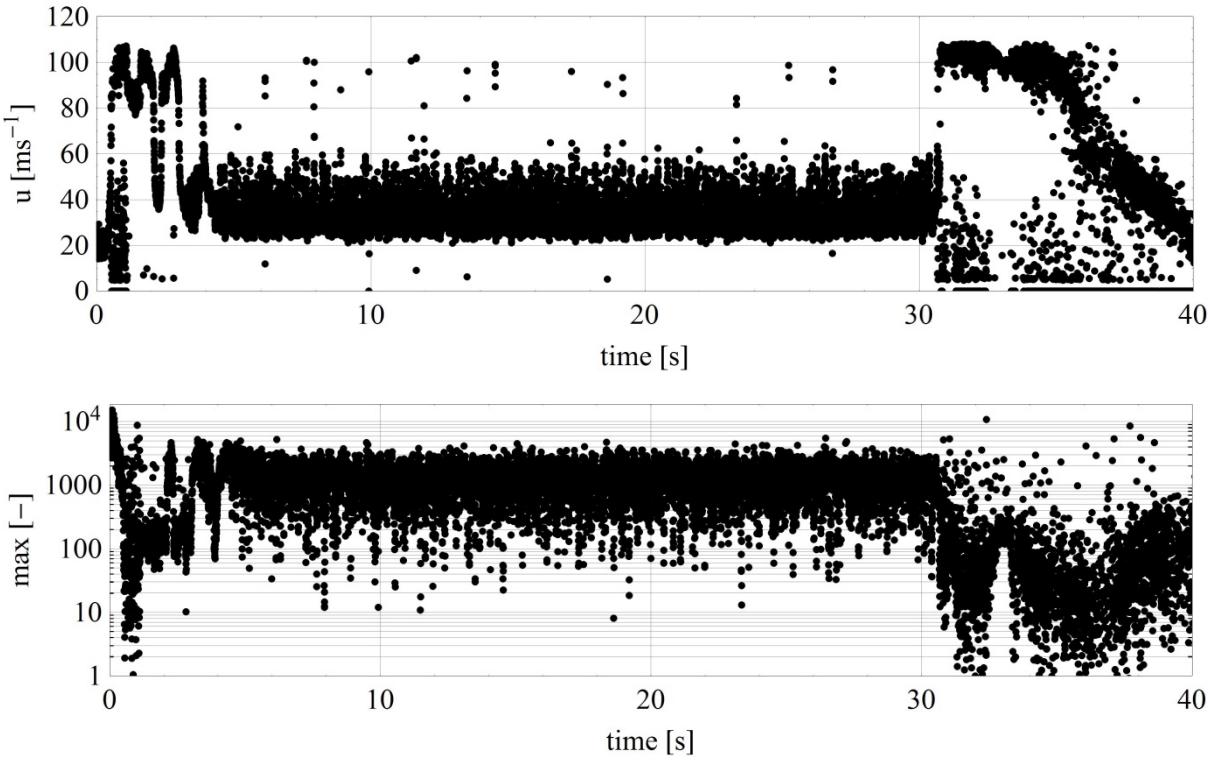

Figure 62 Time series of the velocity and the corresponding maximum value of the laser Doppler spectra of the first run.

Ceramic bolts 0.2 mm @ 50 mm: 70 PSI

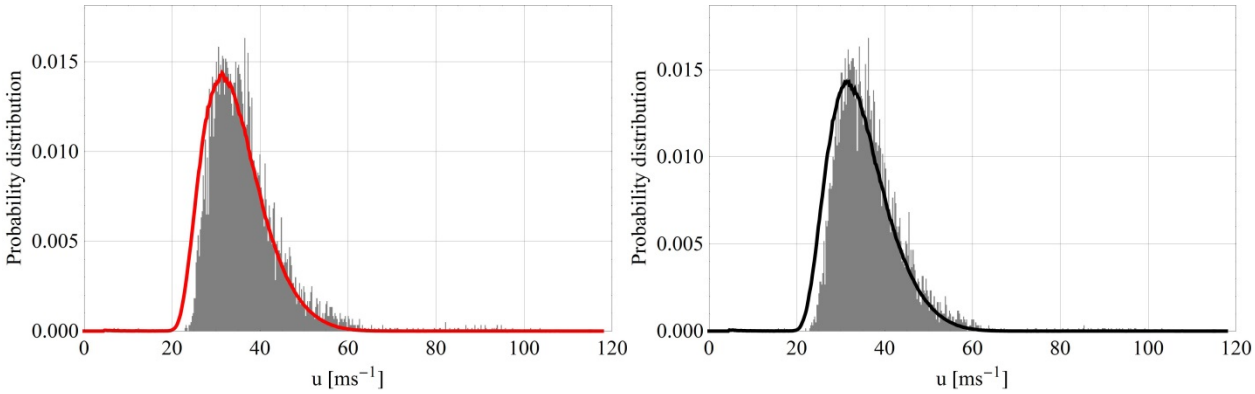

Figure 63 Probability density function and histogram of the measured speeds for two runs.

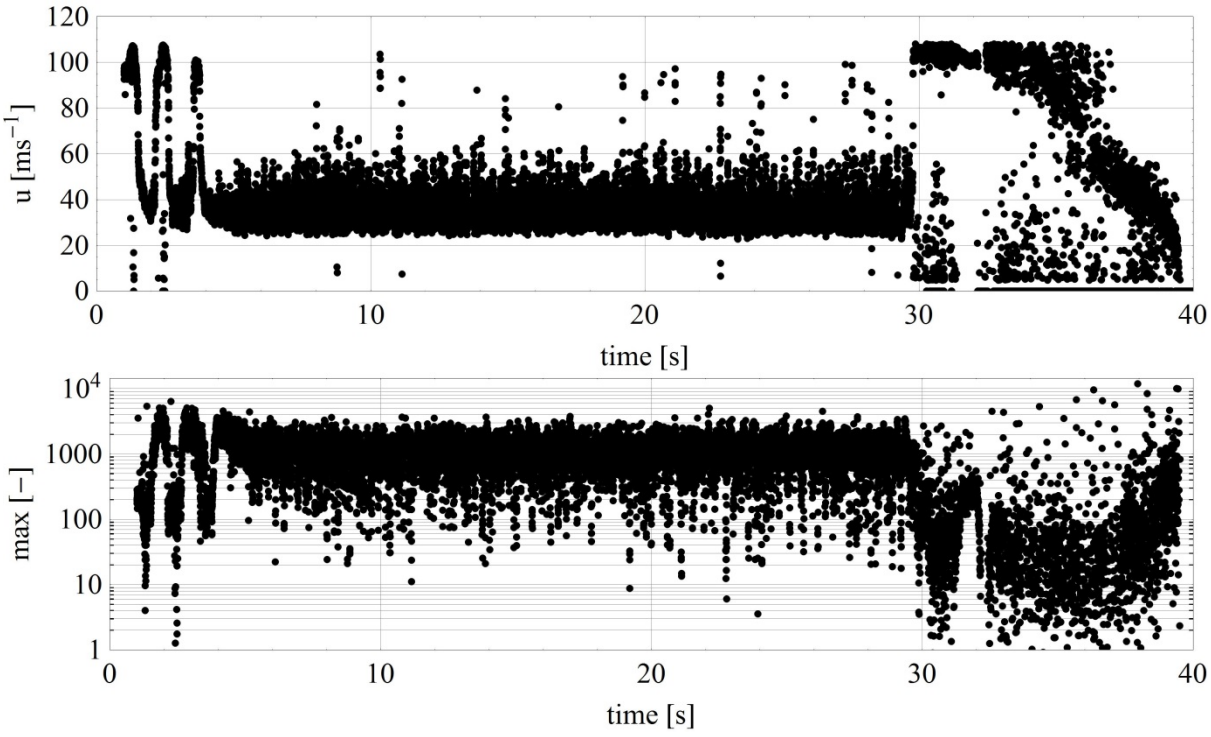

Figure 64 Time series of the velocity and the corresponding maximum value of the laser Doppler spectra of the first run.

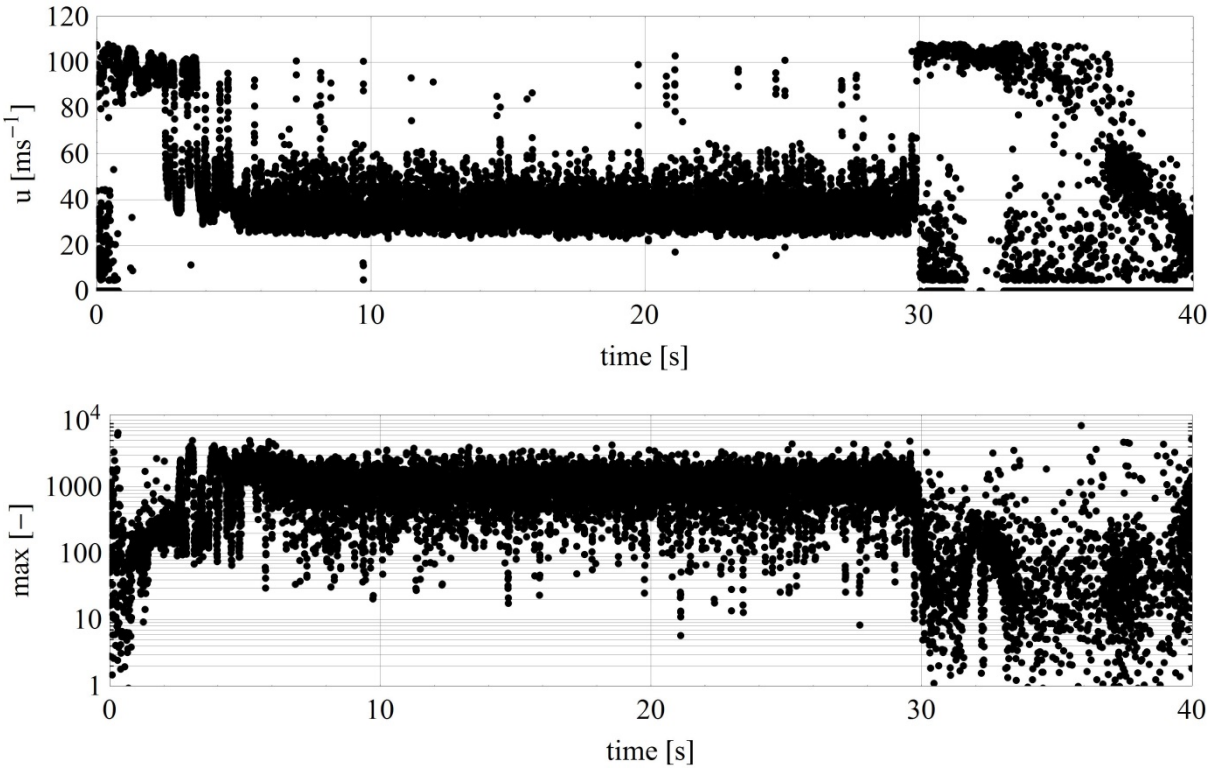

Figure 65 Time series of the velocity and the corresponding maximum value of the laser Doppler spectra of the second run.

Ceramic bolts 0.2 mm @ 50 mm: 80 PSI

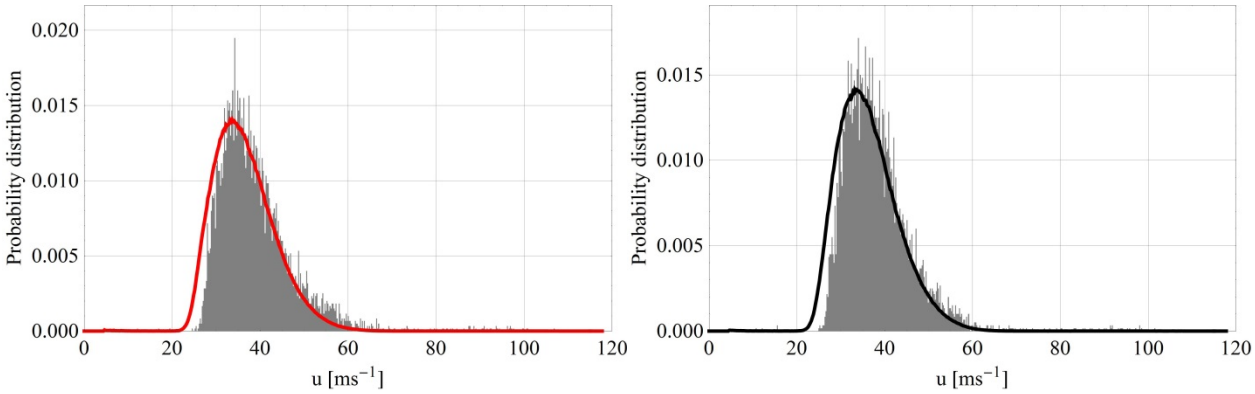

Figure 66 Probability density function and histogram of the measured speeds for two runs.

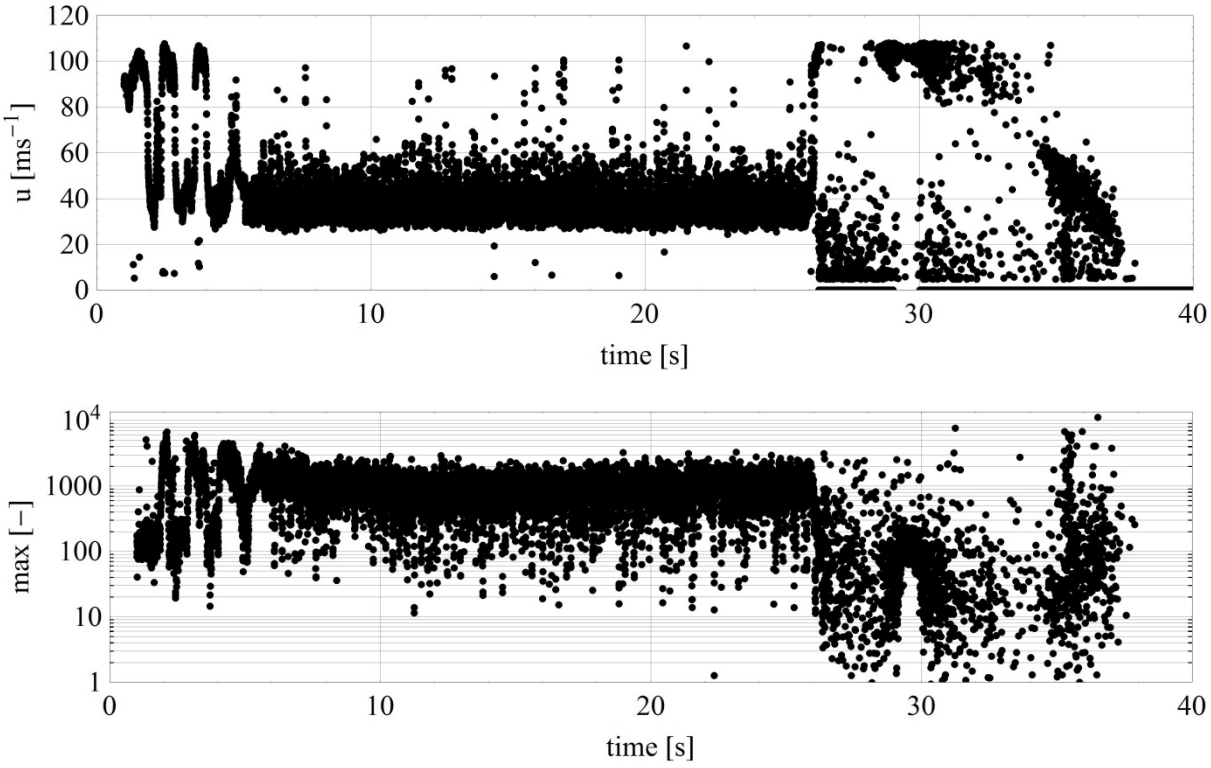

Figure 67 Time series of the velocity and the corresponding maximum value of the laser Doppler spectra of the first run.

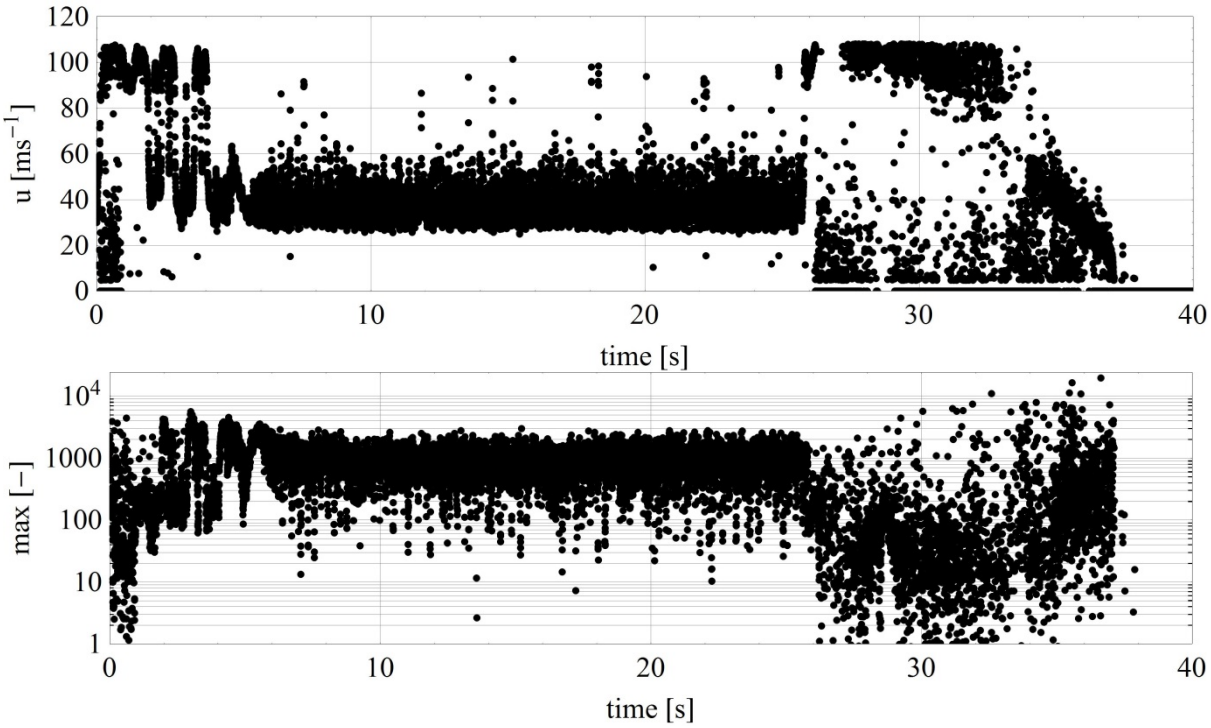

Figure 68 Time series of the velocity and the corresponding maximum value of the laser Doppler spectra of the second run.

Ceramic bolts 0.3 mm @ 50 mm: 40 PSI

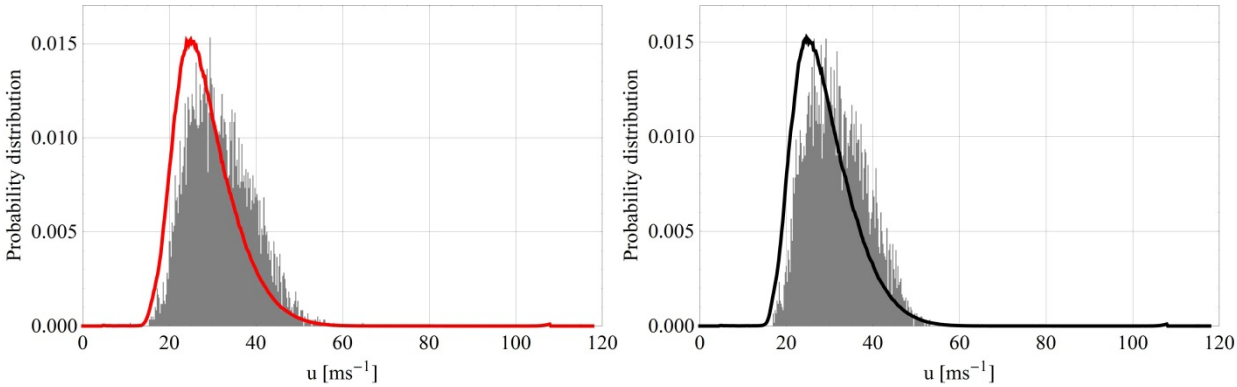

Figure 69 Probability density function and histogram of the measured speeds for two runs.

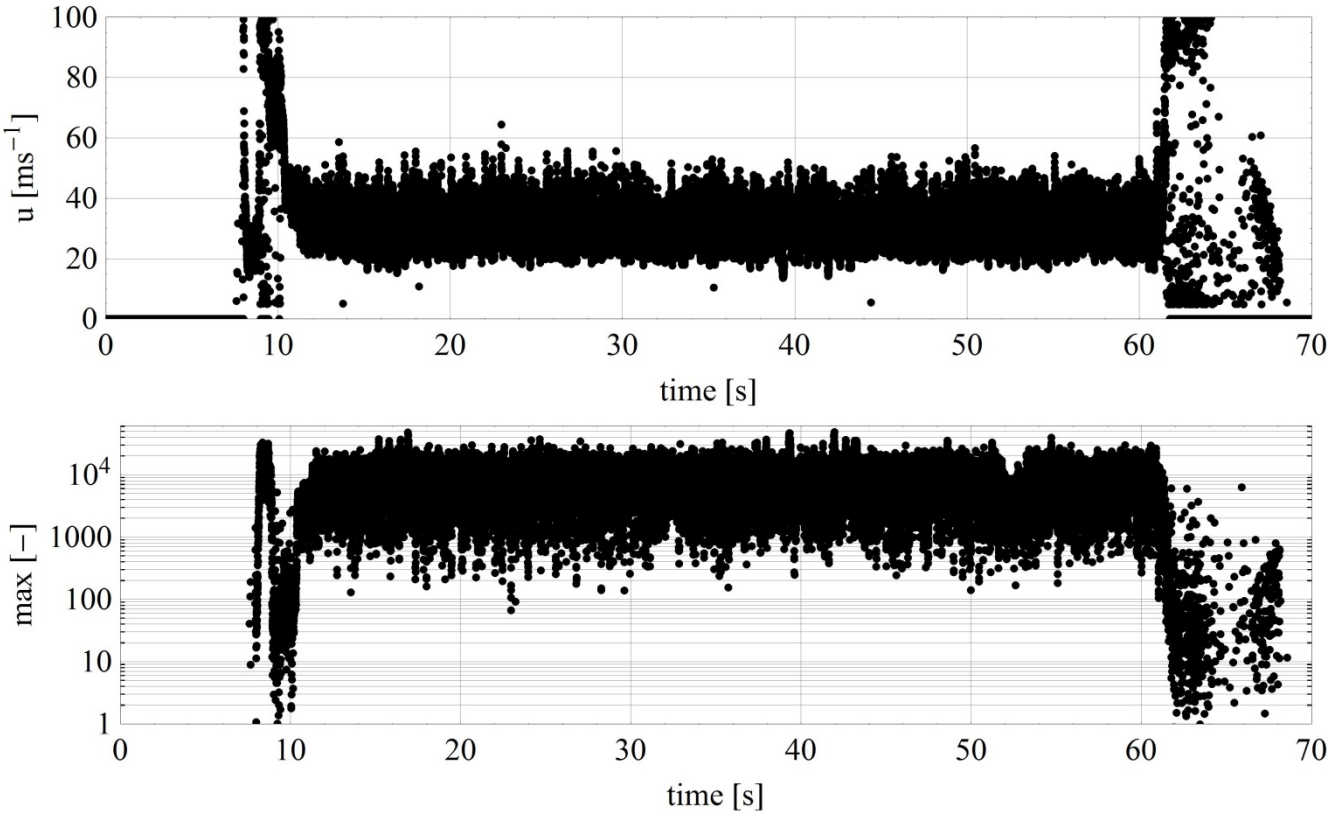

Figure 70 Time series of the velocity and the corresponding maximum value of the laser Doppler spectra of the first run.

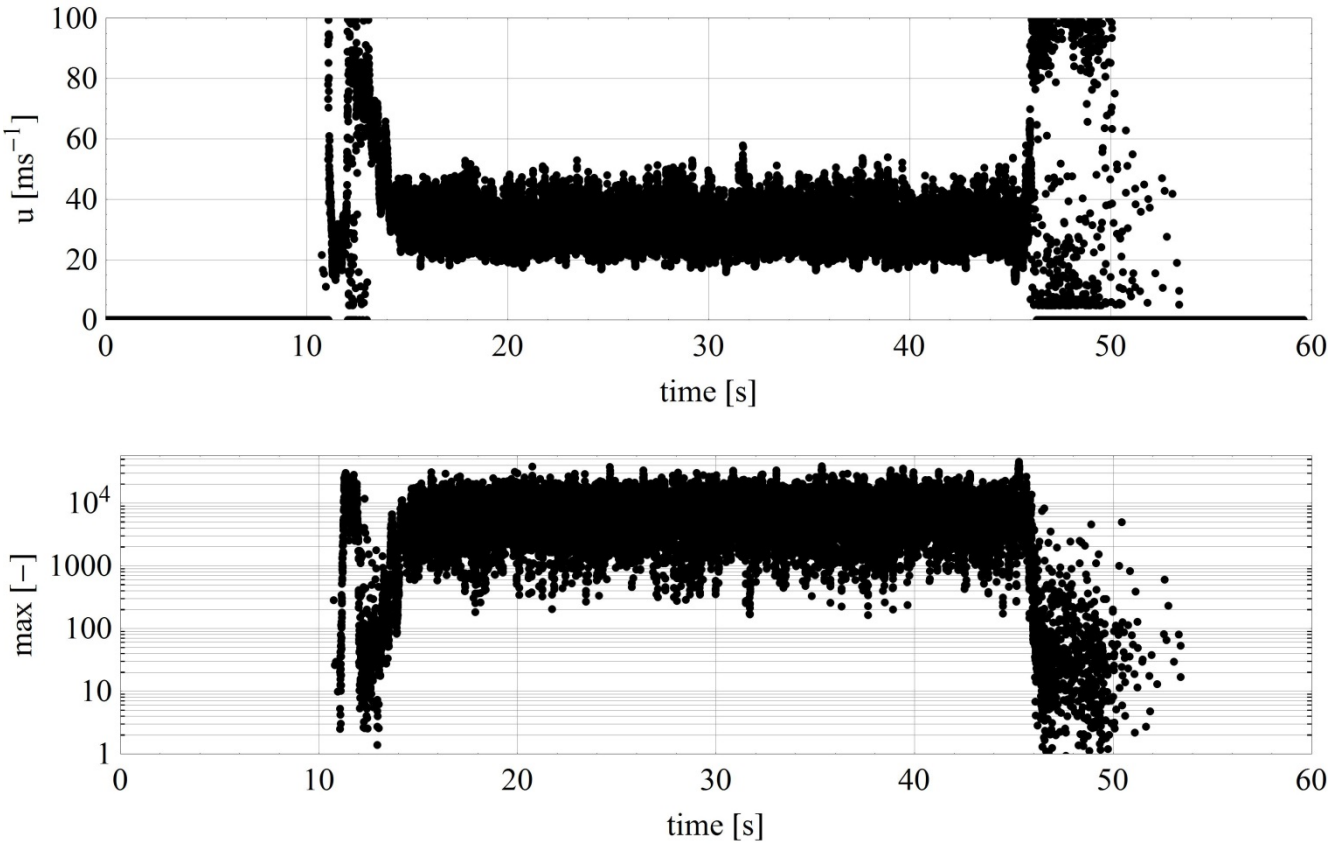

Figure 71 Time series of the velocity and the corresponding maximum value of the laser Doppler spectra of the second run.

Ceramic bolts 0.3 mm @ 50 mm: 50 PSI

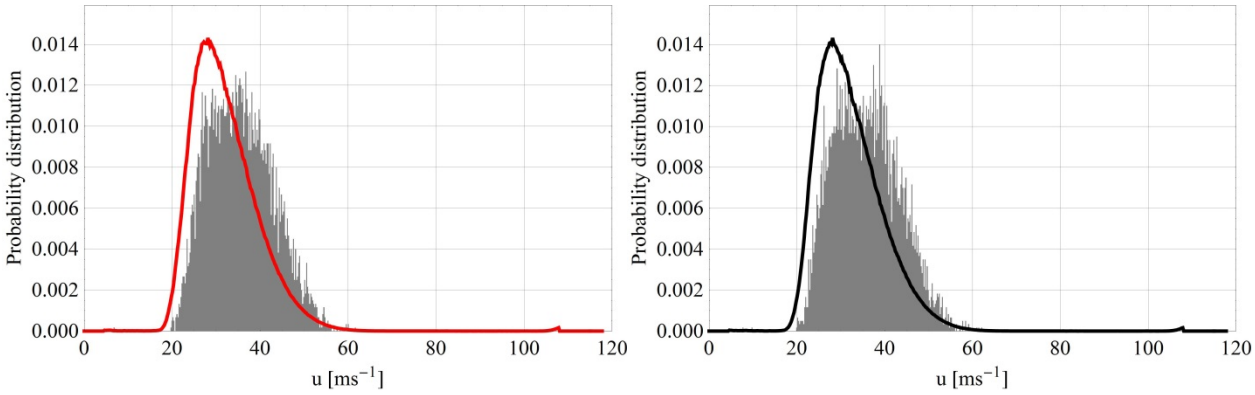

Figure 72 Probability density function and histogram of the measured speeds for two runs.

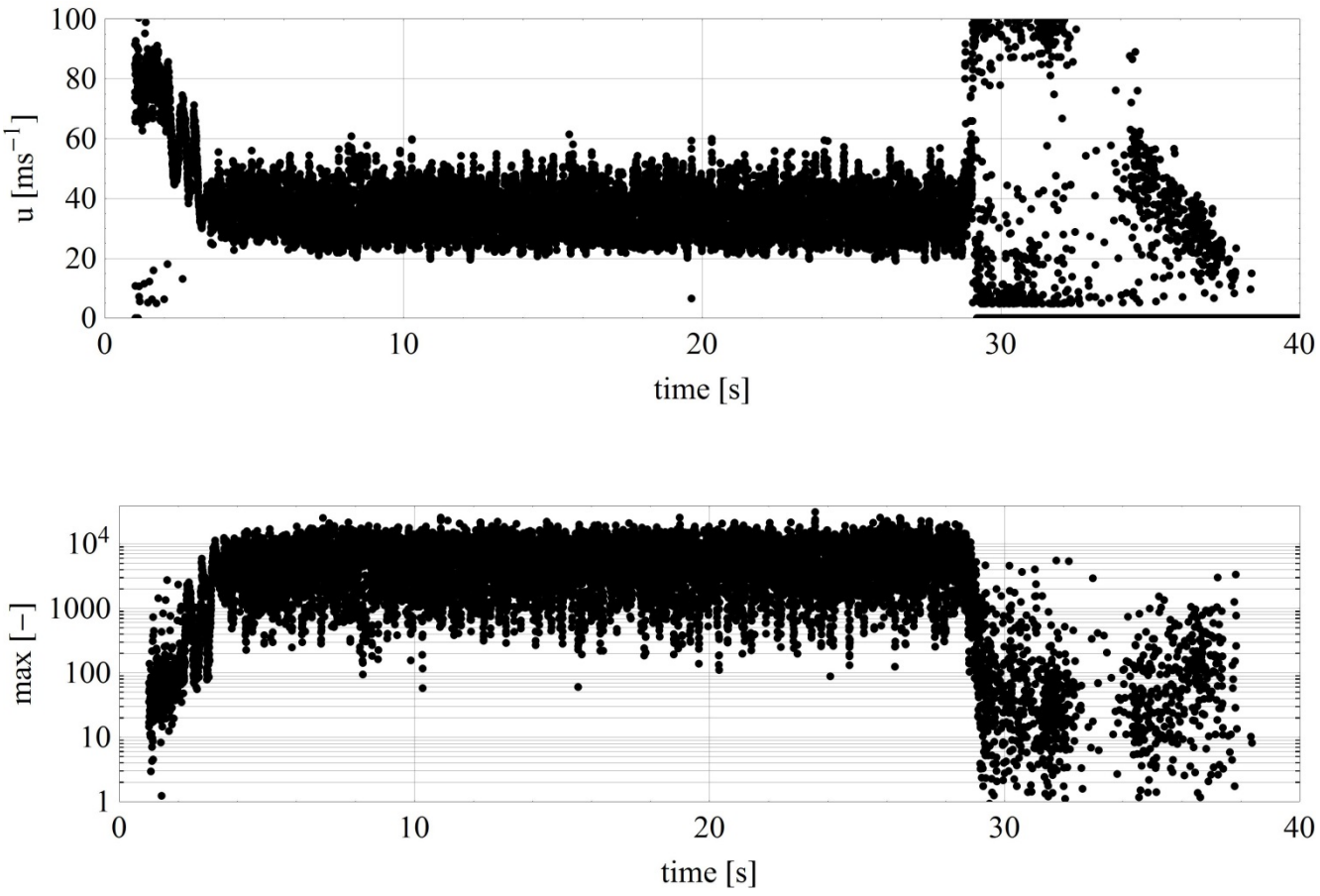

Figure 73 Time series of the velocity and the corresponding maximum value of the laser Doppler spectra of the first run.

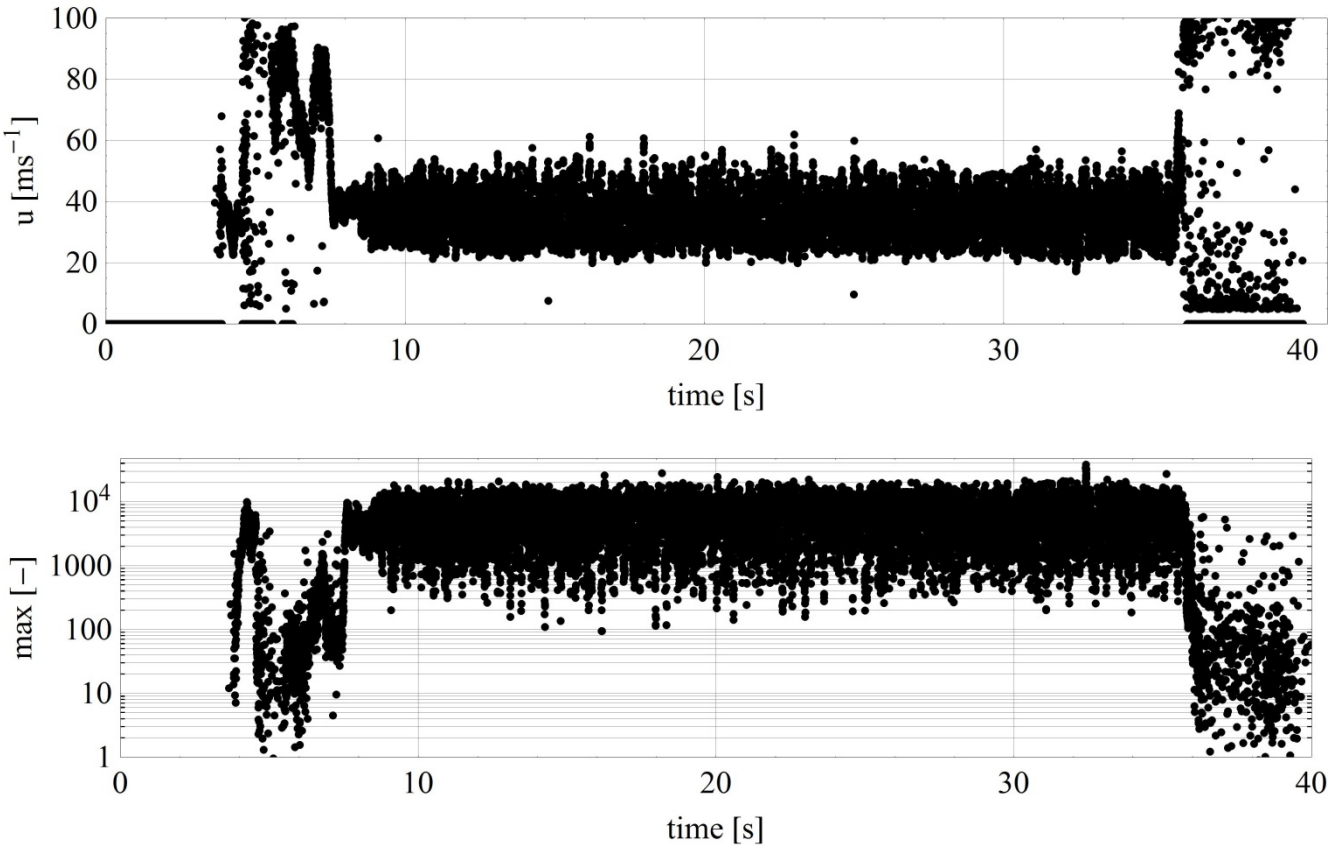

Figure 74 Time series of the velocity and the corresponding maximum value of the laser Doppler spectra of the second run.

Ceramic bolts 0.3 mm @ 50 mm: 60 PSI

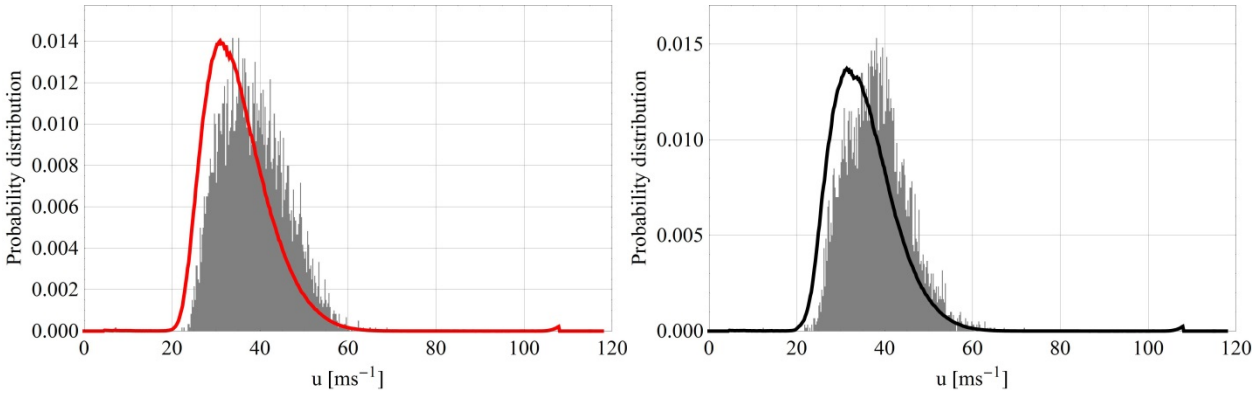

Figure 75 Probability density function and histogram of the measured speeds for two runs.

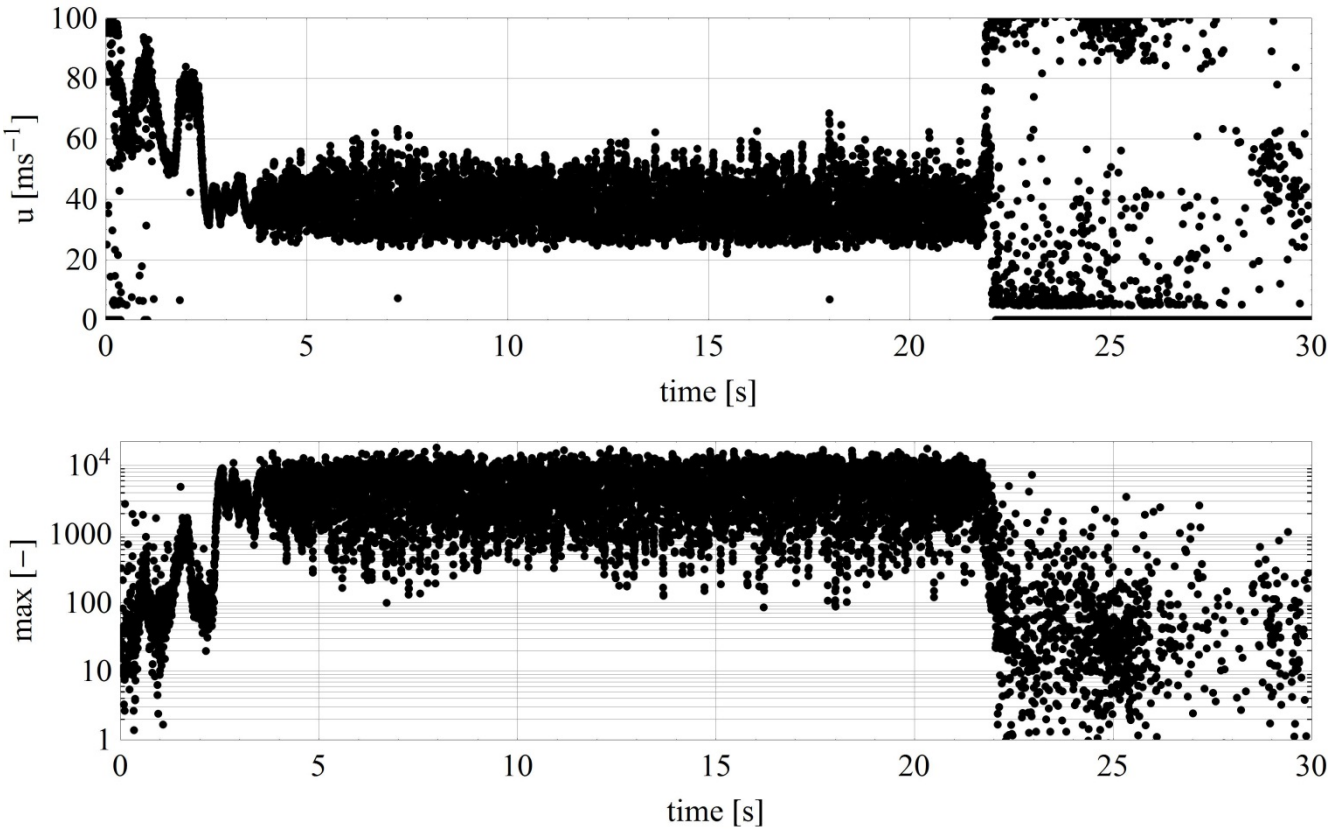

Figure 76 Time series of the velocity and the corresponding maximum value of the laser Doppler spectra of the first run.

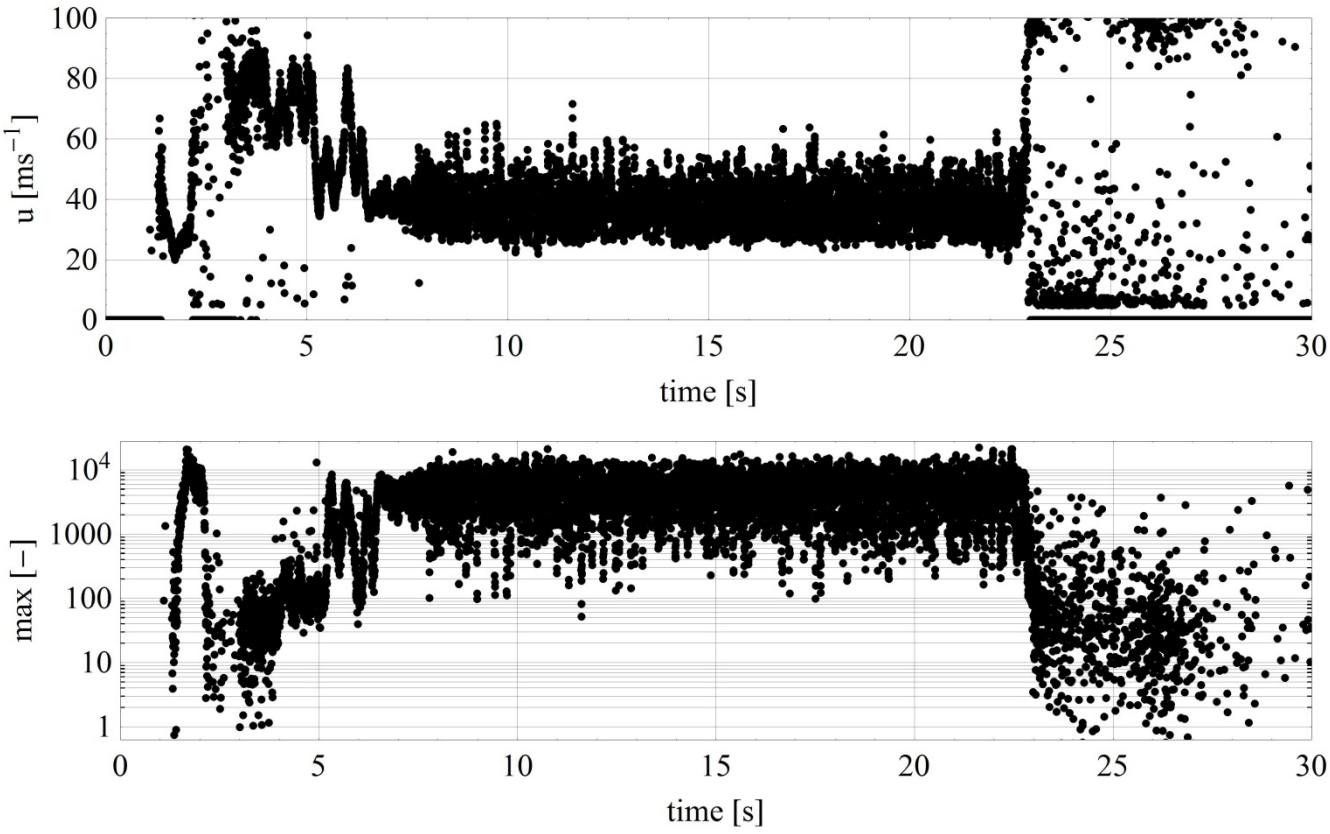

Figure 77 Time series of the velocity and the corresponding maximum value of the laser Doppler spectra of the second run.

Ceramic bolts 0.3 mm @ 50 mm: 70 PSI

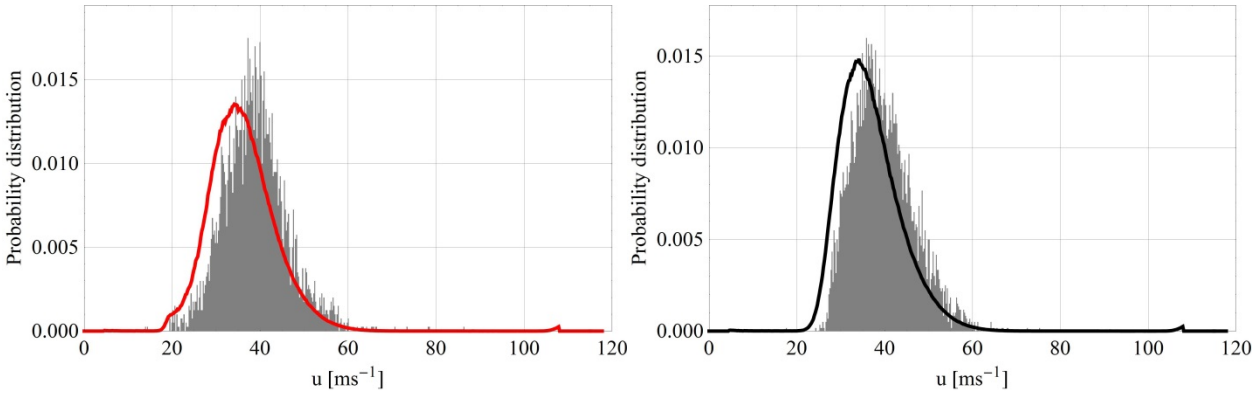

Figure 78 Probability density function and histogram of the measured speeds for two runs.

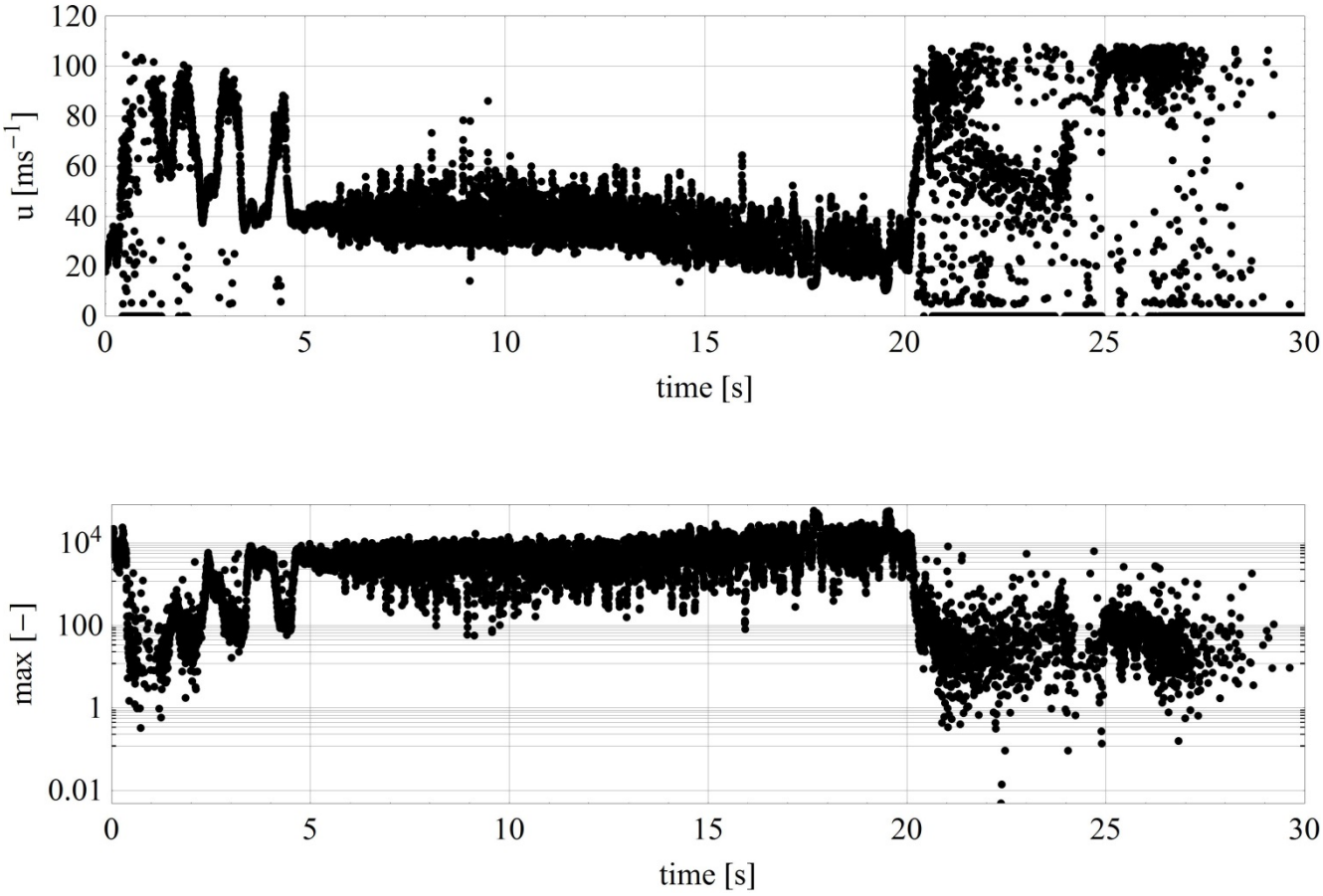

Figure 79 Time series of the velocity and the corresponding maximum value of the laser Doppler spectra of the first run.

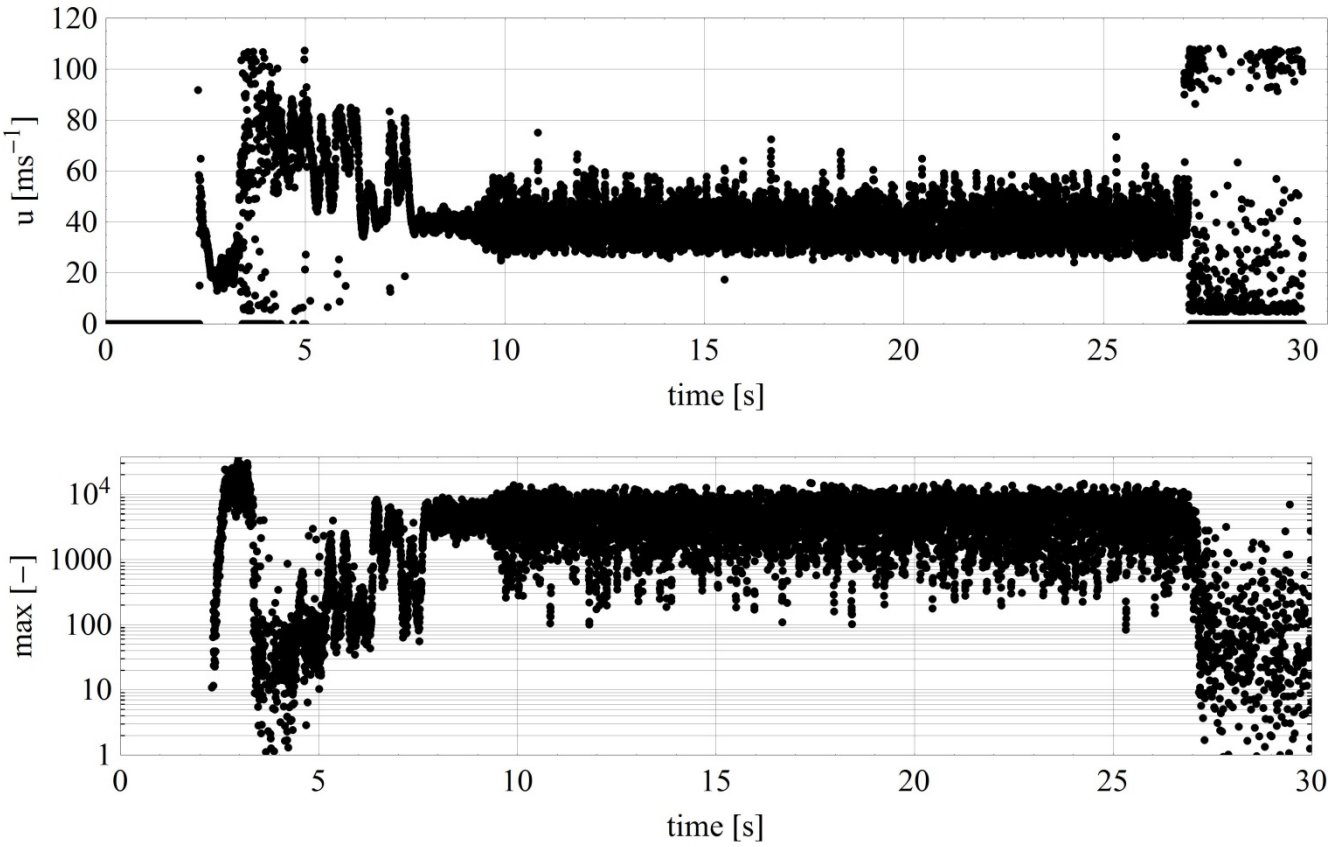

Figure 80 Time series of the velocity and the corresponding maximum value of the laser Doppler spectra of the second run.

Steel bolts 0.6 mm @ 50 mm: 40 PSI

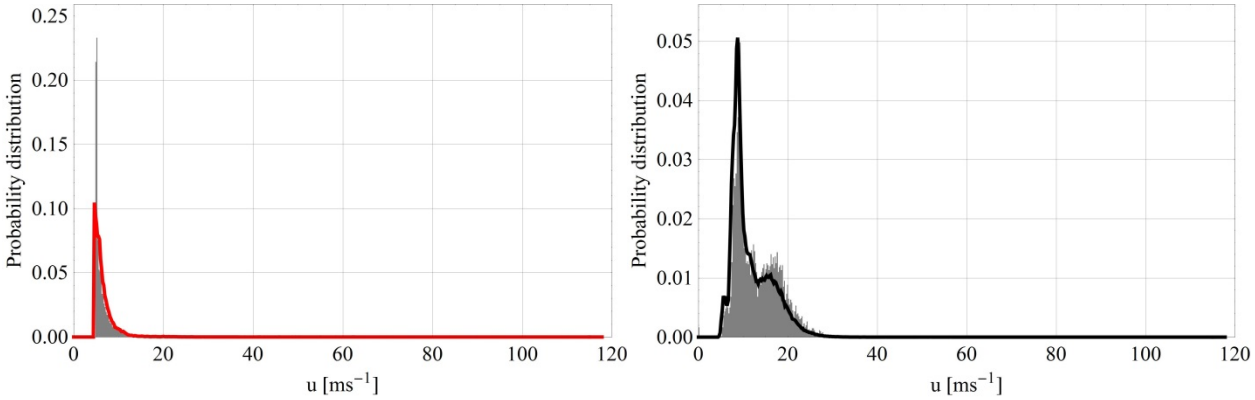

Figure 81 Probability density function and histogram of the measured speeds for two runs.

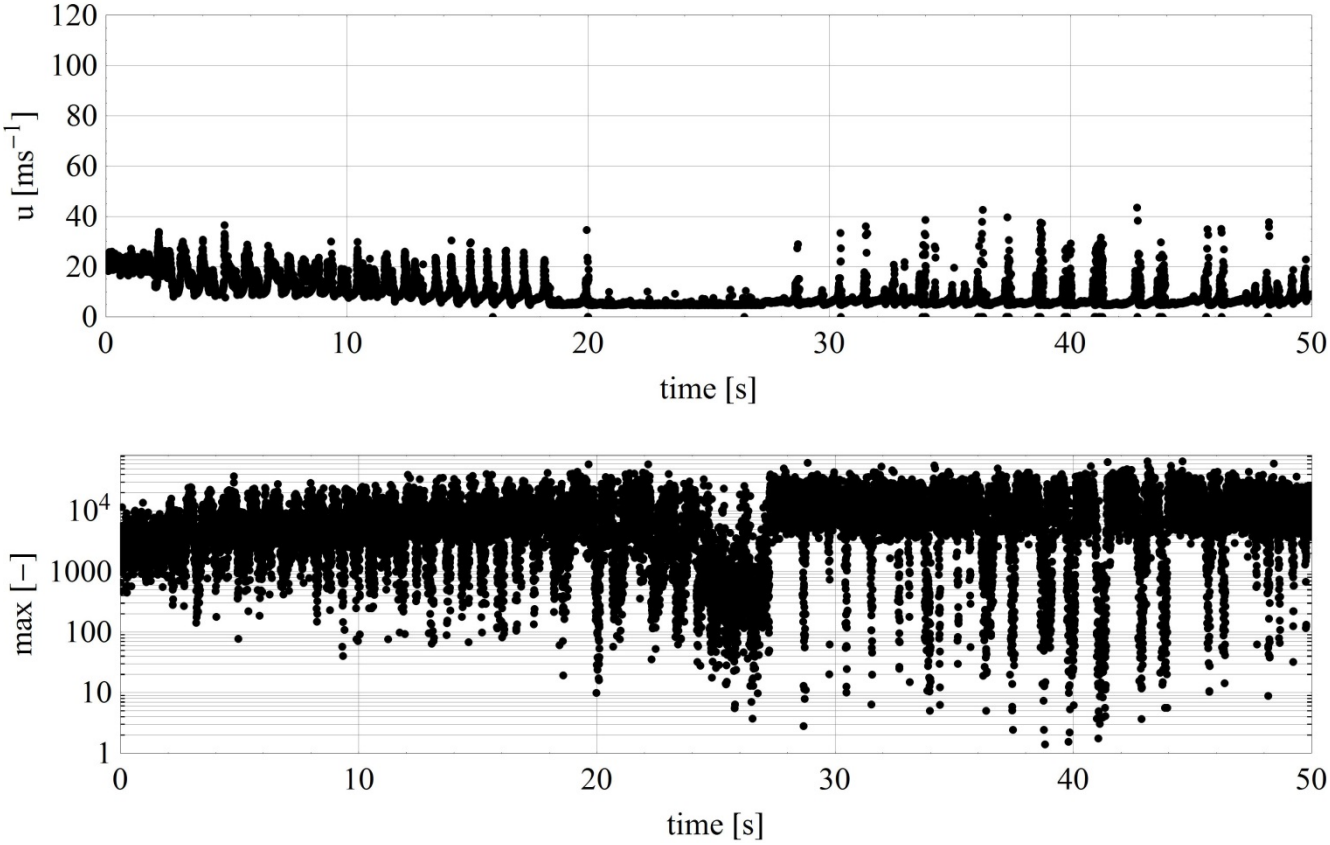

Figure 82 Time series of the velocity and the corresponding maximum value of the laser Doppler spectra of the first run.

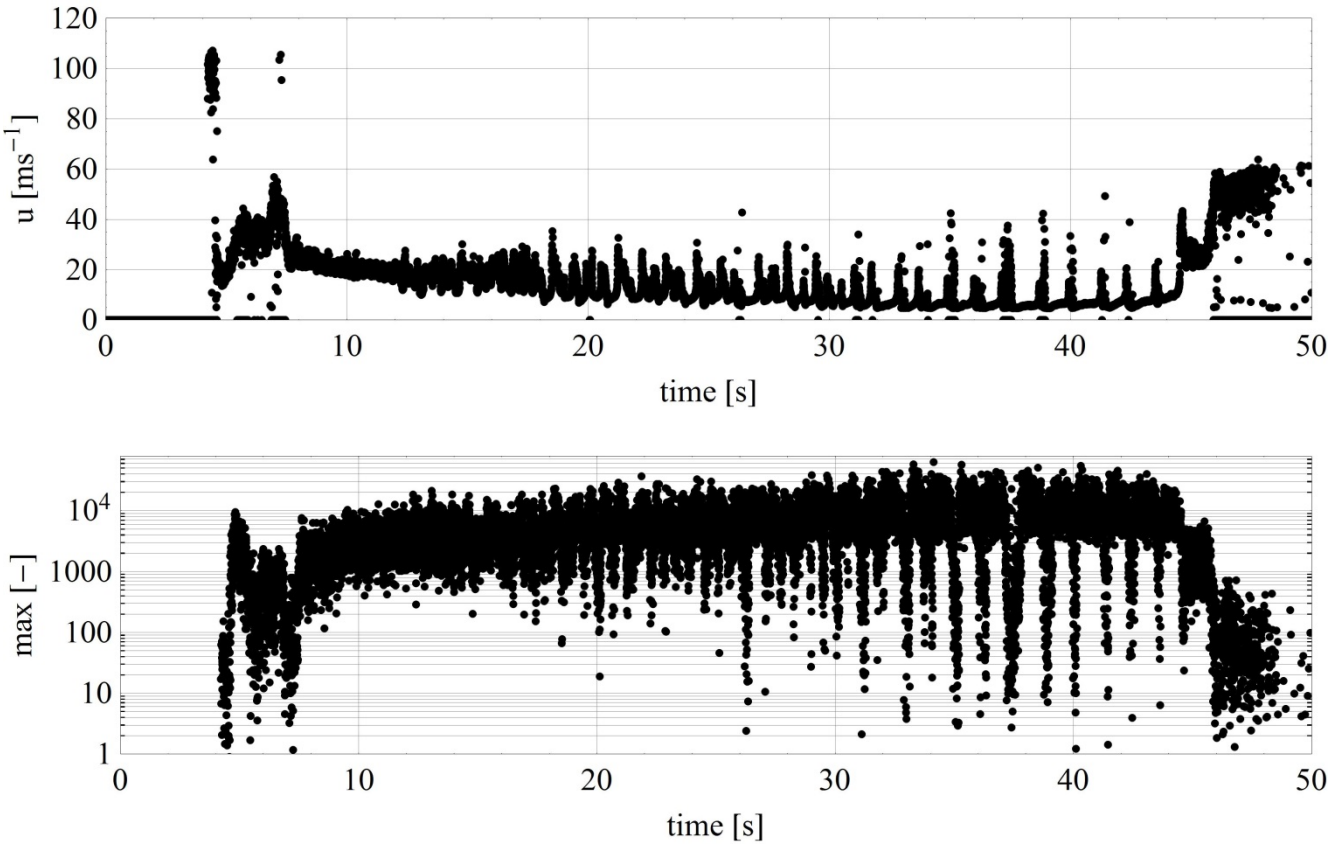

Figure 83 Time series of the velocity and the corresponding maximum value of the laser Doppler spectra of the second run.

Steel bolts 0.6 mm @ 50 mm: 50 PSI

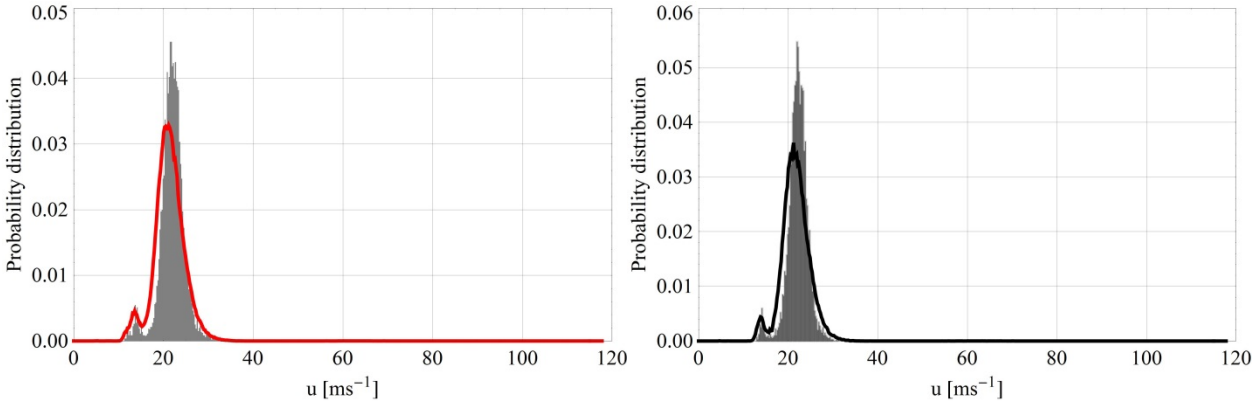

Figure 84 Probability density function and histogram of the measured speeds for two runs.

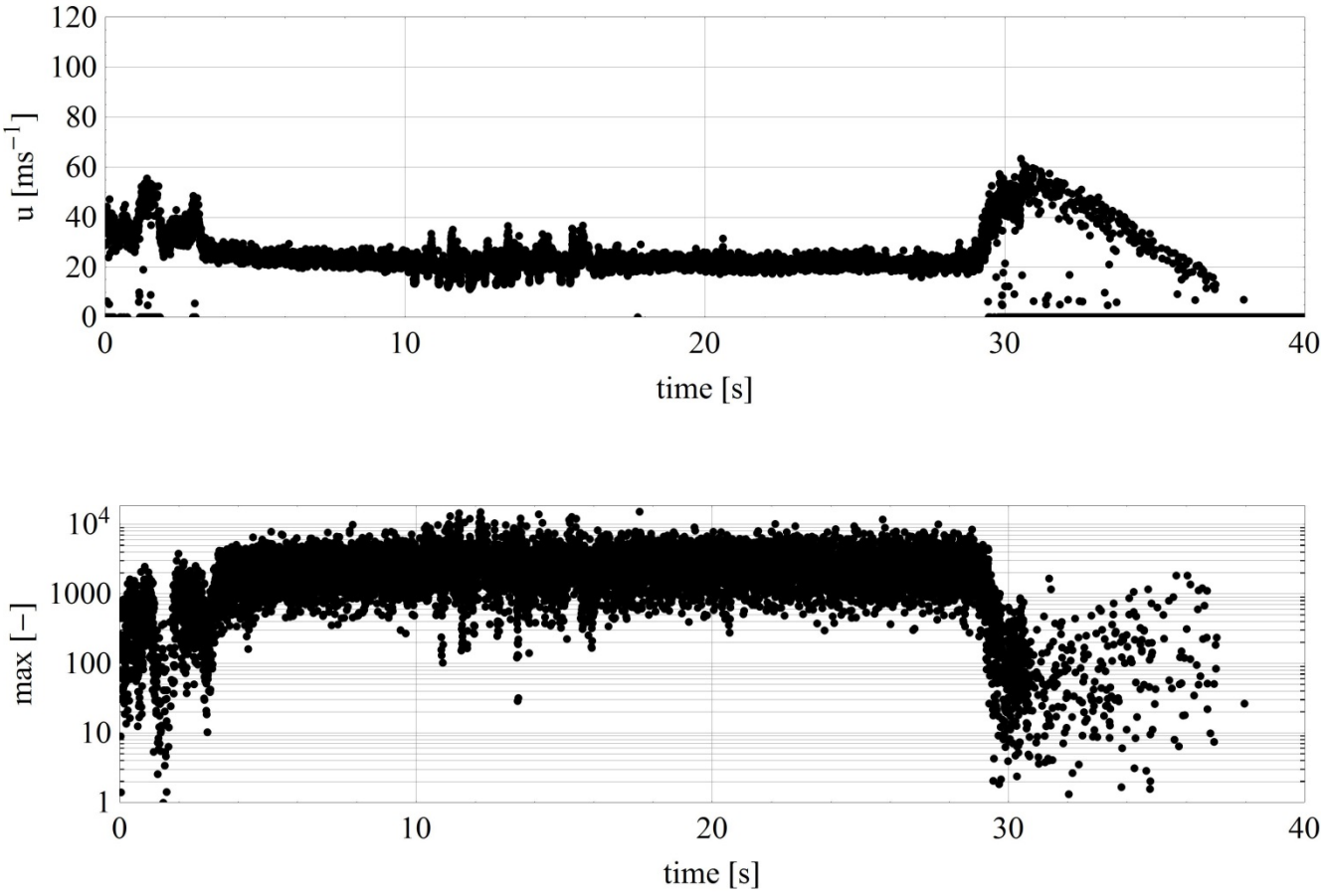

Figure 85 Time series of the velocity and the corresponding maximum value of the laser Doppler spectra of the first run.

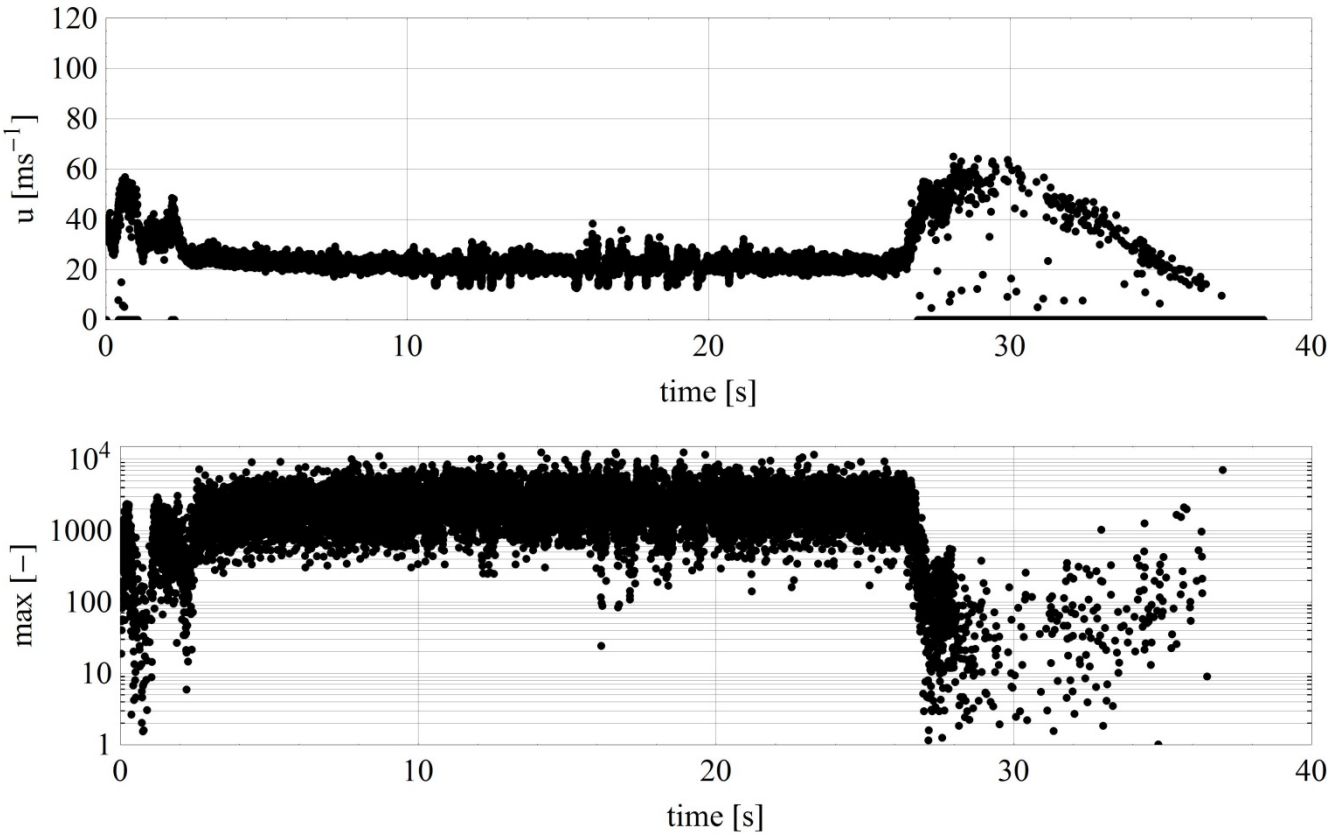

Figure 86 Time series of the velocity and the corresponding maximum value of the laser Doppler spectra of the second run.

Steel bolts 0.6 mm @ 50 mm: 60 PSI

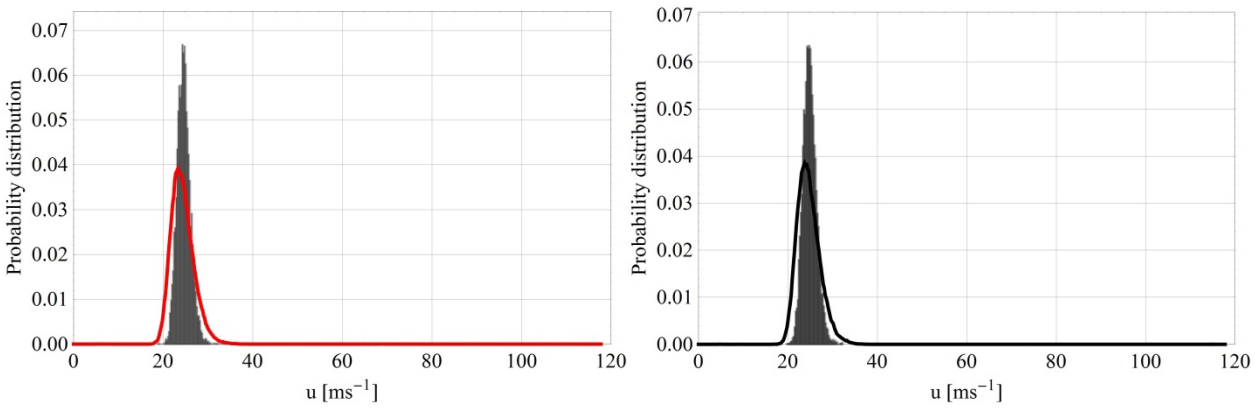

Figure 87 Probability density function and histogram of the measured speeds for two runs.

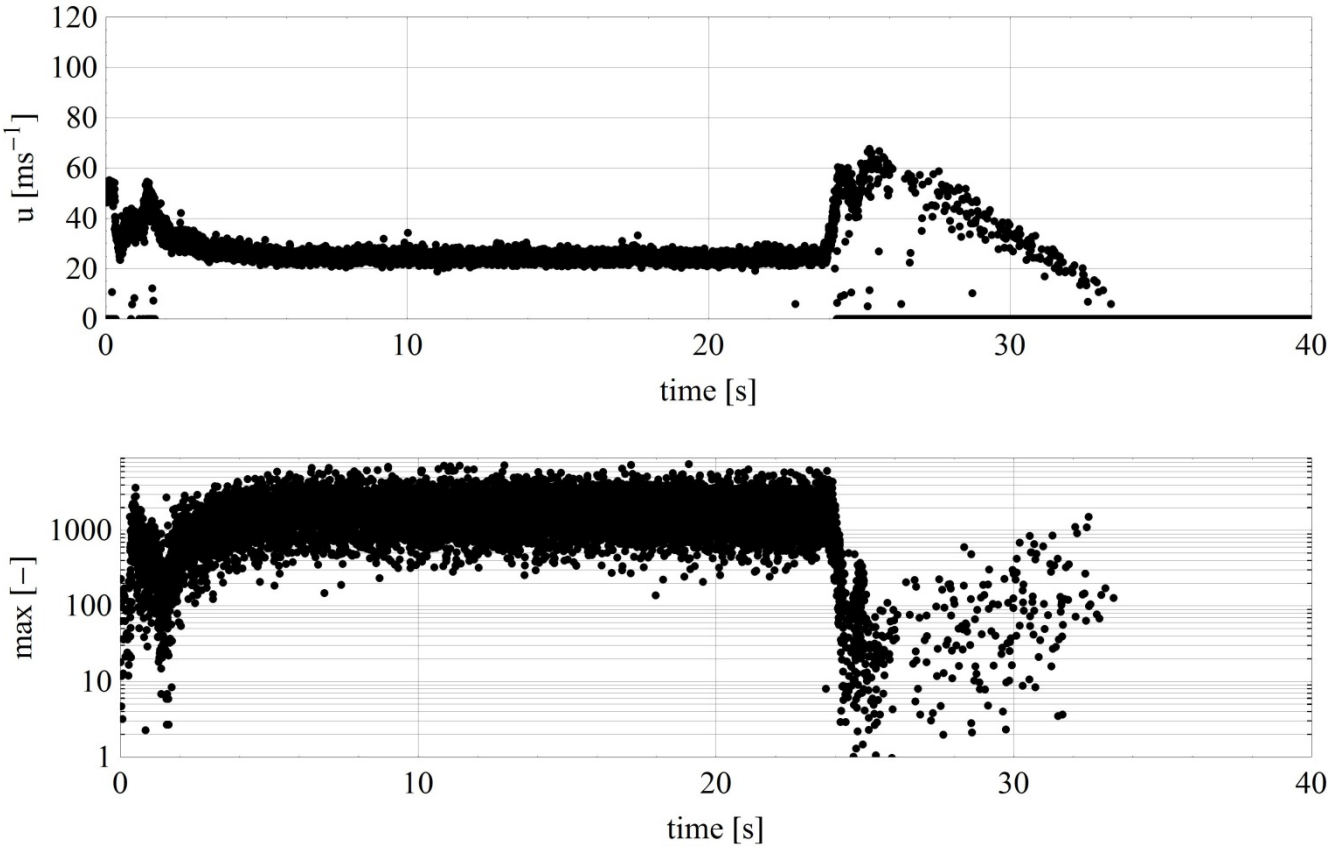

Figure 88 Time series of the velocity and the corresponding maximum value of the laser Doppler spectra of the first run.

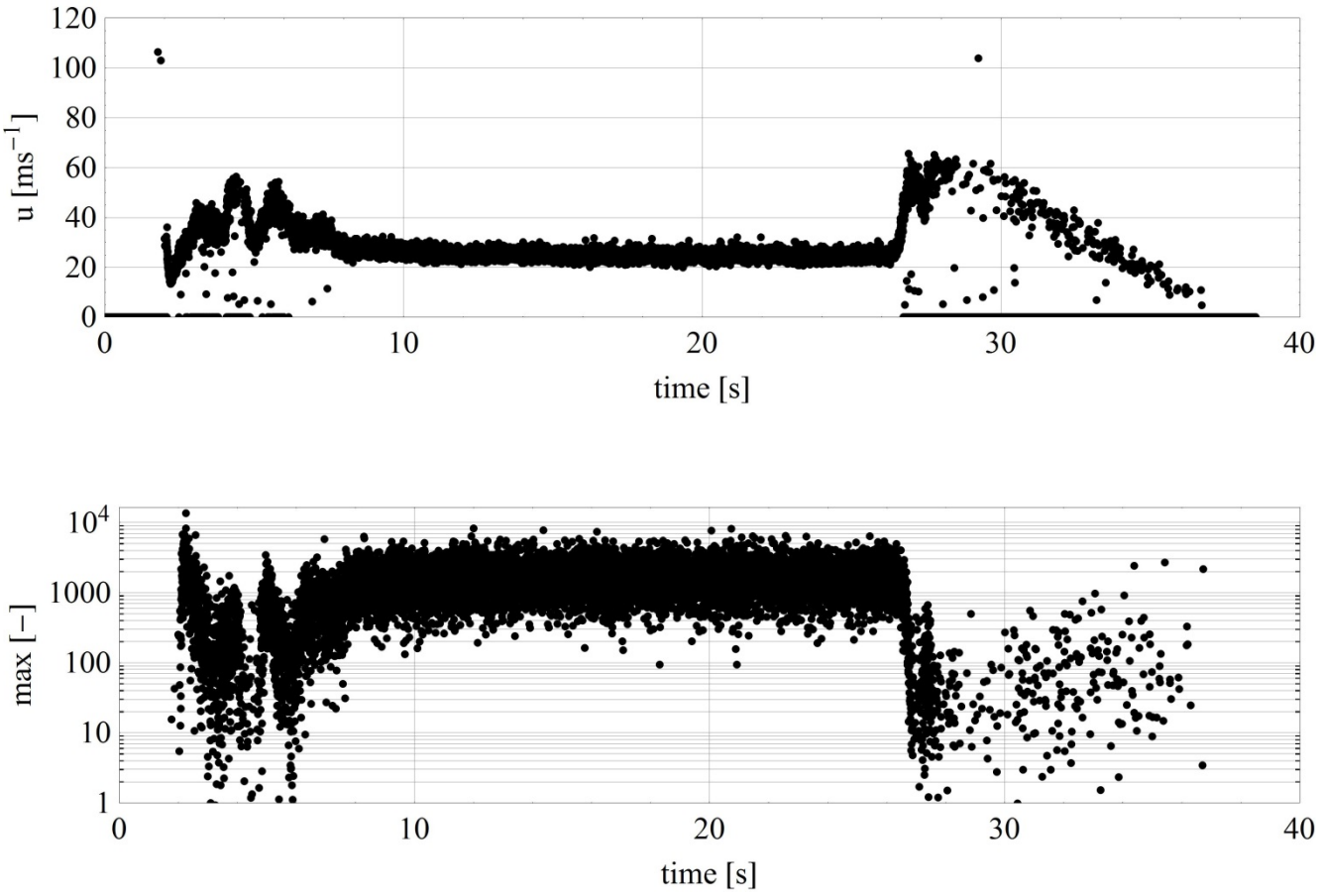

Figure 89 Time series of the velocity and the corresponding maximum value of the laser Doppler spectra of the second run.

Steel bolts 0.6 mm @ 50 mm: 70 PSI

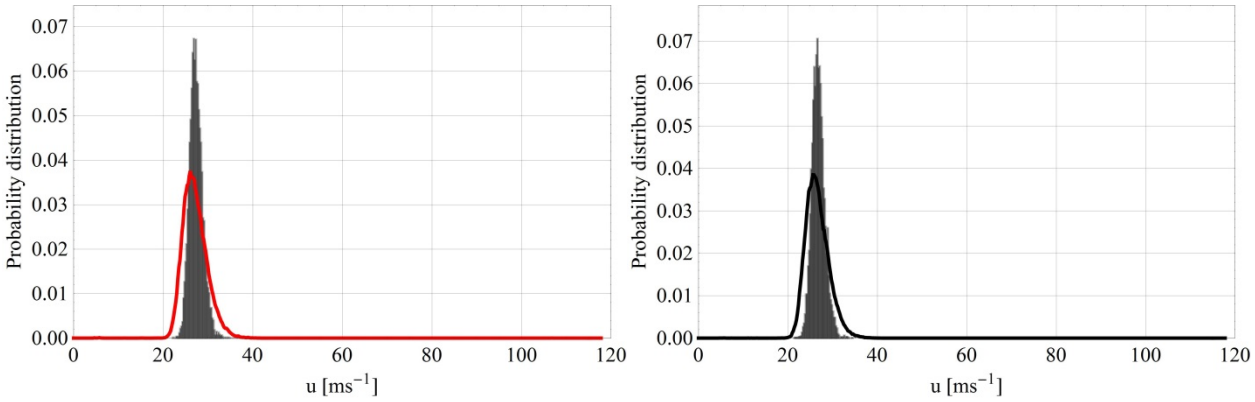

Figure 90 Probability density function and histogram of the measured speeds for two runs.

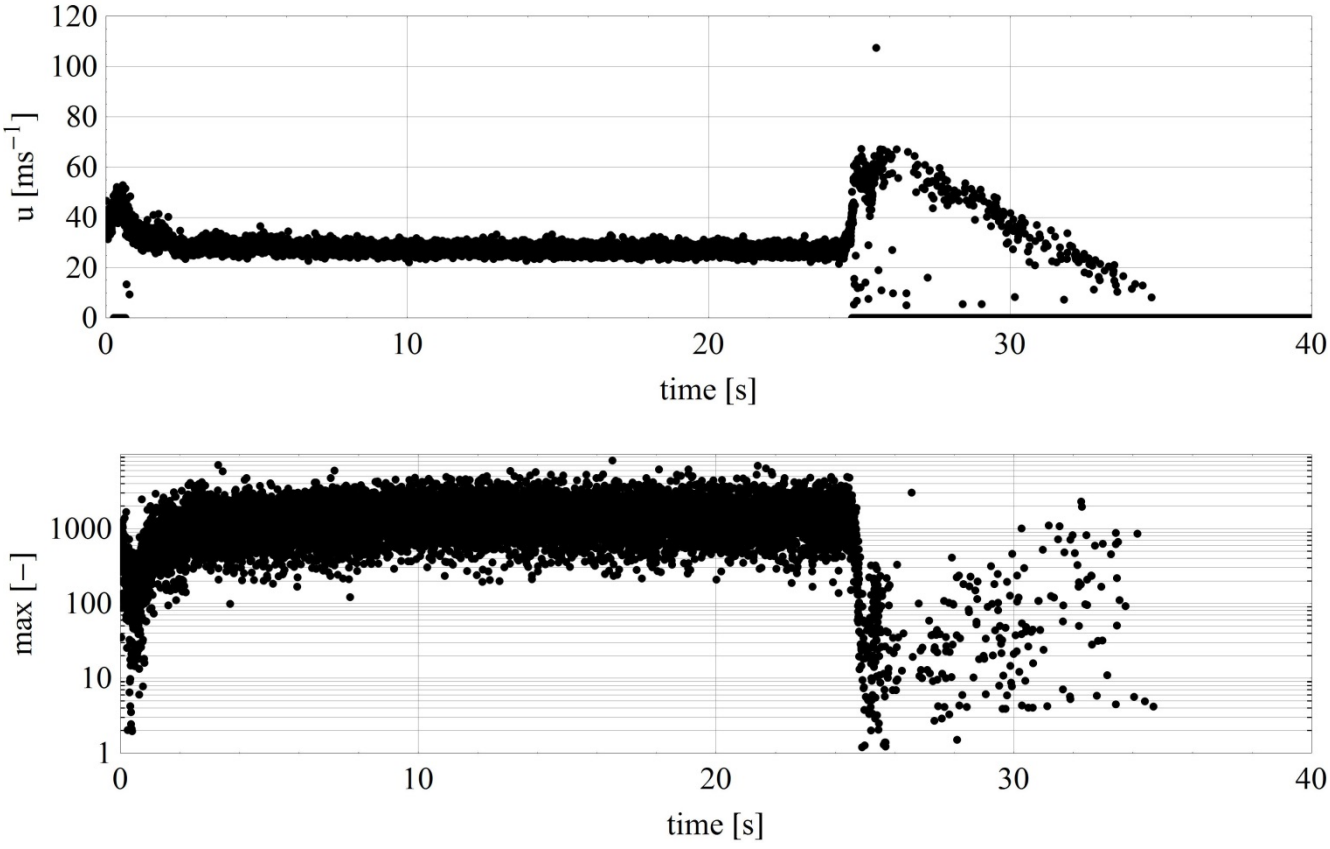

Figure 91 Time series of the velocity and the corresponding maximum value of the laser Doppler spectra of the first run.

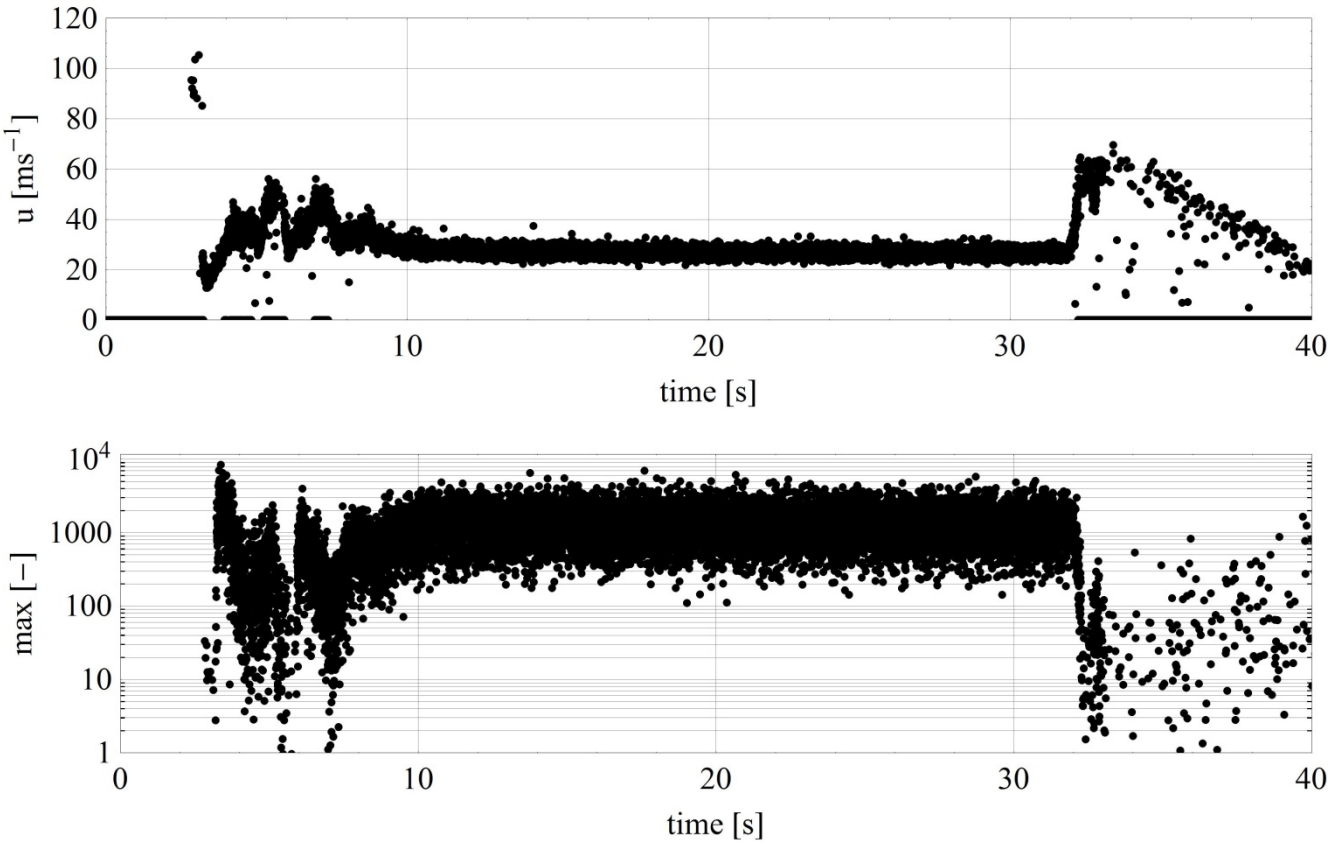

Figure 92 Time series of the velocity and the corresponding maximum value of the laser Doppler spectra of the second run.

Steel bolts 0.6 mm @ 50 mm: 80 PSI

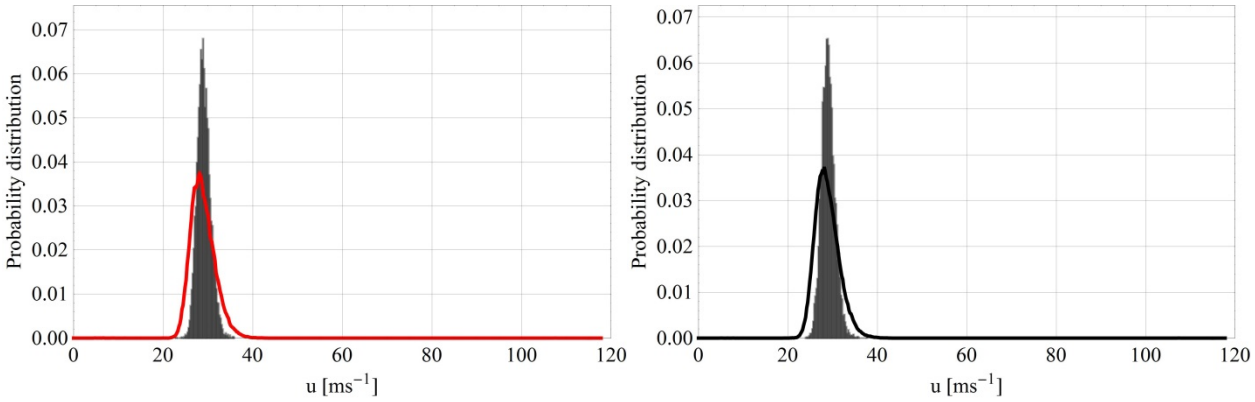

Figure 93 Probability density function and histogram of the measured speeds for two runs.

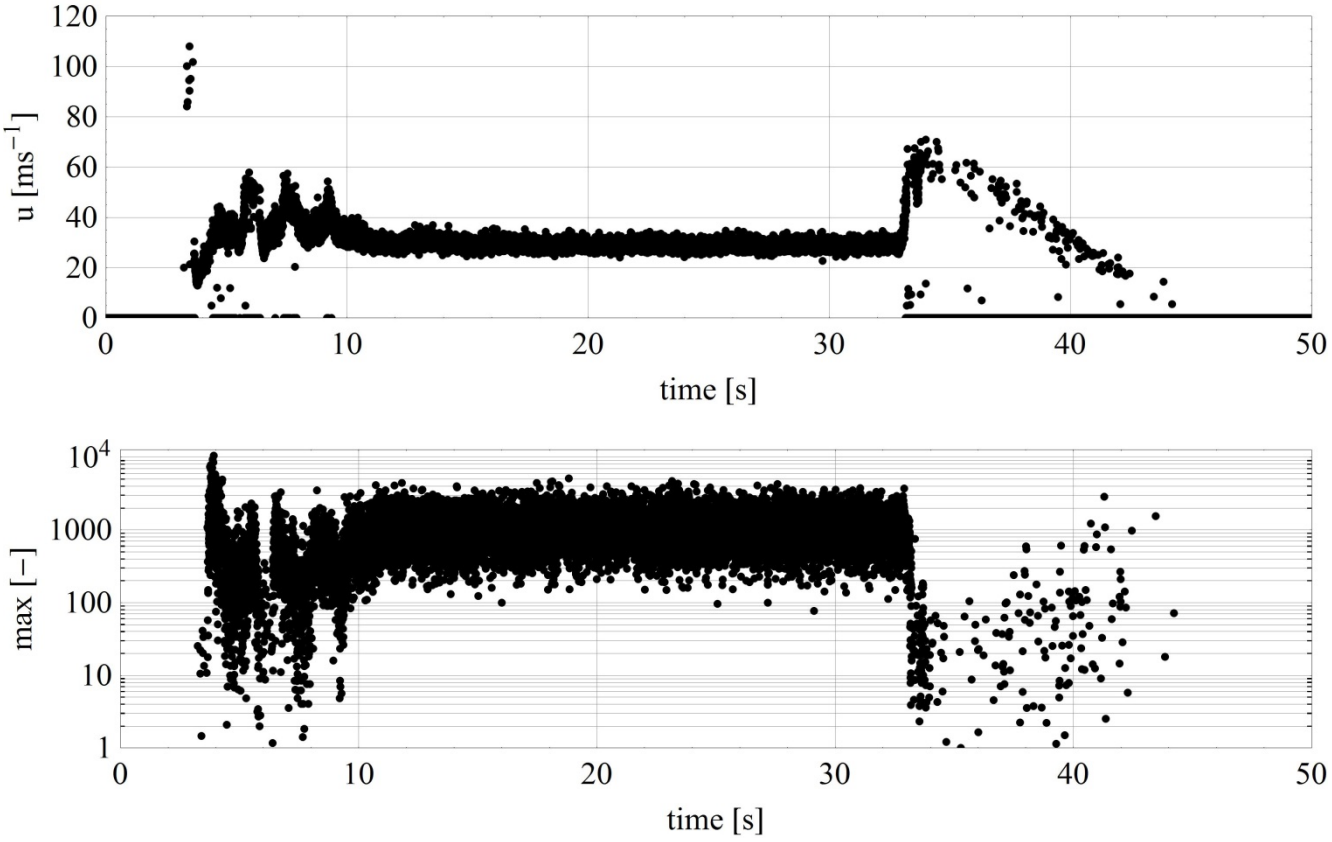

Figure 94 Time series of the velocity and the corresponding maximum value of the laser Doppler spectra of the first run.

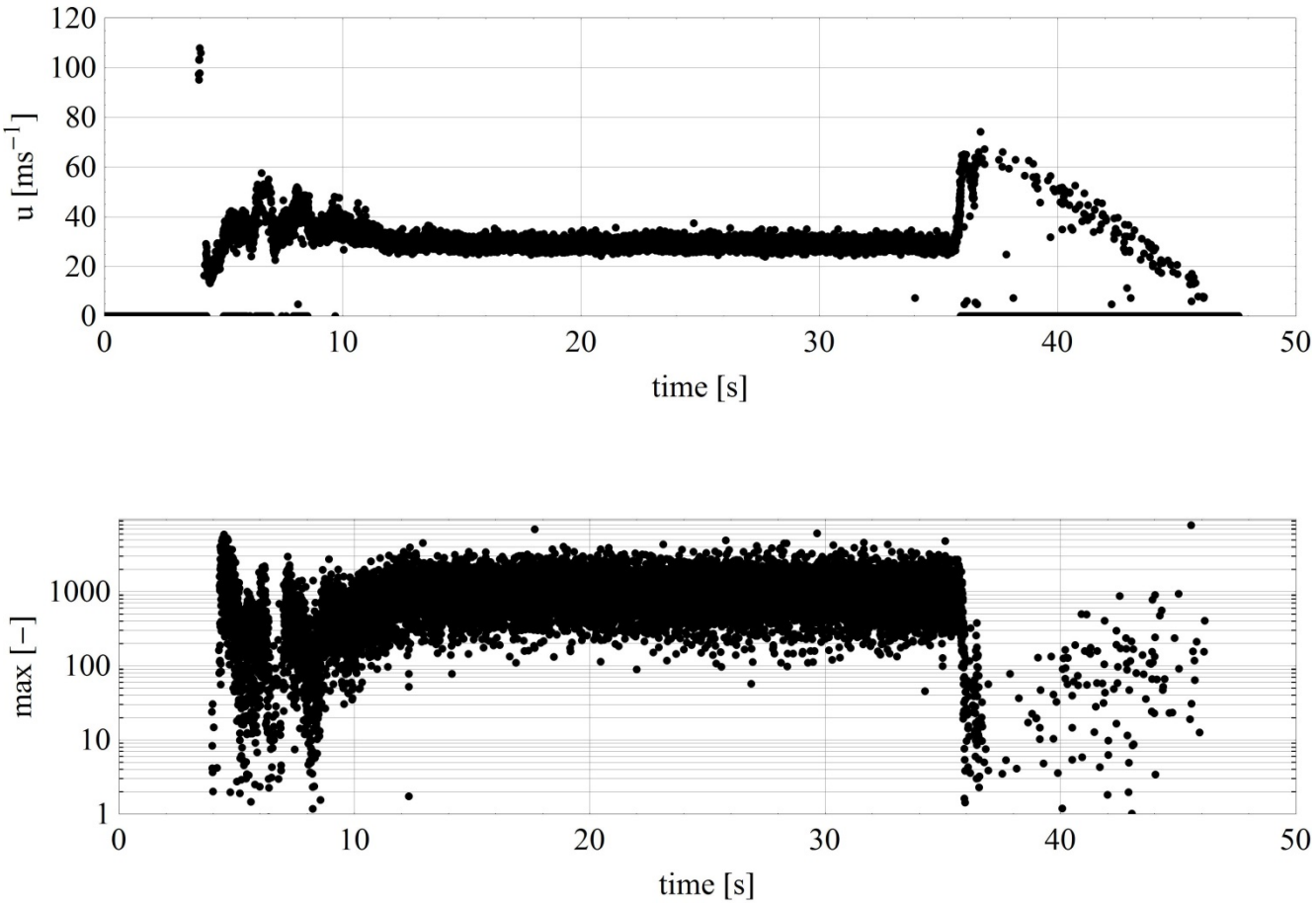

Figure 95 Time series of the velocity and the corresponding maximum value of the laser Doppler spectra of the second run.

Steel bolts 0.6 mm @ 100 mm: 40 PSI

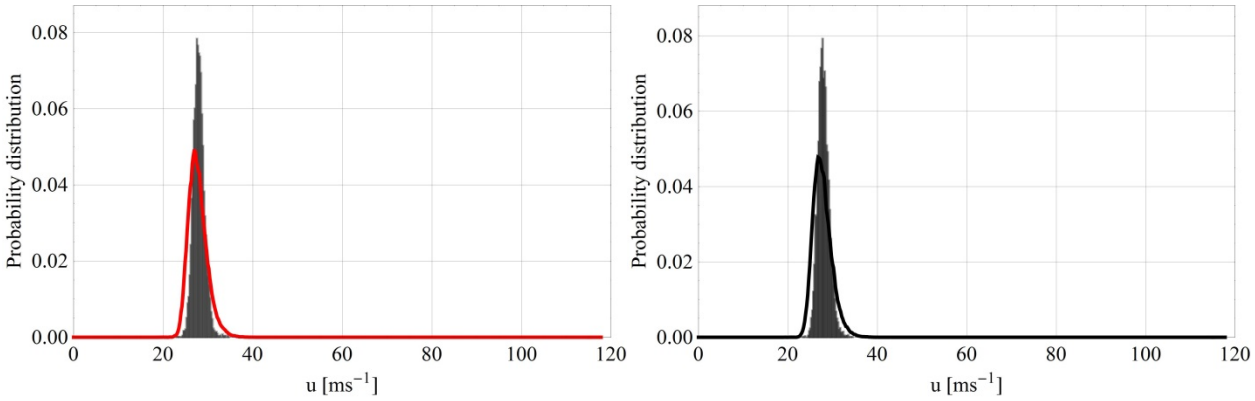

Figure 96 Probability density function and histogram of the measured speeds for two runs.

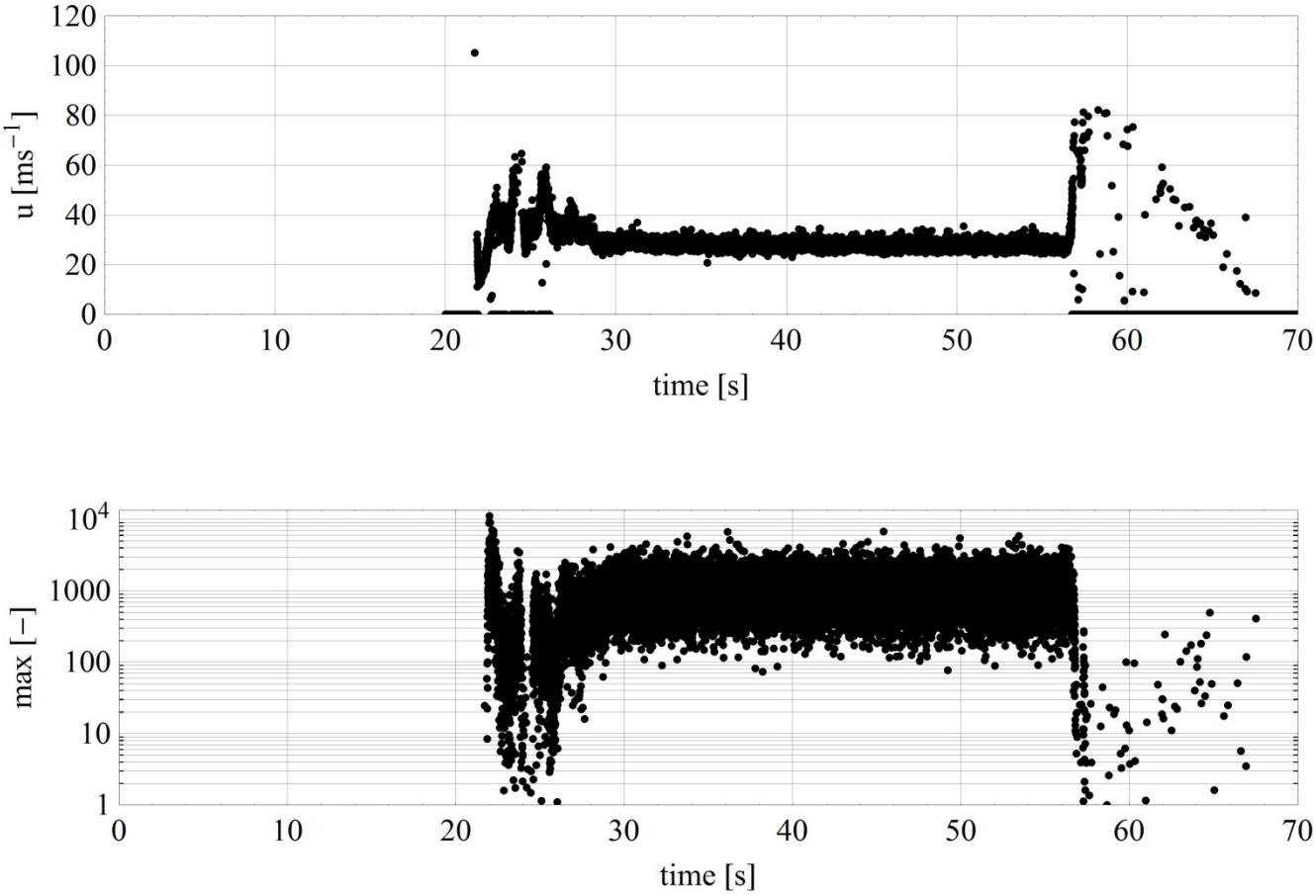

Figure 97 Time series of the velocity and the corresponding maximum value of the laser Doppler spectra of the first run.

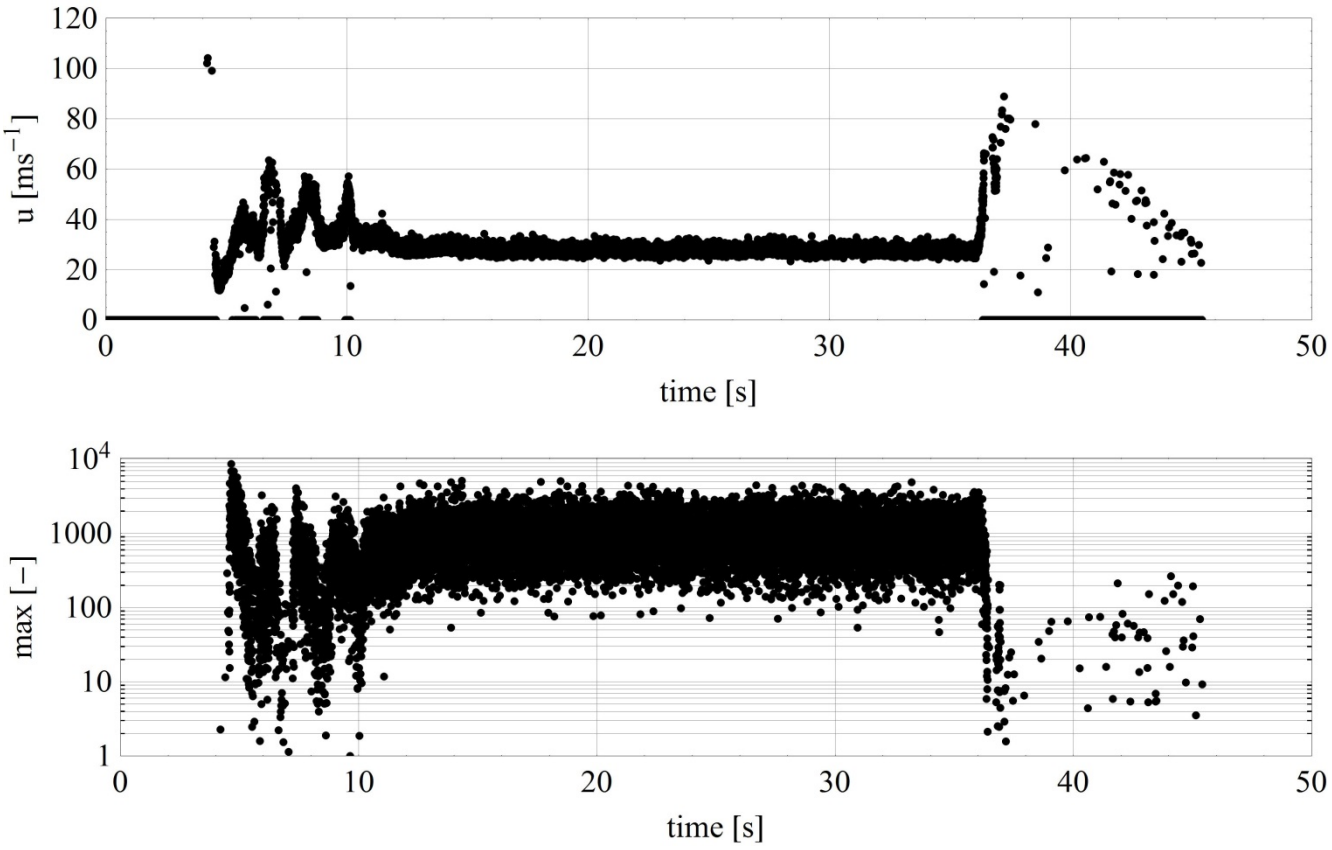

Figure 98 Time series of the velocity and the corresponding maximum value of the laser Doppler spectra of the second run.

Steel bolts 0.6 mm @ 100 mm: 50 PSI

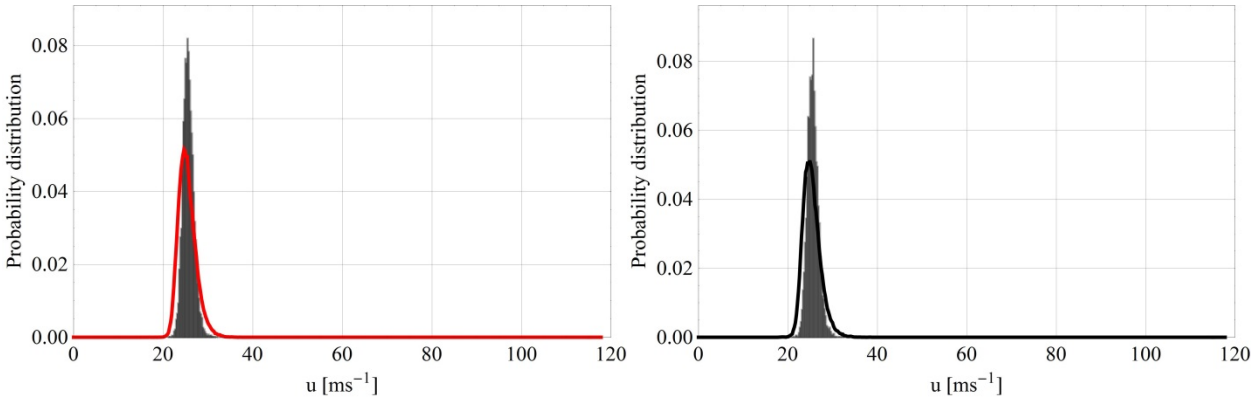

Figure 99 Probability density function and histogram of the measured speeds for two runs.

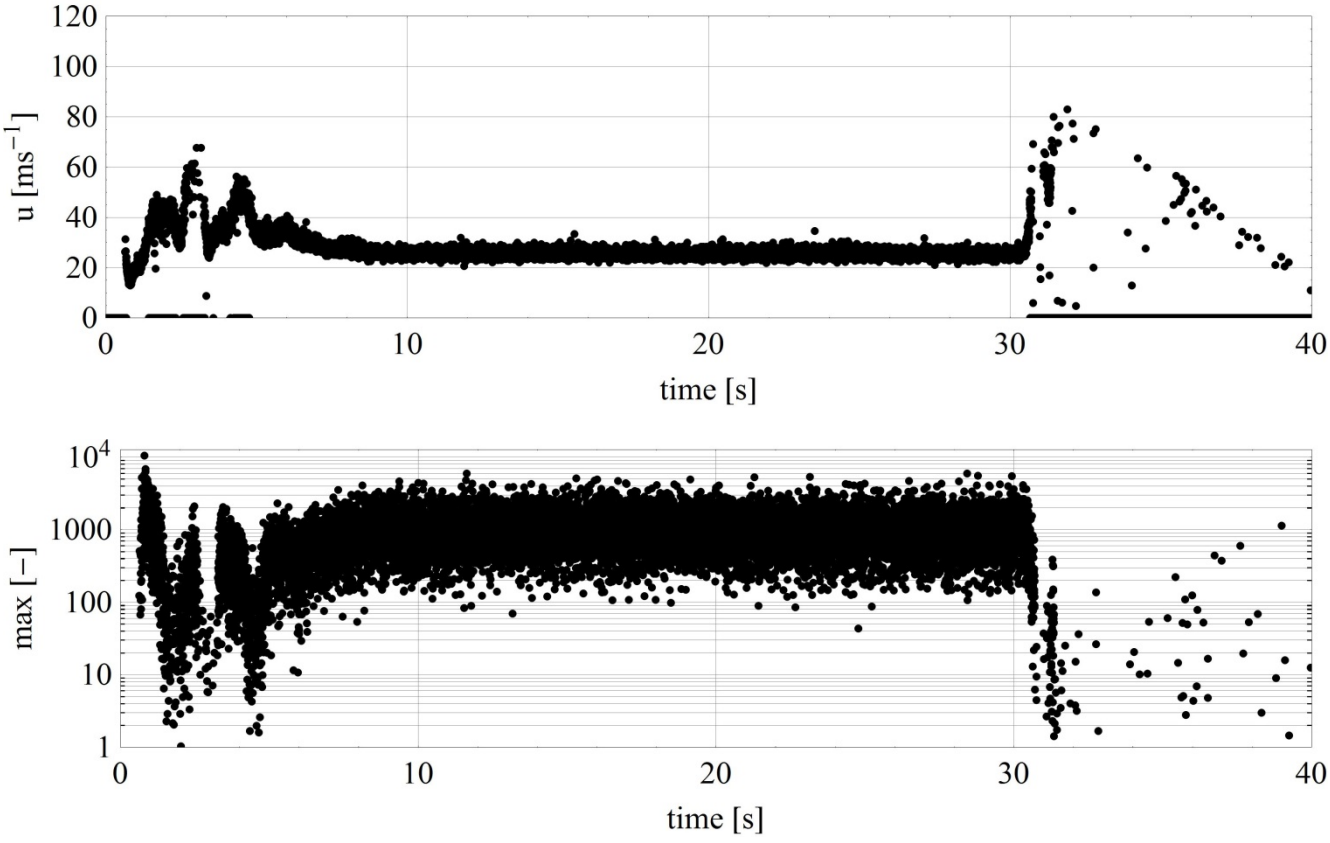

Figure 100 Time series of the velocity and the corresponding maximum value of the laser Doppler spectra of the second run.

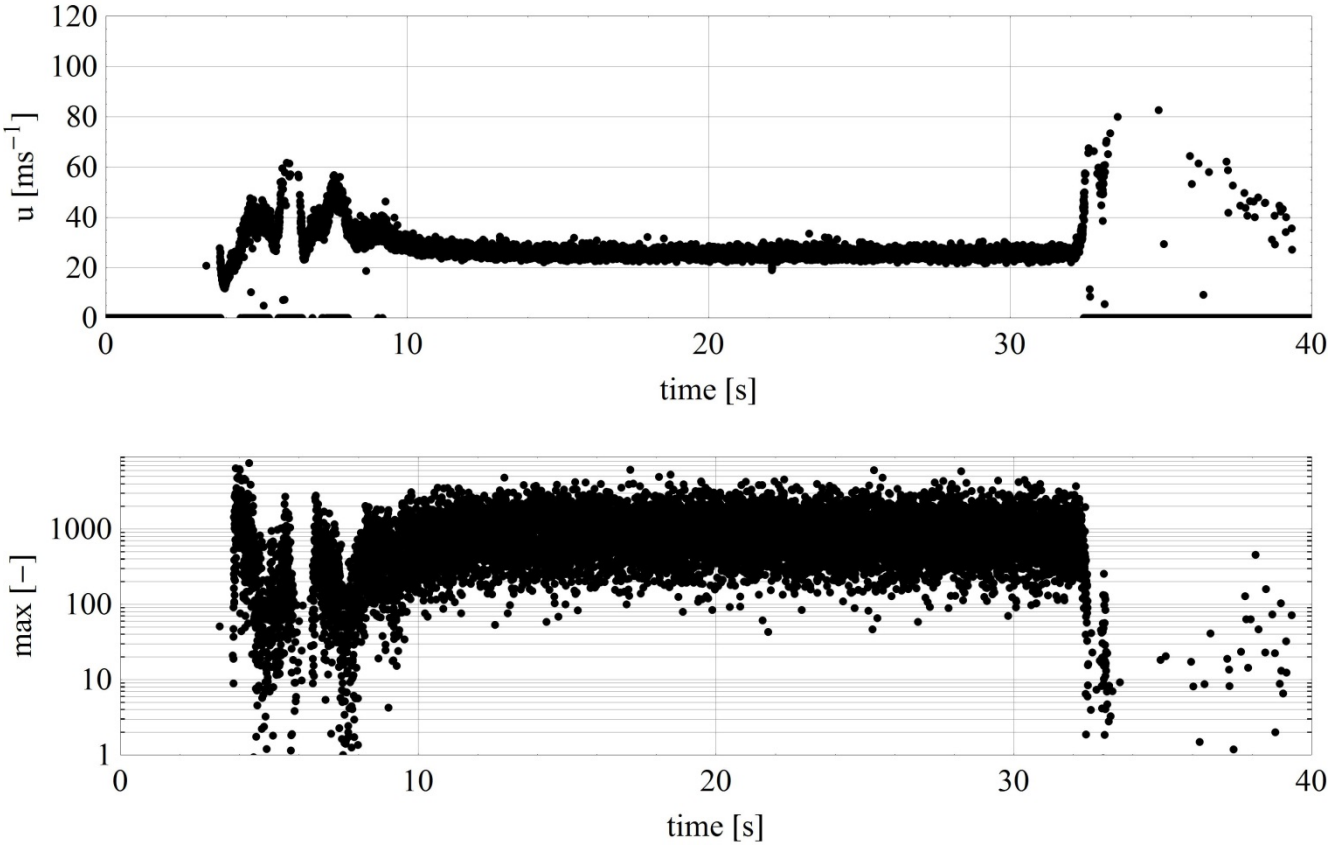

Figure 101 Time series of the velocity and the corresponding maximum value of the laser Doppler spectra of the second run.

Steel bolts 0.6 mm @ 100 mm: 60 PSI

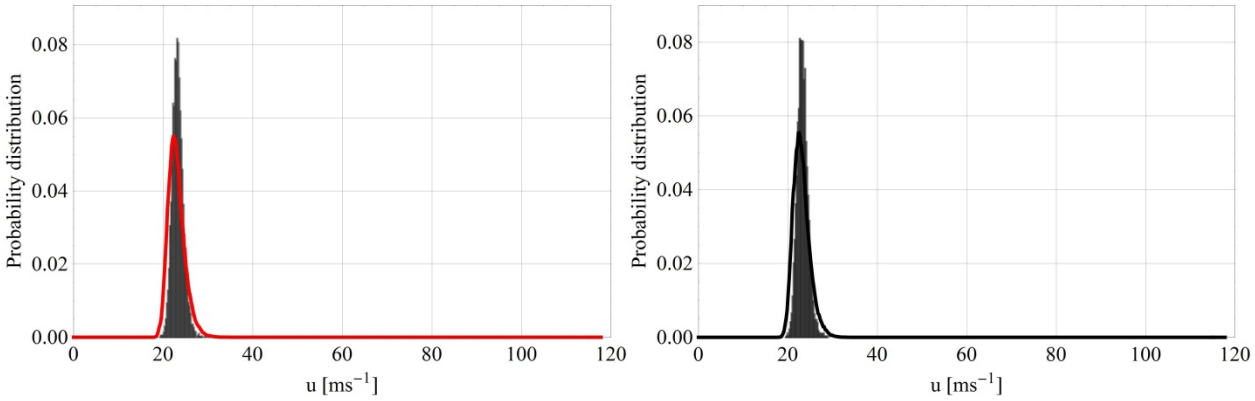

Figure 102 Probability density function and histogram of the measured speeds for two runs.

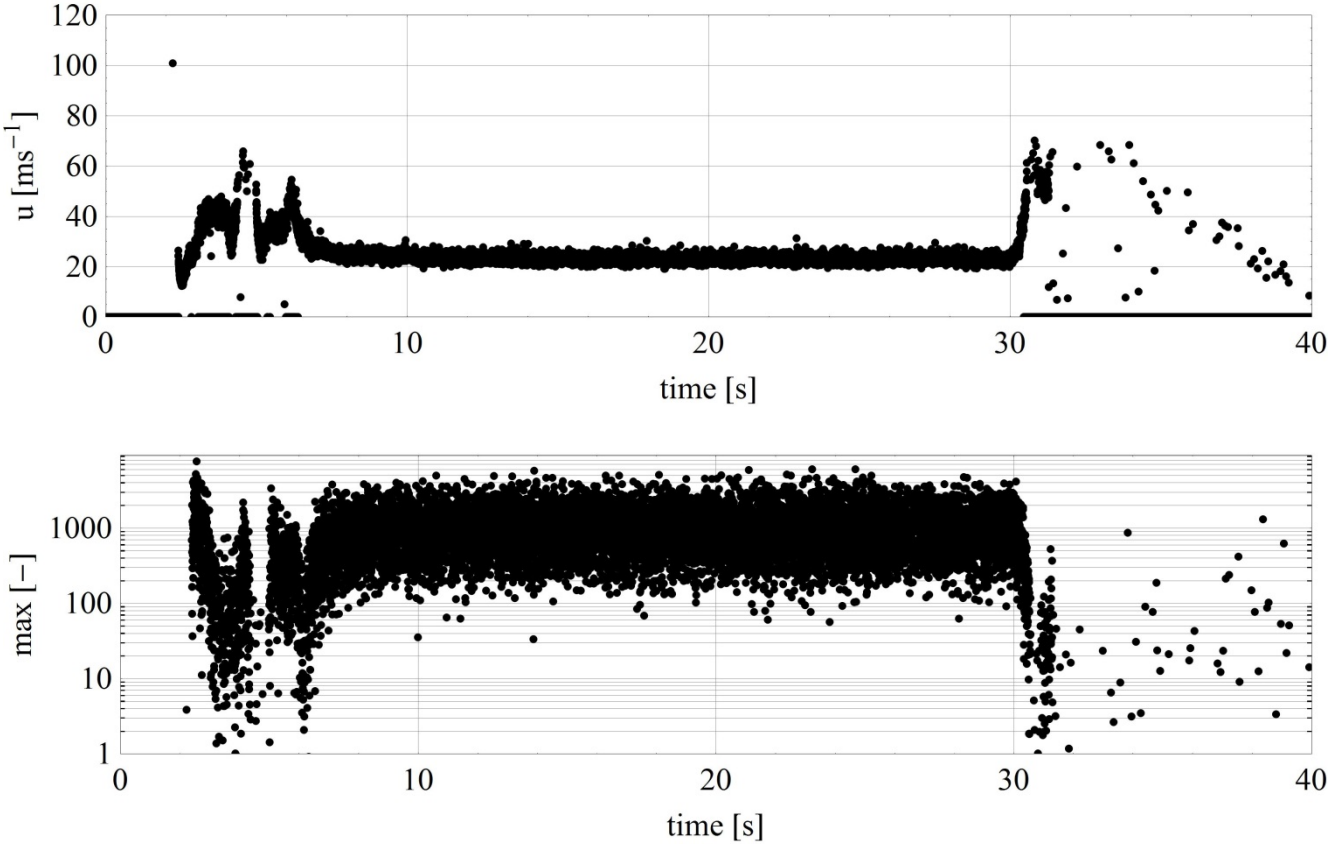

Figure 103 Time series of the velocity and the corresponding maximum value of the laser Doppler spectra of the first run.

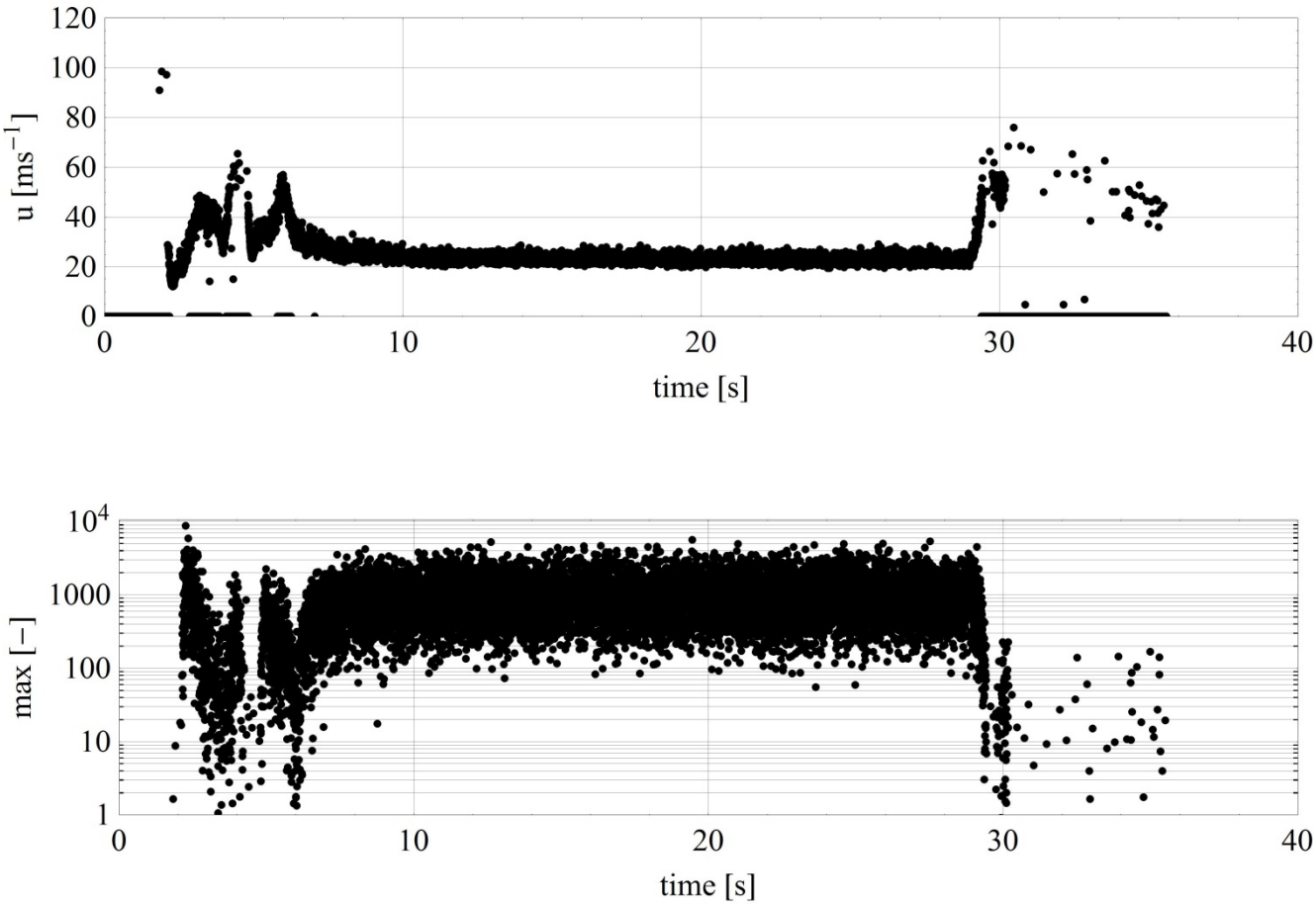

Figure 104 Time series of the velocity and the corresponding maximum value of the laser Doppler spectra of the second run.

Steel bolts 0.6 mm @ 100 mm: 70 PSI

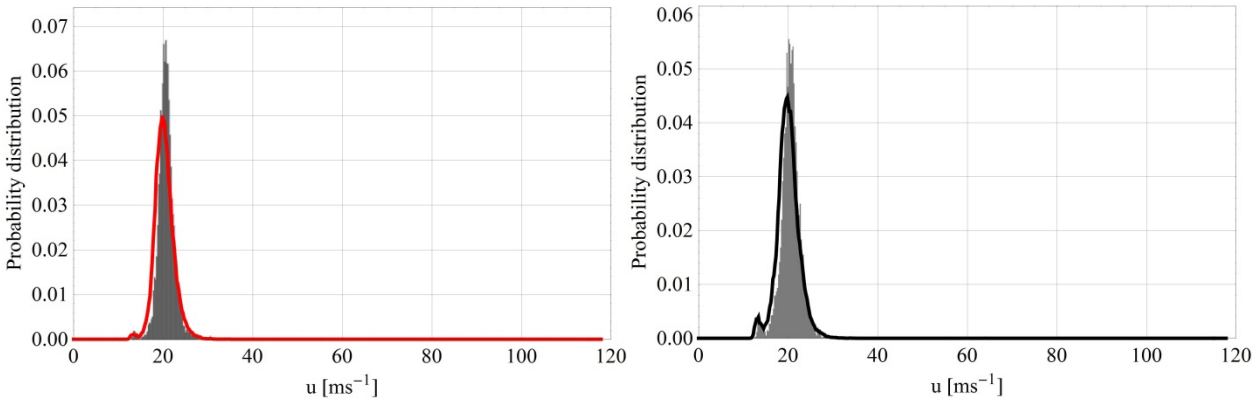

Figure 105 Probability density function and histogram of the measured speeds for two runs.

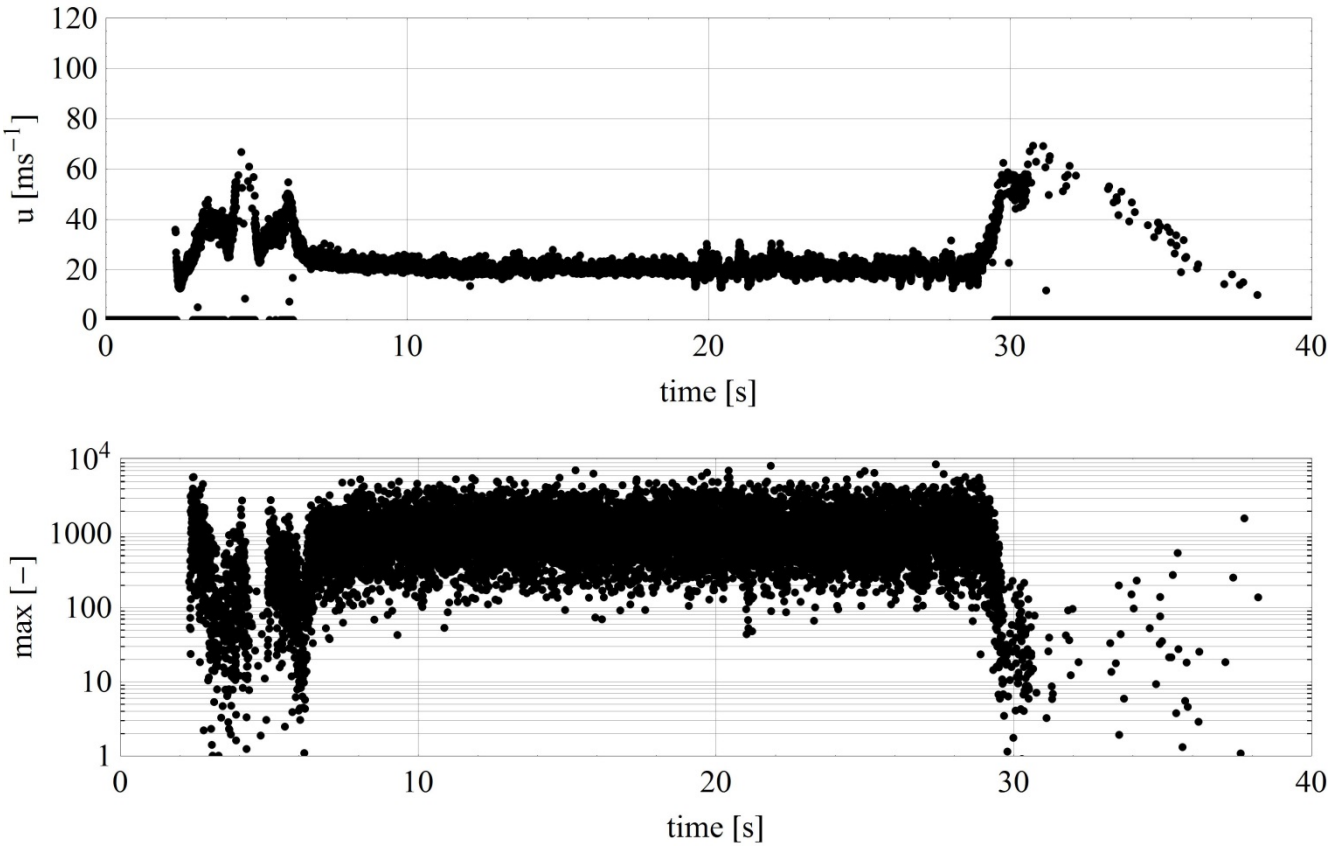

Figure 106 Time series of the velocity and the corresponding maximum value of the laser Doppler spectra of the first run.

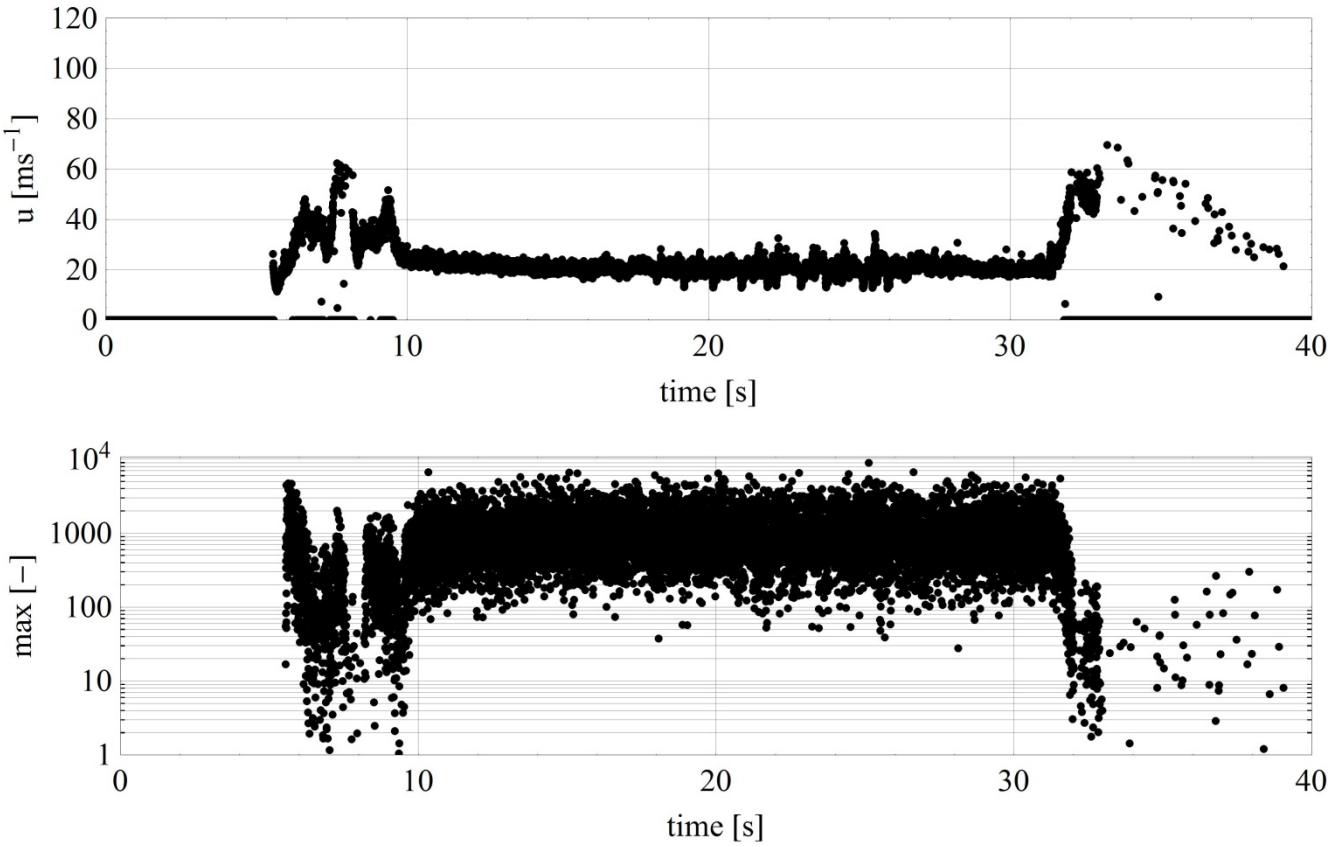

Figure 107 Time series of the velocity and the corresponding maximum value of the laser Doppler spectra of the second run.

Steel bolts 1.0 mm @ 50 mm: 40 PSI

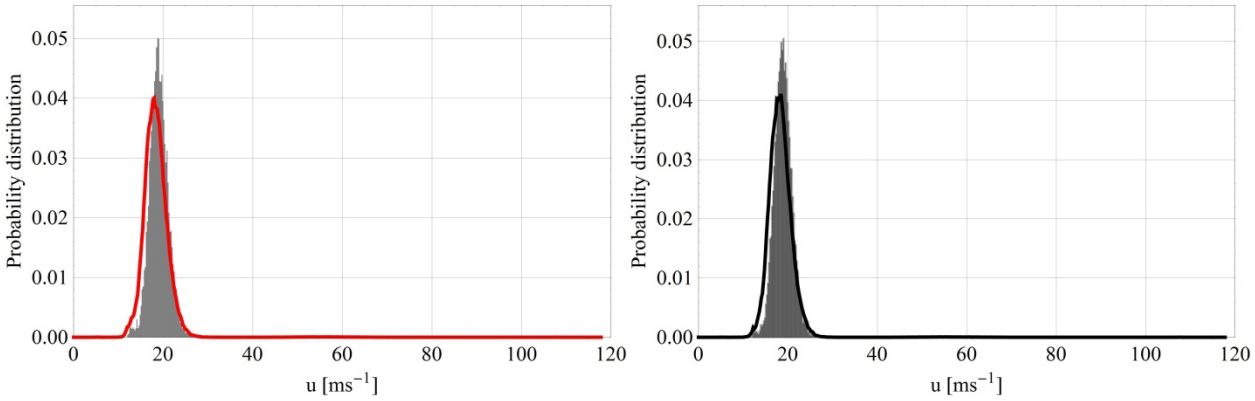

Figure 108 Probability density function and histogram of the measured speeds for two runs.

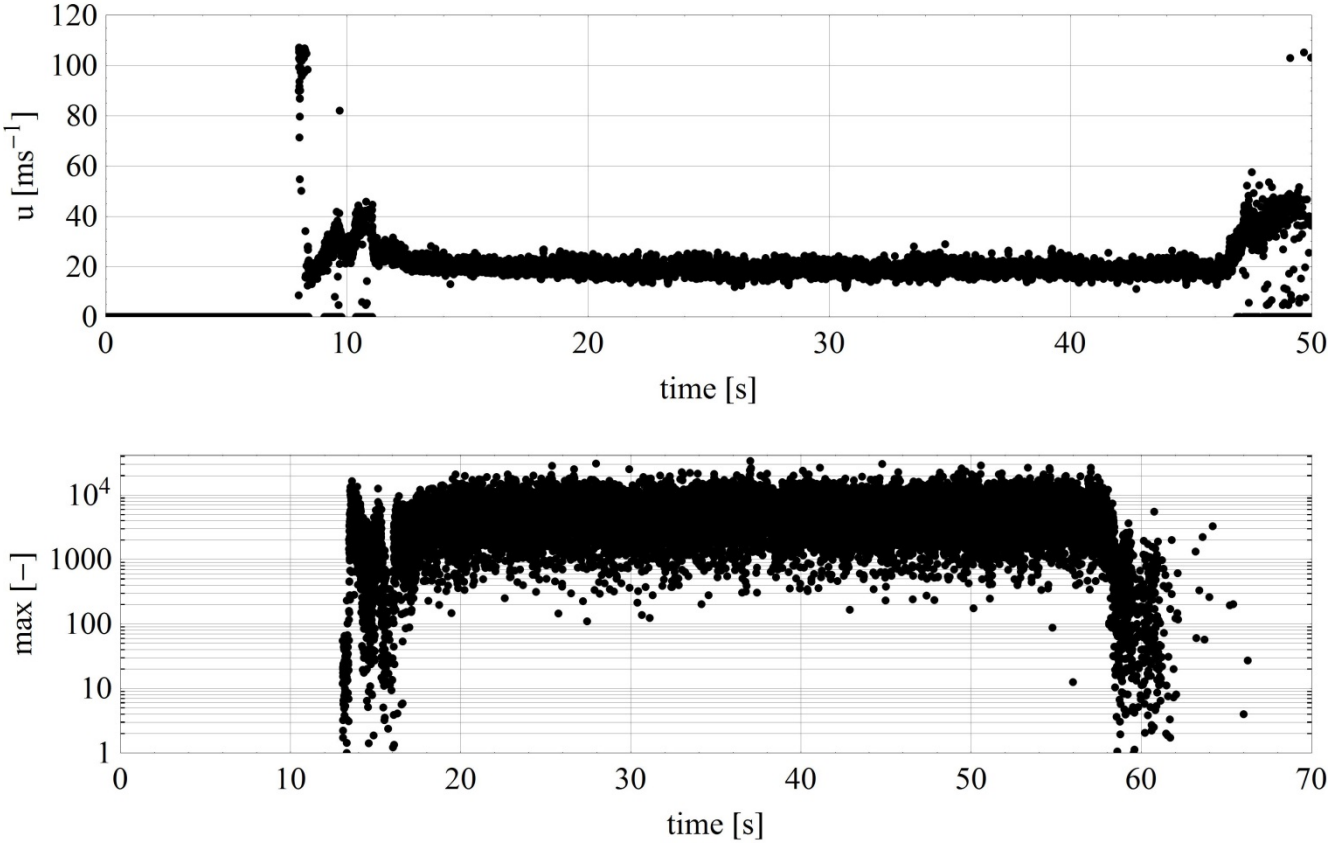

Figure 109 Time series of the velocity and the corresponding maximum value of the laser Doppler spectra of the first run.

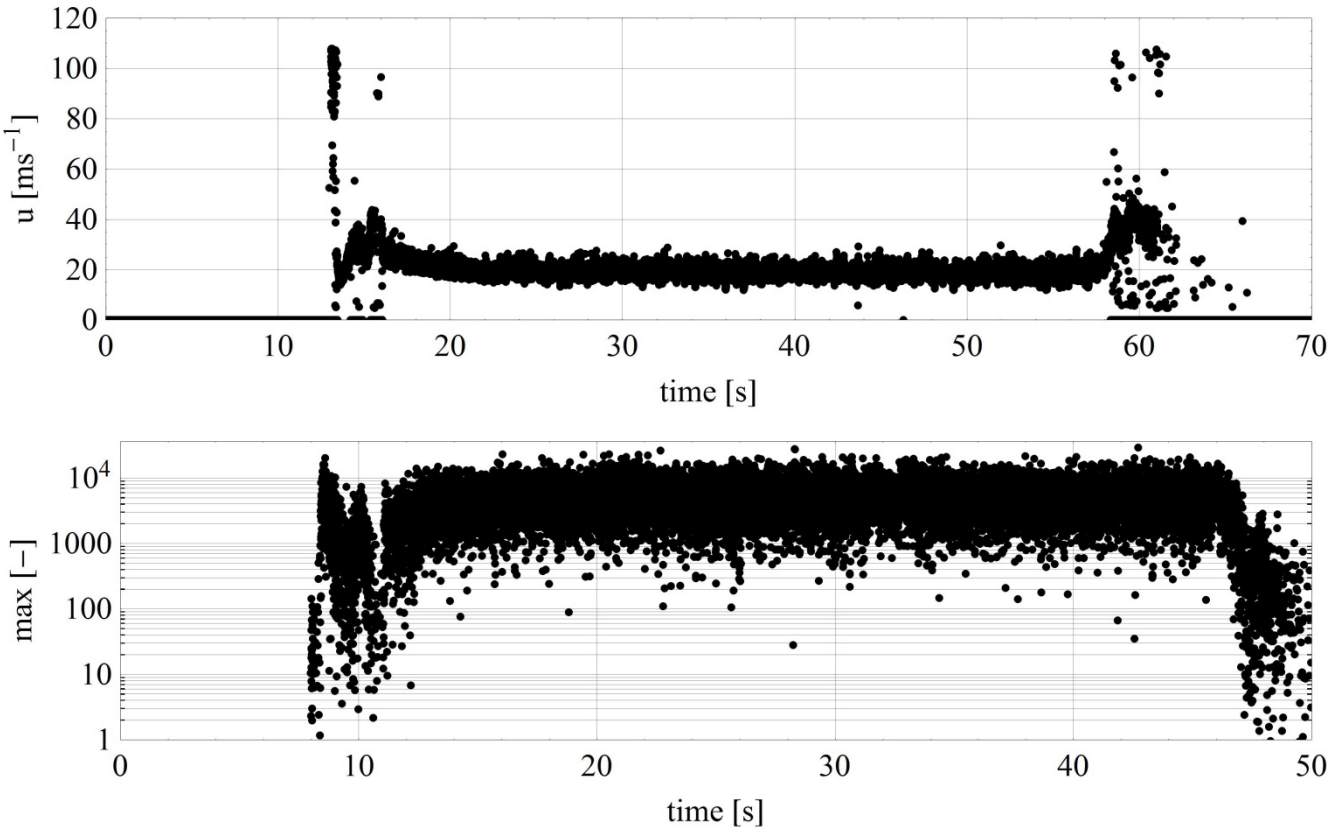

Figure 110 Time series of the velocity and the corresponding maximum value of the laser Doppler spectra of the second run.

Steel bolts 1.0 mm @ 50 mm: 50 PSI

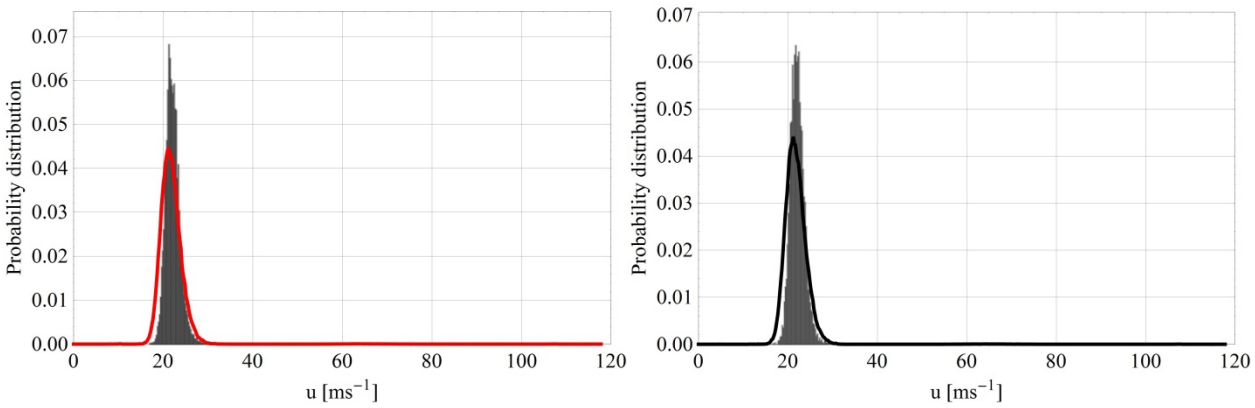

Figure 111 Probability density function and histogram of the measured speeds for two runs.

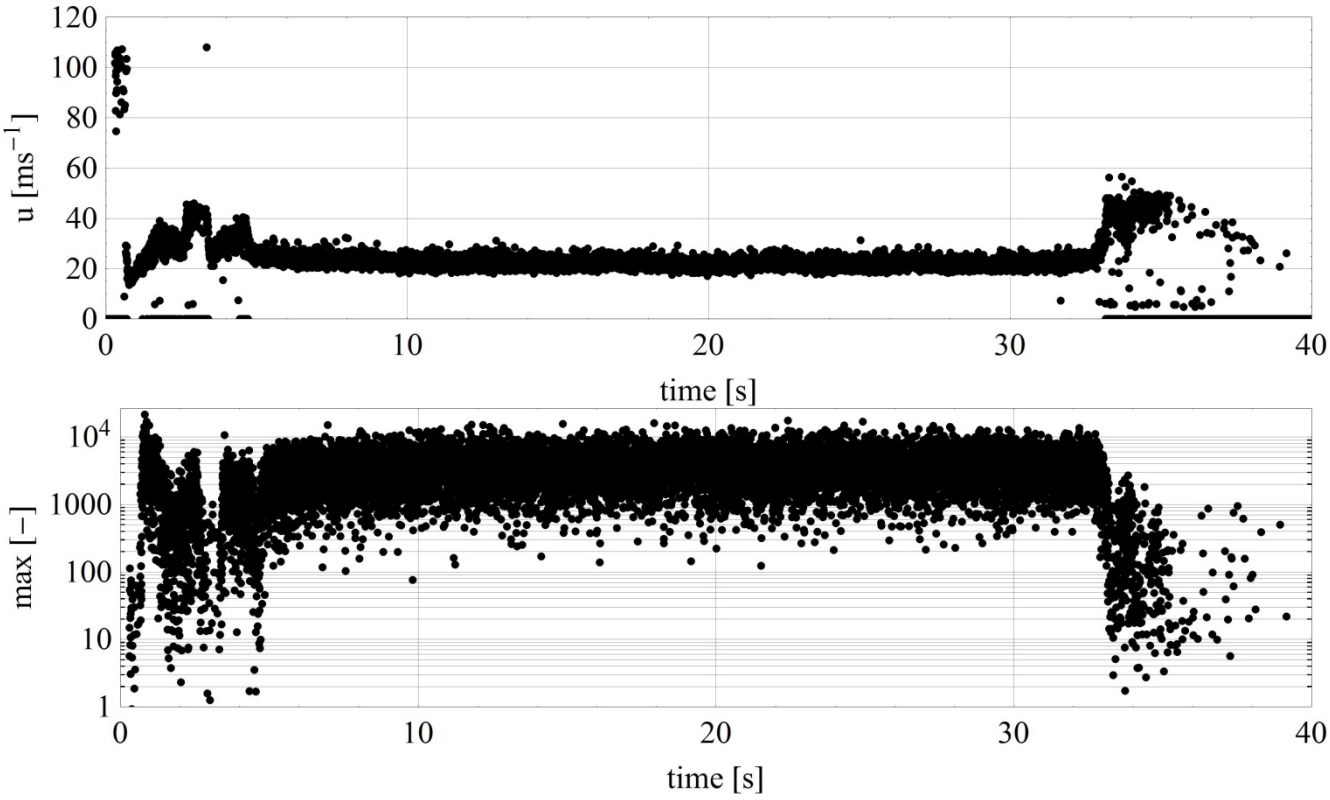

Figure 112 Time series of the velocity and the corresponding maximum value of the laser Doppler spectra of the first run.

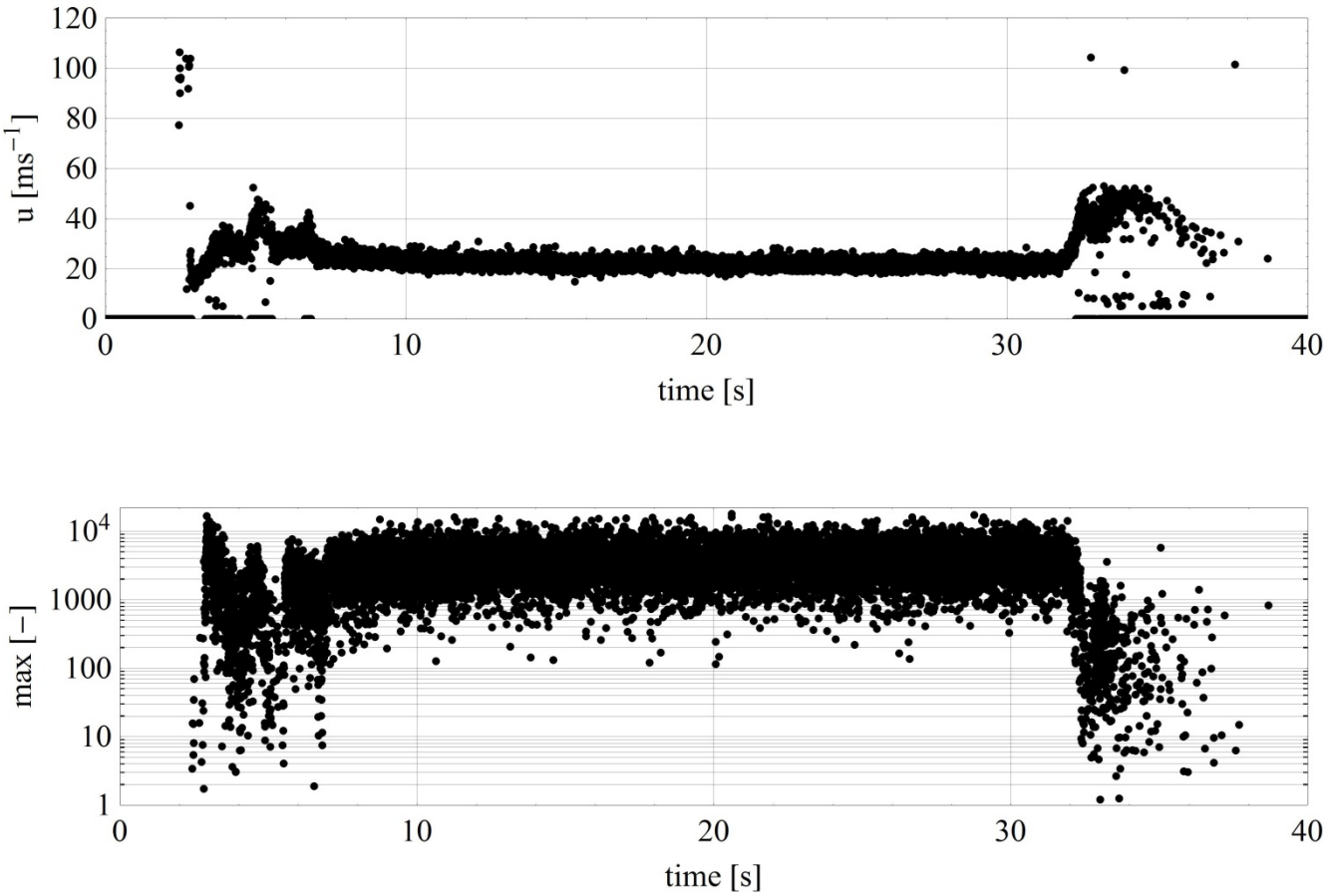

Figure 113 Time series of the velocity and the corresponding maximum value of the laser Doppler spectra of the second run.

Steel bolts 1.0 mm @ 50 mm: 60 PSI

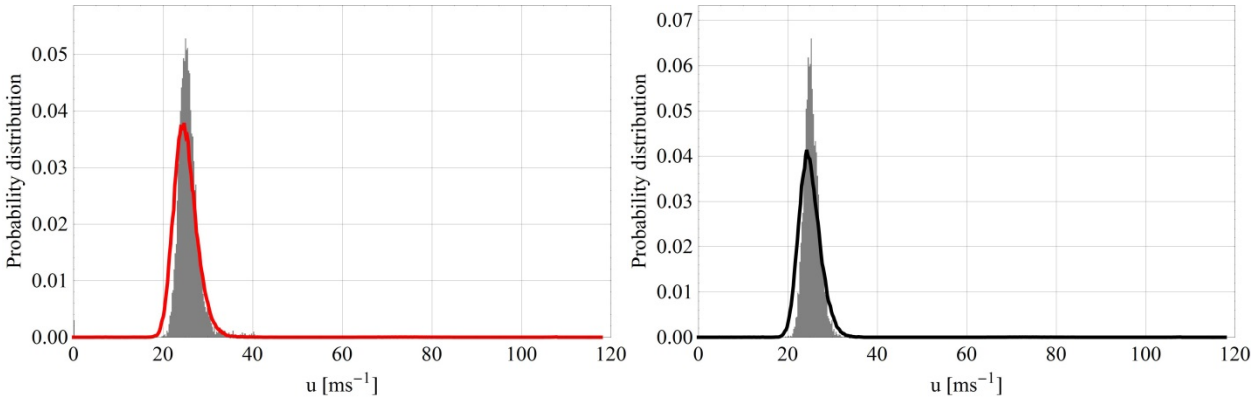

Figure 114 Probability density function and histogram of the measured speeds for two runs.

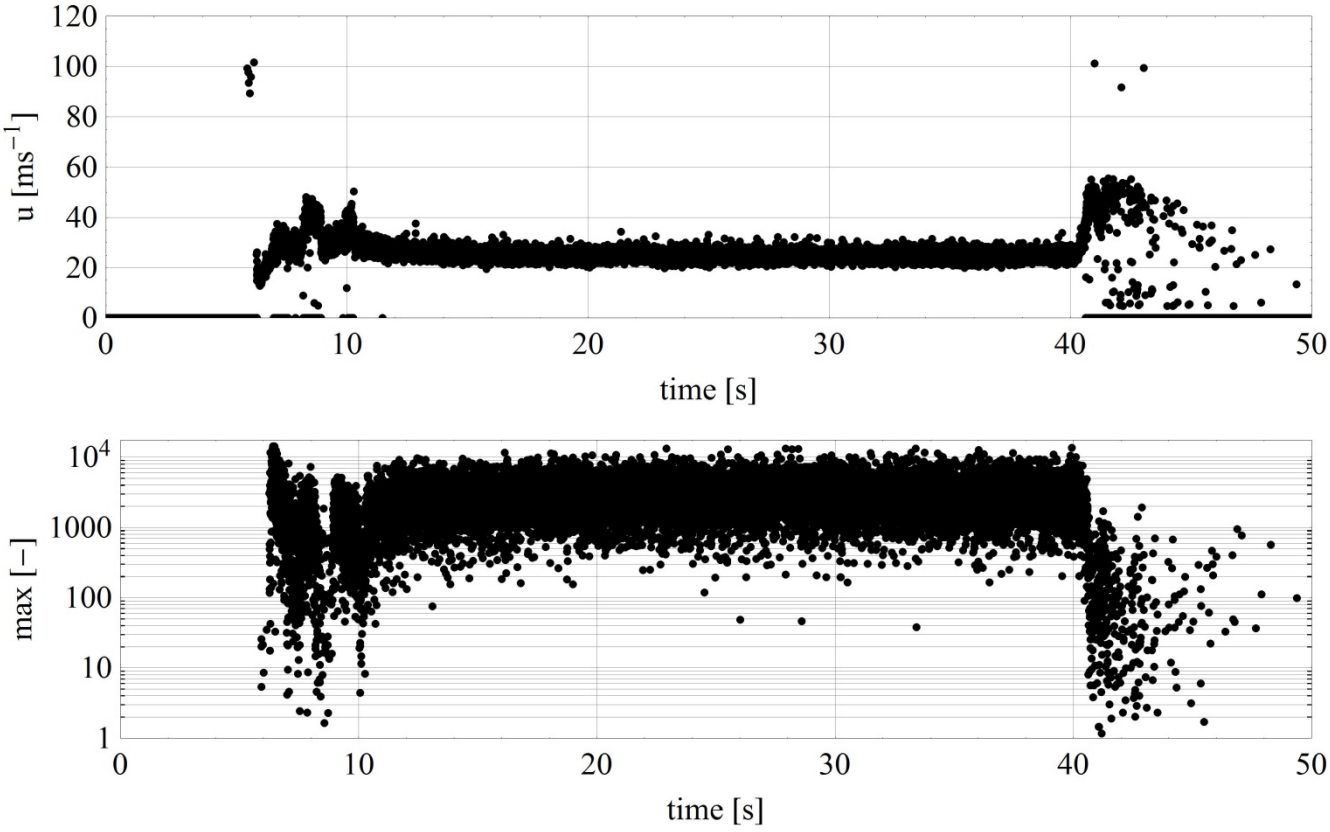

Figure 115 Time series of the velocity and the corresponding maximum value of the laser Doppler spectra of the first run.

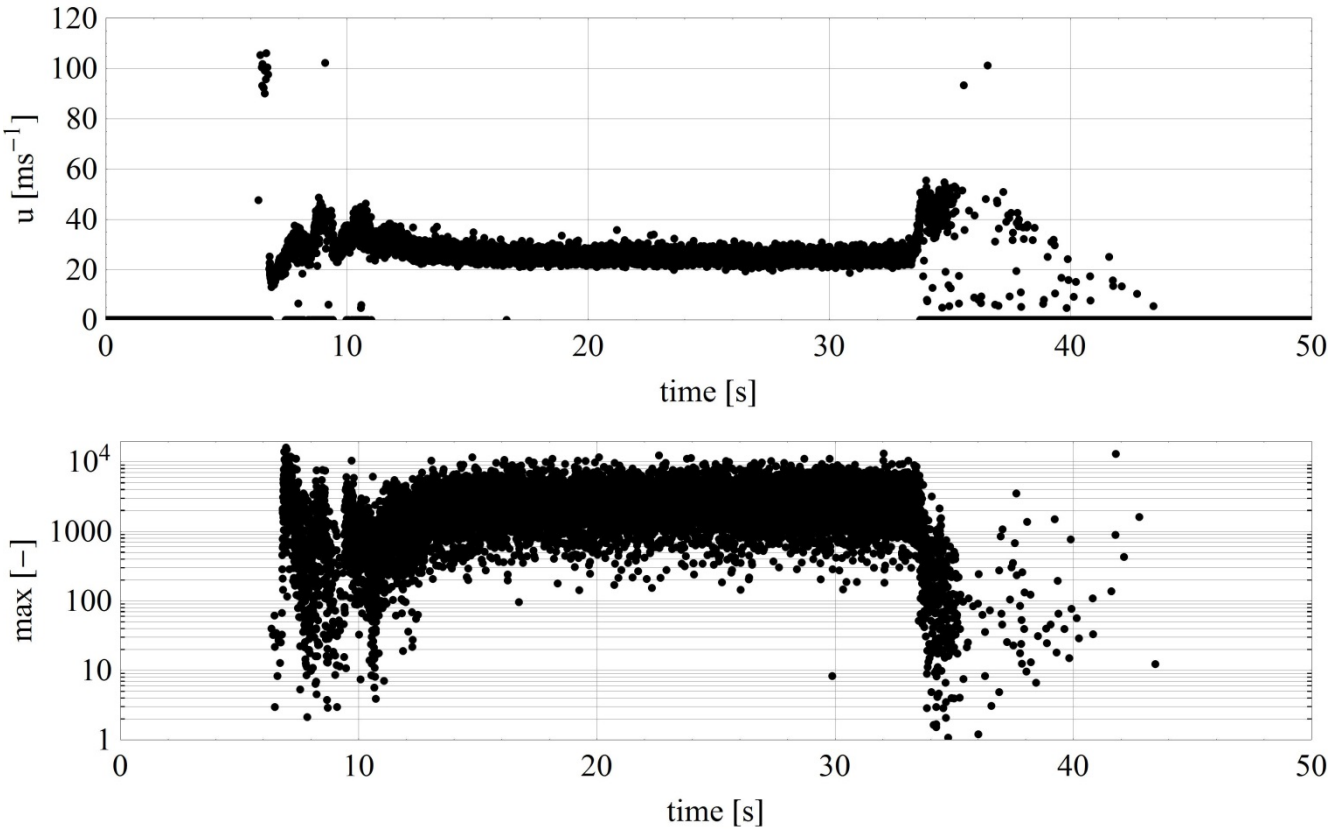

Figure 116 Time series of the velocity and the corresponding maximum value of the laser Doppler spectra of the second run.

Steel bolts 1.0 mm @ 50 mm: 70 PSI

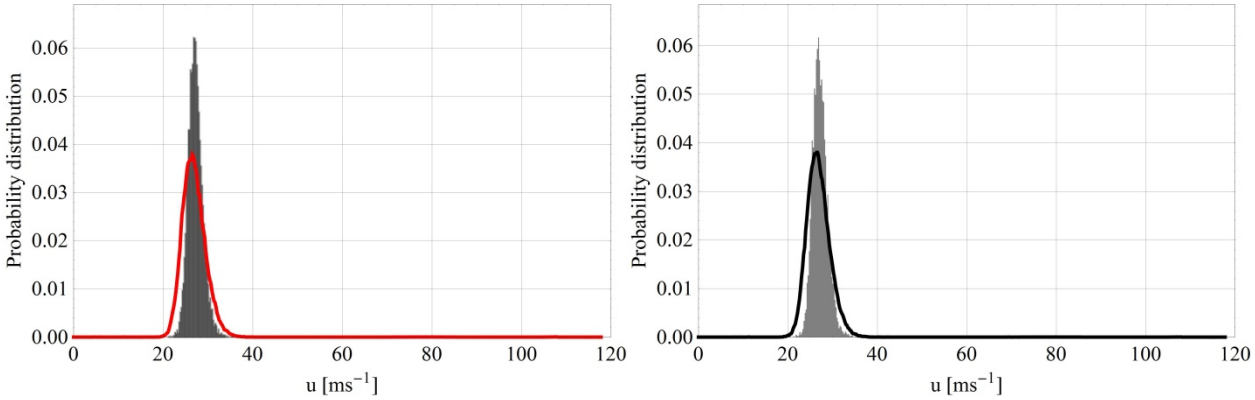

Figure 117 Probability density function and histogram of the measured speeds for two runs.

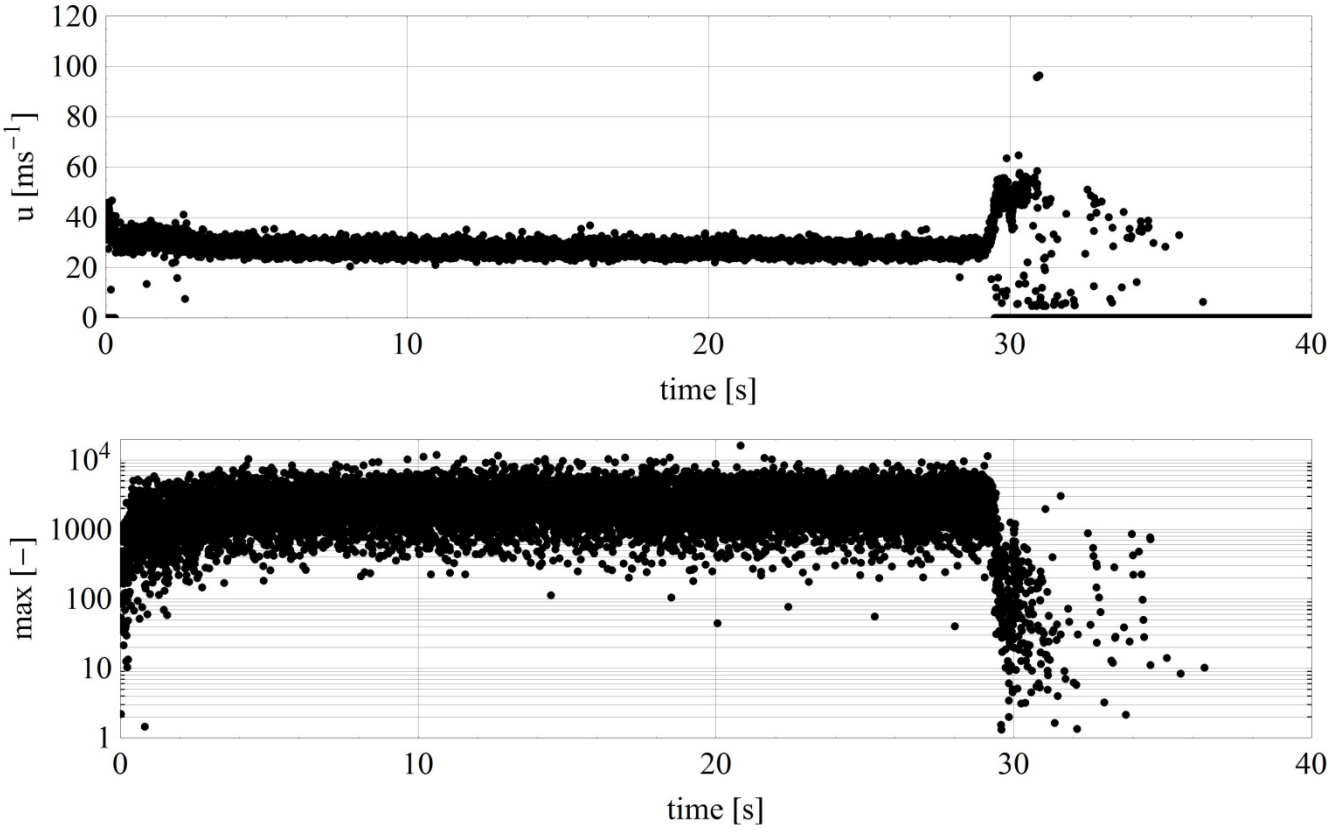

Figure 118 Time series of the velocity and the corresponding maximum value of the laser Doppler spectra of the first run.

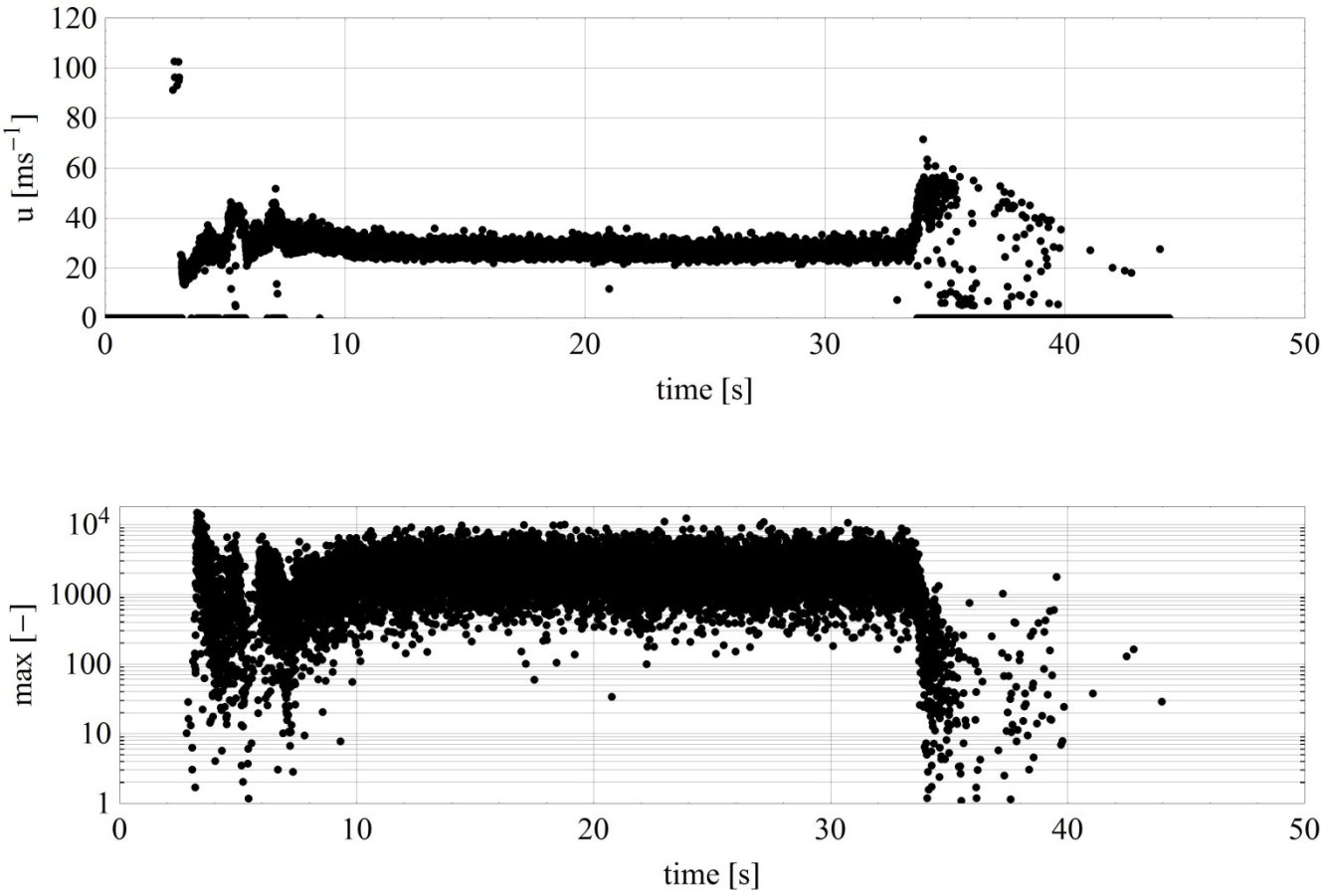

Figure 119 Time series of the velocity and the corresponding maximum value of the laser Doppler spectra of the second run.

Steel bolts 1.0 mm @ 50 mm: 80 PSI

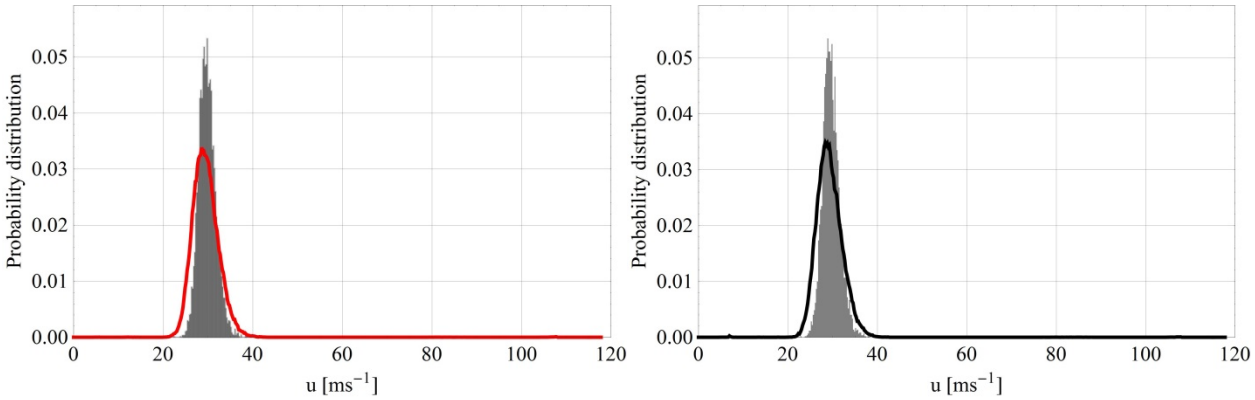

Figure 120 Probability density function and histogram of the measured speeds for two runs.

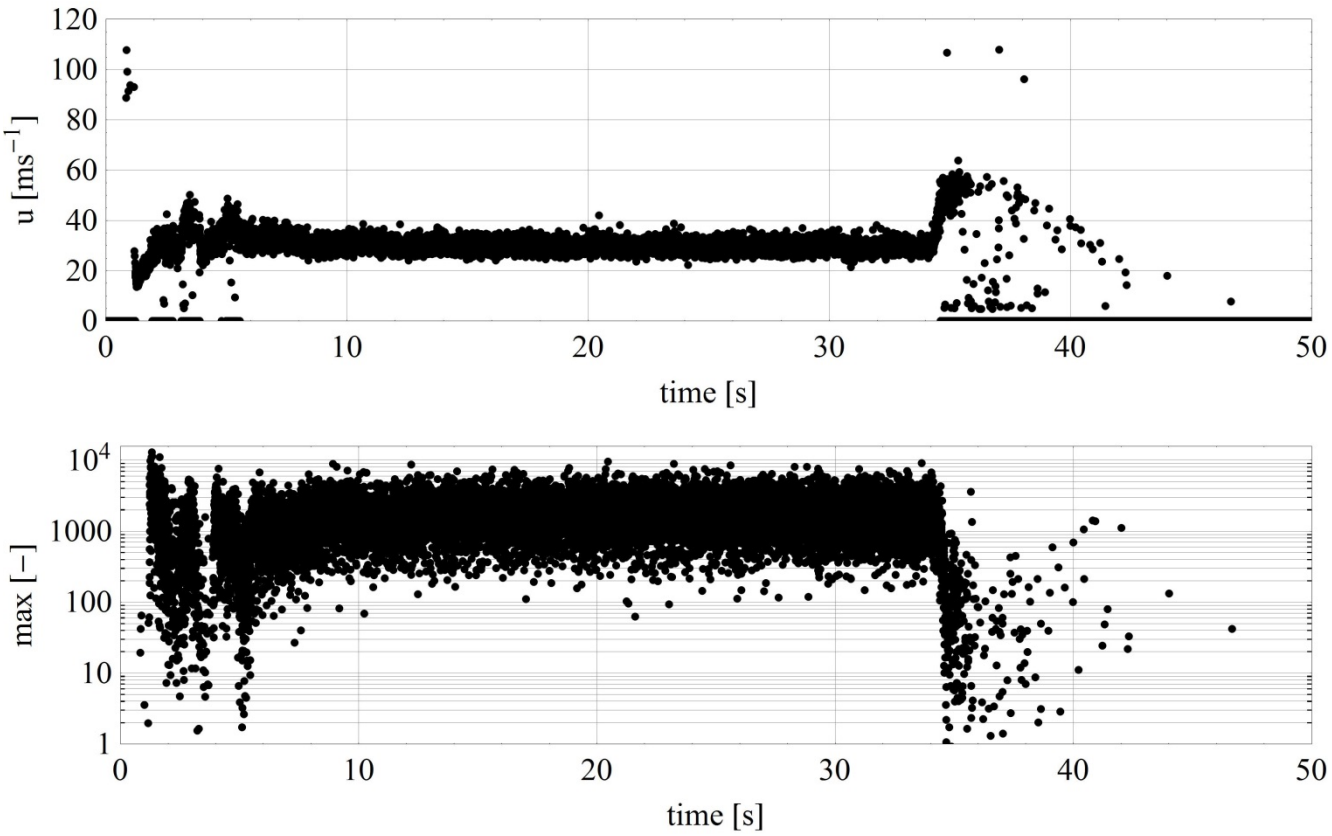

Figure 121 Time series of the velocity and the corresponding maximum value of the laser Doppler spectra of the first run.

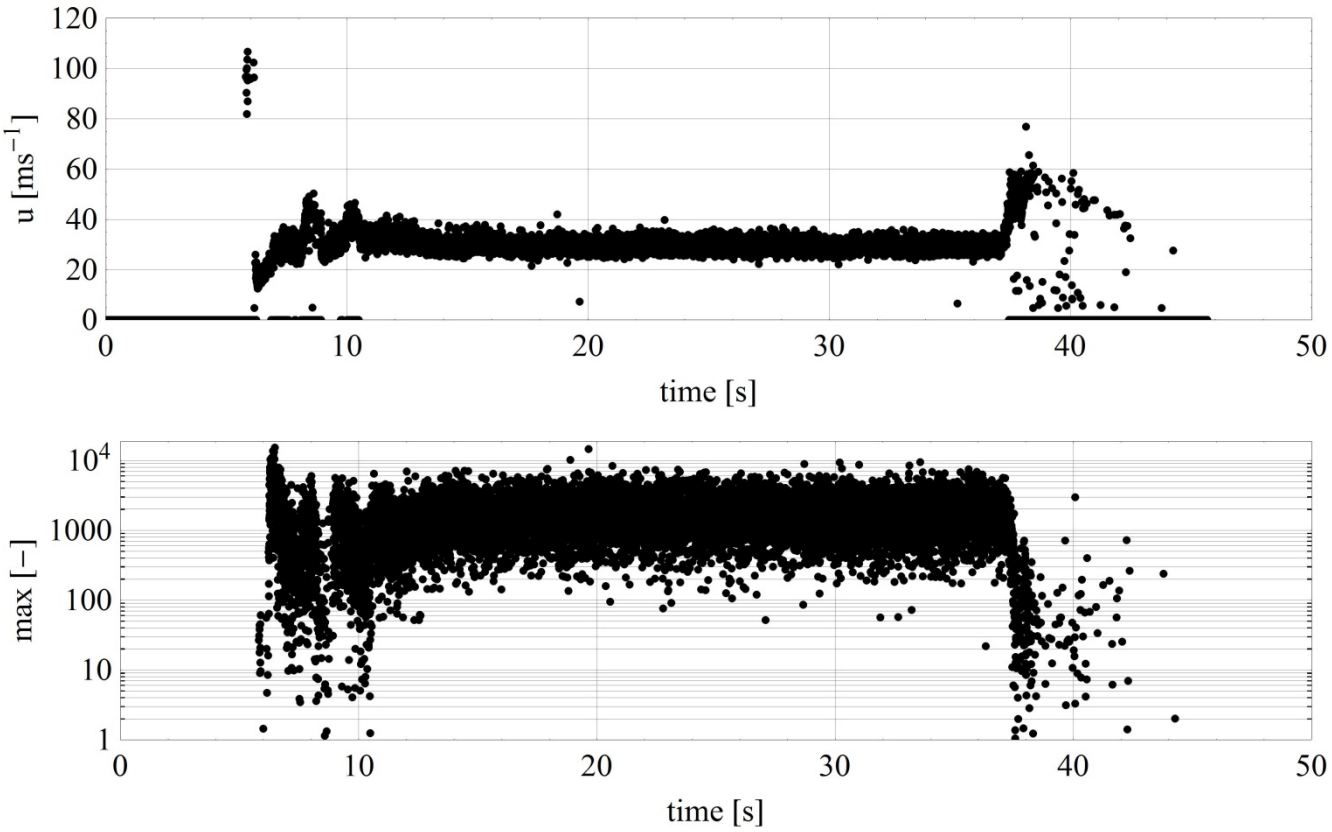

Figure 122 Time series of the velocity and the corresponding maximum value of the laser Doppler spectra of the second run.

DTU Wind Energy
Department of Wind Energy
Technical University of Denmark

Frederiksborgvej 399
DK-4000
Roskilde

http://www.vindenergi.dtu.dk